

UNIVERSITY OF CALGARY

Integration of MEMS Sensors, WiFi, and Magnetic Features for Indoor Pedestrian Navigation
with Consumer Portable Devices

by

You Li

A THESIS
SUBMITTED TO THE FACULTY OF GRADUATE STUDIES
IN PARTIAL FULFILMENT OF THE REQUIREMENTS FOR THE
DEGREE OF DOCTOR OF PHILOSOPHY

GRADUATE PROGRAM IN GEOMATICS ENGINEERING

CALGARY, ALBERTA

DECEMBER, 2015

© You Li 2015

Abstract

Mobile location based services (LBS) is attracting the public attention due to their potential applications in a wide range of personalized services from emergency responders to proximity-based mobile advertising and social networks. As a core technology of LBS, positioning and navigation (i.e., determination of the position, velocity, and attitude of the mobile device) is evidently vital. Most LBS users spend 70% - 90% of their time in indoor environments. Therefore, a highly demanding issue is to provide a trustworthy and real-time indoor navigation solution.

This thesis provides a reliable indoor pedestrian navigation solution by using off-the-self sensors in consumer portable devices, local magnetic features, and existing WiFi infrastructures. By taking better advantage of the merits of dead-reckoning (DR), WiFi fingerprinting, and Magnetic matching (MM), the proposed algorithm can provide a navigation solution that has accuracy of 3-5 m (RMS), and do not suffer from failures or jumps. Furthermore, this algorithm can run in real time on portable devices, and can be easily combined with other techniques such as GNSS and BLE. Compared with previous hybrid navigation algorithms or structures, the main innovation points of this research are:

- 1) This research presents a real-time calibration method for gyro sensors in consumer portable devices. The calibration happens automatically without the need for external equipment or user intervention. Multi-level constraints (i.e., the pseudo-observations, the accelerometer and magnetometer measurements, the norm vector of the accelerometer and magnetometer measurements, and the quasi-static attitude updates) are used to ensure the method is reliable and accurate under natural user motions. This method provided promising calibration results, even under challenging motion modes such as dangling and pocket, and in challenging indoor environments with frequent magnetic interferences.

- 2) This research proposes an autonomous navigation algorithm for challenging indoor environments that do not have any WiFi signal or have WiFi signals with a weak distribution. This algorithm integrates DR and MM, and uses several approaches to improve the DR and MM performance. Furthermore, realizing that the key to enhancing the DR/MM performance is to mitigate the impact of MM mismatches, this research introduces and evaluates two mismatch-detection approaches, including a threshold-based method that sets the measurement noises of MM positions based on their distances to the historical DR/MM position solutions, and an adaptive Kalman filter based method that introduces the estimation of the innovation sequence covariance into the calculation of the Kalman filter gain matrix.
- 3) This research presents a profile-based WiFi fingerprinting algorithm by using the short-term trajectories from DR and geometrical relationships of various RPs in the space. The Multi-Dimensional Dynamic Time Warping (MD-DTW) algorithm is introduced to match with inaccurate profile length for such a multi-dimensional system. The use of the profile-based approach can reduce the probability of mismatches. Furthermore, the profile-based approach is especially useful to provide a more accurate initialization for position as soon as a user starts navigating.
- 4) This research proposes a WiFi-aided MM algorithm, which uses the WiFi results to limit the MM search space to reduce both the mismatch rate and computational load. The complementary characteristics of WiFi and MM are especially useful for improving the navigation applications that use consumer devices not equipped with gyros (e.g., many medium- and low-end smartphones contain accelerometers and magnetometers but do not

have gyros). Furthermore, when aided by WiFi (or DR/WiFi) to remove mismatches, MM results can be used as reliable updates in the position-tracking KF.

- 5) This research provides designs for and evaluates two hybrid integration structures that uses off-the-shelf sensors in consumer portable devices and existing WiFi infrastructures. Structure #1 utilizes the WiFi-aided MM algorithm, while Structure #2 uses both DR and WiFi results (i.e., the integrated DR/WiFi solutions) to limit the MM search space. Furthermore, a multi-level quality control mechanism is designed based on the interaction between different techniques and utilized in Structure #2. This mechanism has at least one more level than those in previous DR/WiFi/MM structures. Therefore, Structure #2 is more effective than previous structures at detecting MM mismatches, even in areas with limited WiFi RSS or weak RSS distribution. This structure reduced dependency on both navigation environments and motion condition. It provided consistent positioning accuracy in indoor environments with frequent magnetic interferences, and under different motion conditions.

Therefore, by taking better advantage of the merits of DR, WiFi, and MM, the proposed algorithm has the following advantages:

- 1) The algorithm can significantly improve the attitude-determination and DR results with commercial-grade MEMS gyros (typically have biases of up to several deg/s) without the need for any external calibration equipment or user intervention.
- 2) The algorithm can provide reliable and continuous indoor navigation results when external positioning technologies (e.g., WiFi and BLE) are not available; also, it can achieve optimal system performance when an external technology is available.

- 3) The algorithm can reduce dependency on navigation environments. For example, the algorithm works in indoor environments that have weak WiFi signal distribution, or in environments with frequent magnetic interferences.
- 4) The algorithm can reduce dependency on device motion conditions. Specifically, the algorithm can work under natural motion conditions such as handheld, phoning (i.e., close to the ear), dangling (i.e., walking with phone in hand), and in pants pockets.

There are various potential applications for the outcomes of this research, for example:

- Mobile LBS that use consumer portable devices;
- Indoor photogrammetry and mapping;
- Crowdsourcing of WiFi/magnetic DBs by using daily-life data from users;
- To augment smartphone-based GNSS positioning (e.g., precise point positioning);
- Integration with other available technologies (e.g., BLE, LED, and map matching).

Acknowledgements

I would like to thank Dr. Naser El-Sheimy and Dr. Xiaoji Niu for being the most considerate and trusted supervisors. Dr. El-Sheimy, thank you for giving me too many supports on my study and life. Because of your trust and selflessness, I always feel you are on my side. Also, your wisdom and energy have inspired me deeply, and let me known why you are so successful in both academic and industrial fields. Dr. Niu, thank you for leading me into the treasure house of research and enjoy the happiness it brings to me. You encourage me to publish my first article, complete my first project, attend my first international conference, and go aboard to obtain eye-opening experiences. You are the best supervisor who always considers for the students more than yourself.

I would like to thank my colleagues at the Mobile Multi-Sensor System (MMSS) Research Group, University of Calgary (Dr. Hsiu-Wen Chang, Dr. Yuan Zhuang, Dr. Daihong Chao, Dr. Xing Zhao, Dr. Adel Moussa, Dr. Sara Saeedi, Dr. Zahra Lari, Haiyu Lan, Chunyang Yu, Qifan Zhou, Navid Mostofi, Hussein Sahli, Hani Mohamme, Naif Alsubaie, and Mostafa Sakr) for their friendship and support. Special thanks to Dr. Yuan Zhuang and Haiyu Lan for the so many valuable discussions in multi-sensor navigation systems. Also, I would thank Dr. Tao Lin and Dr. Zhe He at the PLAN Group, University of Calgary for their beneficial suggestions on research and life.

I would also like to thank all the team members at the Trusted Positioning Inc. (currently InvenSense Canada) for giving me the opportunity to work with the most talented and impassioned navigation team in the world. Special thanks to Dr. Jacques Georgy, Dr. Zanaib Syed, and Dr. Chris Goodall for being my supervisors and friends, and thanks to Dr. Tao Li, Dr. Zhi Shen, Dr. Da Wang, and Dr. Abdelrahman Ali, Dr. Mostafa Elhoushi, Dr. Medhat Omr, Ahmed Wahdan, Walid Abdelfatah, and Amr Al-Hamad for always being my trustable friends and colleagues.

I would like to thank my supervisors and colleagues at the GNSS Research Center, Wuhan University. Special thanks to Dr. Jingnan Liu, Dr. Chuang Shi, Dr. Hongping Zhang, Dr. Qile Zhao, Dr. Guigen Nie, Dr. Yidong Lou, Dr. Weiming Tang, and Dr. Tao Li for giving me valuable guidance in the positioning and navigation field. Also, I would like to give my thanks to Dr. Wenfei Guo, Dr. Tisheng Zhang, Dr. Quan Zhang, Dr. Rongxin Fang, Peng Zhang, Yalong Ban, Zhouzheng Gao, Weiwei Cheng, Qijin Chen, Qingjiang Wang, and all the team members at the GNSS/INS Group for their support.

There are so many people that have supported me in my life. I could not list all your names in this acknowledgements, but thank you all for every moment we shared and every help you gave me. I really appreciate them. This thesis should be a gift for all of you: I could not make it without everything you have gave to me.

Dad and Mom, thank you for giving the best things to me but never asking for any return. You are always the idols in my life, who lead me to be a man with integrity and enthusiasm. Father-in-law and Mother-in-law, thank you for being my parents and giving me every support you can. Thank you for encouraging us to choose our own life. Your kindness and love inspires me to become a better man.

Lujie, my lovely wife, thank you for accompanying me at Wuhan, Calgary, and everywhere. We have experienced joys, achievements, and setbacks together, and will continue to face everything hand in hand in the future. Thank you for loving me, encouraging me, and being proud of me. Without your love, I might have never achieved this milestone and have the confidence to moving to bigger and bigger milestones. Luana, my princess, thank you for coming to our family and giving us a source of joys. You are everything for me.

Dedication

To my family

For being my greatest source for happiness, joys,
and energy

Table of Contents

CHAPTER 1: INTRODUCTION	17
1.1 Background and Problem Statement.....	17
1.2 Literature Review.....	23
1.3 Research Objective	37
1.4 Innovation Points	39
1.5 Thesis Outline	41
CHAPTER 2: FUNDAMENTALS FOR NAVIGATION	43
2.1 Reference Systems	43
2.2 WiFi Fingerprinting	45
2.3 Sensor-based Navigation	47
2.4 Magnetic Matching	53
2.5 Kalman Filter	56
CHAPTER 3: AUTONOMOUS GYRO CALIBRATION AND ATTITUDE DETERMINATION	60
3.1 Introduction.....	60
3.2 Calibration Approaches	64
3.3 Algorithm Description	67
3.4 Tests and Results.....	77
3.5 Summary	88
CHAPTER 4: SELF-CONTAINED NAVIGATION WITH SENSORS AND MAGNETIC FEATURES	91

4.1 Introduction.....	91
4.2 Magnetic Matching	93
4.3 Hybrid DR/MM Navigation.....	97
4.4 Tests and Results.....	101
4.5 Summary	114
CHAPTER 5 HYBRID DR/WIFI/MM INDOOR NAVIGATION.....	116
5.1 Introduction.....	116
5.2 WiFi Fingerprinting	118
5.3 Integration of WiFi and Magnetic Matching	132
5.4 Integration of Dead-reckoning, WiFi, and Magnetic Matching	134
5.5 Tests and Results.....	137
5.6 Summary	159
CHAPTER 6 CONCLUSIONS AND FUTURE WORKS.....	162
6.1 Conclusions.....	162
6.2 Recommendations for Future works	167
LIST OF PUBLICATIONS DURING PHD PERIOD	169
REFERENCES	172

List of Tables

Table 1-1. Some companies that provide indoor positioning and navigation solutions	19
Table 1-2. Comparison of professional and mass-market indoor positioning applications.....	21
Table 1-3. Limitations for indoor navigation technologies	34
Table 3-1. Performance of MEMS sensors in smartphones and that in tactical IMU	61
Table 3-2. Comprehensive characteristics of previous works and proposed method.....	67
Table 3-3. Rough reference values of gyro biases	78
Table 3-4. Statistical results of the calibration errors under all scenarios	82
Table 3-5. Statistical results of the calibration errors under all scenarios	82
Table 3-6. Statistical results of the calibration errors under all scenarios	85
Table 3-7. Statistical results of the calibration errors under all scenarios	85
Table 4-1. RMS of position errors at E.....	110
Table 4-2. RMS of position errors at B.....	114
Table 5-1. Statistical values of position errors of WiFi (point), WiFi (profile), and their integration with DR at E	144
Table 5-2. Statistical values of position errors at E	151
Table 5-3. Statistical values of position errors at B	157

List of Figures and Illustrations

Figure 1-1. Accuracy requirements for indoor positioning (modified on (Mautz, 2012))	20
Figure 1-2. Thesis outline and detailed issues	42
Figure 2-1. Coordinate systems used in navigation	45
Figure 2-2. Procedure of training and positioning	46
Figure 2-3. Diagram of the INS mechanization (Shin, 2005b).....	49
Figure 2-4. Diagram of PDR.....	50
Figure 2-5: Earth's main dipole magnetic field, modified on (Benenson and St öcker, 2002)	53
Figure 2-6. Diagram of Kalman filter	58
Figure 3-1. Structure of proposed calibration algorithm	68
Figure 3-2. The flowchart of using magnetometer data during QSMF periods.....	75
Figure 3-3. Tested motion conditions and corresponding gyro and accelerometer signals.....	78
Figure 3-4. Magnetometer readings and calibrated LMF when walking (handheld) outdoors and indoors	79
Figure 3-5. Outdoor test environment and trajectory.....	80
Figure 3-6. Figures of calibration results in outdoor tests (magenta dots indicate the availability of magnetometer measurements)	81
Figure 3-7. Indoor test environment trajectory	83
Figure 3-8. Figures of calibration results in indoor tests (magenta dots indicate the availability of magnetometer measurements)	84
Figure 3-9. Indoor test environment trajectory	86
Figure 3-10. Heading provided by magnetometers indoors.....	87
Figure 3-11. Indoor pedestrian navigation results	88
Figure 3-12. Gyro biases without and with the proposed real-time calibration.....	89
Figure 3-13. Calibration errors under typical motions both indoors and outdoors.....	90
Figure 4-1. Aligning two sequences using DTW (Zhen et al., 2012)	96

Figure 4-2. Two-filter based DR algorithm	98
Figure 4-3. Trajectories used to generate magnetic DB	103
Figure 4-4. Distribution of magnetic intensities at E.....	104
Figure 4-5. Magnetic ranges in magnetic profiles in one test.....	104
Figure 4-6. Positioning results at E (handheld)	106
Figure 4-7. Positioning results at E (dangling)	107
Figure 4-8. Position errors and corresponding CDF with different combinations of PDR and MM at E	109
Figure 4-9. Indoor test environment at B	111
Figure 4-10. Magnetic intensities on test trajectory at B	111
Figure 4-11. Positioning results at B (handheld)	112
Figure 4-12. Position errors and corresponding CDF with different combinations of PDR and MM at B (handheld).....	113
Figure 5-1. Flow chart of positioning phase of WiFi fingerprinting	119
Figure 5-2. Case 1 using single-point-based WiFi positioning.....	127
Figure 5-3. Case 2 using single-point-based WiFi positioning.....	127
Figure 5-4. Case 2 using profile-based WiFi positioning	128
Figure 5-5. Flow chart of profile-based WiFi fingerprinting.....	129
Figure 5-6. Flow chart of MD-DTW algorithm.....	132
Figure 5-7. Process of training and positioning for WiFi and magnetic matching.....	133
Figure 5-8. Using WiFi positioning results to limit search space for magnetic matching.....	133
Figure 5-9. Structure #1 for DR/WiFi/MM integration	135
Figure 5-10. Structure #2 for DR/WiFi/MM integration	135
Figure 5-11. Position uncertainties when using different levels of quality controls	137
Figure 5-12. Distribution of WiFi signals at E	138

Figure 5-13. AP localization results.....	139
Figure 5-14. Propagation-parameter determination results	139
Figure 5-15. Results of WiFi (point), WiFi (profile), and their fusion with DR, phoning	140
Figure 5-16. Results of WiFi (point), WiFi (profile), and their fusion with DR, pocket.....	141
Figure 5-17. Errors in WiFi (point) and WiFi (profile) results.....	142
Figure 5-18. Errors in DR/WiFi (point) and DR/WiFi (profile) results	143
Figure 5-19. Results of MM, MM (WiFi aided), and MM (DR/WiFi aided), phoning.....	145
Figure 5-20. Results of MM, MM (WiFi aided), and MM (DR/WiFi aided), pocket	146
Figure 5-21. Errors in MM, MM (WiFi aided), and MM (DR/WiFi aided) results <i>DR/WiFi/MM results</i>	147
Figure 5-22. Results of DR/WiFi/MM (WiFi aided) and DR/WiFi/MM (DR/WiFi aided), phoning	148
Figure 5-23. Results of DR/WiFi/MM (WiFi aided) and DR/WiFi/MM (DR/WiFi aided), pocket	148
Figure 5-24. Errors in DR/WiFi/MM (WiFi aided) and DR/WiFi/MM (DR/WiFi aided) results	149
Figure 5-25. CDF of position errors when using different strategies	150
Figure 5-26. RMS values of position errors under different motions.....	152
Figure 5-27. RSS distribution on test trajectory at B	153
Figure 5-28. Position results when using different strategies (handheld).....	154
Figure 5-29. Errors in results of WiFi (point) and WiFi (profile), and their integration with DR, handheld	155
Figure 5-30. Errors in results of MM, MM (WiFi aided), and MM (DR/WiFi aided), handheld	156
Figure 5-31. CDF of position errors when using different strategies	158
Figure 5-32. RMS values of position errors when using different technologies or combinations in two different environments	158

List of Abbreviations

Acronyms/Abbreviations	Definition
AKF	Adaptive Kalman Filter
AP	Access Point
BLE	Bluetooth Low Energy
CDF	Cumulative Distribution Function
COR	Cross-correlation
DB	Database
DOP	Dilution of Precision
DR	Dead Reckoning
DTW	Dynamic Time Warping
EKF	Extended Kalman Filter
FCC	Federal Communications Commission
GNSS	Global Navigation Satellite Systems
ICCP	Iterative Closest Contour Point
ICP	Iterated Closest Point
IGRF	International Geomagnetic Reference Field
INS	Inertial Navigation System
KF	Kalman Filter
KNN	K-Nearest Neighbour
LBS	Location Based Services
LED	Light-Emitting Diode
LMF	Local Magnetic Field
LS	Least Squares
MAD	Mean Absolute Difference
MD-DTW	Multi-Dimensional Dynamic Time Warping
MEMS	Micro-Electromechanical Systems

MMSE	Minimum Mean Square Error
MM	Magnetic Matching
MSD	Mean Square Difference
NED	North-East-Down
NHC	Non-Holonomic Constraints
PDR	Pedestrian Dead Reckoning
PF	Particle Filter
QSMF	Quasi-Static Magnetic Field
QSAU	Quasi-Static Attitude Updates
RF	Radio Frequency
RFID	Radio Frequency Identification
RP	Reference Point
RTLS	Real-Time Location Systems
RMS	Root Mean Square
RSS	Received Signal Strength
SLAM	Simultaneous Localization and Mapping
TERCOM	Terrain Contour Matching
UKF	Unscented Kalman Filters
UWB	Ultra Wideband Beacons
WGS	World Geodetic System
WiFi	Wireless Fidelity
WLAN	Wireless Local Area Networks
ZARU	Zero Angular Rate Update
ZUPT	Zero Velocity Update

CHAPTER 1: INTRODUCTION

1.1 Background and Problem Statement

1.1.1 Background

Mobile location based services (LBS) are attracting increasing public attention due to their potential applications in a wide range of personalized services from emergency responders to proximity-based mobile advertising and social networks ([Herrera et al., 2013](#), [Dos Santos et al., 2014](#)). Meanwhile, the popularization of consumer portable devices, such as smartphones, tablets, and the emerging wearable devices (e.g., smart glasses, watches, armbands, etc.), has stimulated the development of mobile LBS. In fact, the total LBS service revenues reached US\$ 1.8 billion in North America and € 735 million in the European Union in 2013, and will potentially grow to US \$ 3.8 billion in North America and €2.3 billion in Europe by 2018 ([BergInsight, 2014](#)). As a core technology of LBS, positioning and navigation (i.e., determination of the position, velocity, and attitude) of the mobile device is vital. Moreover, because most LBS users spend 70% - 90% of their time indoors ([Rahim, 2012](#)), there is a high demand is to provide trusted and real-time indoor navigation solutions ([Mokbel and Levandoski, 2009](#)).

During the last decade, especially the last five years, indoor pedestrian navigation has become a hot topic in both industrial and academic fields. To the best of our knowledge, there are currently over 150 companies involved in Real-Time Location Systems (RTLS), indoor mapping, indoor tracking, and other indoor pedestrian applications. These companies include not only startups that are paving innovation in this space, but also large companies such as Apple, Google, Qualcomm, Intel, Cisco, and Alibaba. Also, there are several well-known happenings in this field. To name a few, in March 2013, Apple spent \$20 million to acquire WiFiSlam, which used WiFi as well as

Micro-electromechanical Systems (MEMS) sensors to provide indoor positioning; in March 2014, Google released the development kits of Project Tango and set indoor mapping as a research point in for next decade; in July 2014, InvenSense spent \$81 million to acquire the outdoor/indoor motion solution providers Movea and Trusted Positioning; in September 2014, Baidu invested \$10 million to IndoorAtlas, which develops indoor navigation technology that uses magnetic features; in May 2015, General Electric jointed with Qualcomm and Apple to develop new Light-Emitting Diode (LED) light bulbs to transmit customized coupons to shoppers based on their location; also, China started the construction of “XIHE” Wide Area Network high precision indoor (3 m) and outdoor (1 m) positioning and navigation systems ([Deng et al., 2013](#)). Meanwhile, in the academic arena, there are many international conferences that opened sessions on the next-generation indoor pedestrian navigation techniques; also, there are numerous journal articles devoted to this topic.

There are various technologies for indoor positioning, including Wireless Local Area Net (WLAN, also known as WiFi), Bluetooth Low Energy (BLE), Radio Frequency Identification (RFID), ZigBee, Ultra Wideband Beacons (UWB), pseudolites, video cameras, LED modulation, magnetic, sound/ultrasound, sensor-based dead-reckoning (DR), etc. Based on our survey, Table 1-1 lists the typical companies that provide indoor positioning and navigation solutions, as well as the main technologies they utilize, their reported accuracy, and their main applications.

As shown in Table 1-1, technologies and positioning accuracy are significant dissimilar between solutions from different companies. Therefore, before discussing indoor positioning techniques, this thesis first clarifies the accuracy requirements of indoor positioning applications, as the requirements will drive the choice of technologies.

Table 1-1. Some companies that provide indoor positioning and navigation solutions

Company / product	Main Technology	Reported Accuracy	Main Application	Website
Skyhook	WiFi	99.8 % in 20 m	Urban or indoor	www.skyhookwireless.com/optimized-location
Ekahau	WiFi	3 m (mean)	Network Provider	www.ekahau.com/real-time-location-system/blog/2011/03/04/how-accurate-is-it-part-13/
Cisco	WiFi	50% 5 m; 90 % 10 m	Network Provider	www.cisco.com/en/US/docs/solutions/Enterprise/Mobility/emo30dg/Locatn.html
Guardly	WiFi	Room-level	Safety	www.guardly.com/technology/indoor-positioning-system
Wifarer	WiFi	3 m	Consumer devices	gigaom.com/2012/08/01/wifarers-mobile-app-doesnt-just-map-the-indoors-it-maps-the-objects-within/
Lighthouse Signal Systems	WiFi	5-7 m (sparse RF); 1-3 m (rich RF)	Malls	www.lighthousesignal.com/technology/
Iway	WiFi/GSM/3G/4G	1-5 m (mean)	Indoor services	www.iway.nl/en/index.php/purpose/
Ericsson	WiFi/LTE	97% in 50 m	Tracking	www.ericsson.com/research-blog/lte/indoor-positioning-in-lte/
Indoo.rs	WiFi/iBeacon	5 m	Consumer devices	indoo.rs
Insiteo	BLE/WiFi	2 m	Malls	www.insiteo.com/joomla/index.php/en/plateform
Meridian / Aruba	BLE /WiFi	1-3 m	Indoor navigation	meridianapps.com
SenionLab	WiFi/BLE	1 – 5 m	Consumer devices	senionlab.com/venues/system-integrators/
Sensewhere	WiFi/BLE	10 m	Mobile advertising	sensewhere.com
Estimote	iBeacon	1.5 – 4 m in tests	Navigation	blog.estimote.com/post/11829444205/super-simple-and-accurate-indoor-positioning-with-quuppa
Quuppa	BLE	1 m	Object-tracking	quuppa.com/technology/
Combain	Cell ID/WiFi	40 m	Urban areas	combain.com
9Solutions	BLE/RFID	1 m	Healthcare, safety	www.9solutions.com
InvisiTrack	LTE	3 m for each direction	Customer tracking	www.komindesign.com/oma/Invisitrack.pdf
Loctronix / TCS	GSM□	15 m	E 911	www.loctronix.com
NaciFloor	RFID	50 cm	Robot navigation	www.future-shape.com/en/technologies/32
Kimaldi	RFID	Meter-level	Hospital	www.kimaldi.com/kimaldi_eng
Trusted positioning / InvenSense	Sensors	4-8% of distance; 1% of distance (fixed)	Motion tracking and navigation	www.trustedpositioning.com
NavShoe	Sensors	0.3 % of distance	Foot-mounted	www.wpi.edu/Images/CMS/PPL/InterSense.pdf
aisle411	WiFi/Sensors	3-10 m	Malls, mapping	aisle411.com
CSR / Broadcom	WiFi/Sensors/BLE	50 % in 5 m	Malls	www.csr.com/products/sirfusion
Motorola Solutions	Sensor/RF/Map	Real-time < 7 m; Post-process < 4 m	Military/Emergency	www.motorolasolutions.com/content/dam/msi/docs/business/product_lines/apx/documents/mot_trx_neon_indoor_location_data_sheet.pdf
Qualcomm Atheros	WiFi/Sensor	3-5 m	Chipset	www.qualcomm.com/products/qualcomm-izat/
Pole Star	WiFi/BLE/Sensors	5 m (mean)	Airports	www.polestar.eu/en/
WiFiIslam / Apple	Wifi/Sensors	2.5 m	Consumer devices	angel.co/wifislam
BlinkSight	Special signal	< 10 cm	Chipset	www.blinksight.com
Broadcom	Special signal	Sub-meter	Chipset	www.broadcom.com/press/release.php?id=s836818
NextNav	Special Signal	50% 20 m; 90% 47 m	E911	www.nextnav.com/proven-performance
Nokia	Special Signal	0.3 m	Business	www.nokia.com/en_int
Nanotron	Specific signal	1 m	Mines	nanotron.com/EN/PR_find.php
Ubisense	UWB	15 cm	Business	ubisense.net/en
Zebra	UWB	Sub-meter	Logistics	www.zebra.com/content/dam/zebra/white-papers/en-us/uwb-architecture-en-us.pdf
My - Bodyguard	Zigbee	Zoom level	Tracking	www.x-guard.nl/download/EN/Products/My-Bodyguard-en.pdf
Locata	Pseudolites	Centimeter-level	Industrial-grade	www.locata.com/technology
Trimble	Pseudolites	cm-dm level	Mines	www.trimble.com/mining/Terralite-XPS-Solutions/Position-Infrastructure.aspx
Sonitor	Ultrasound	Subroom	Hospitals, mines	www.sonitor.com/products-sonitor-sense.html
Cricket	Ultrasound	1-2 cm	Smart tracking	cricket.csail.mit.edu
ByteLight / Acuity	LED	Sub-meter	Malls	www.bytelight.com
HW Communications	LED light	10 cm	Business	www.hwcomms.com/VLC
SkyTrax	Industrial Camera	2- 30 cm	Industrial vehicles	www.baxtek.com/products/skytrax/index.php
StarGazer	Industrial Camera	Centimeter-level	Robot localization	www.gbotic.com/index.php?dispatch=products.view&product_id=1173
AICON ProCam	Infrared Camera	0.1 mm	Industrial vehicles	aicon3d.com/products/moveinspect-technology/procam/
IndoorAtlas	Magnetic features	1 – 2 m	Consumer devices	www.indooratlas.com/static/magnetic_positioning_opus_jun2014.pdf

1.1.2 Accuracy Requirements for indoor positioning

Figure 1-1 demonstrates the accuracy requirements for various indoor applications ([Mautz, 2012](#)). According to Table 1-1 and Figure 1-1, indoor positioning and navigation applications can be generally divided into two classes: professional applications and mass-market applications. These classes are highlighted respectively by the blue-dash and red-solid circles in Figure 1-1. Furthermore, Table 1-2 illustrates some characteristics of the professional and mass-market applications.

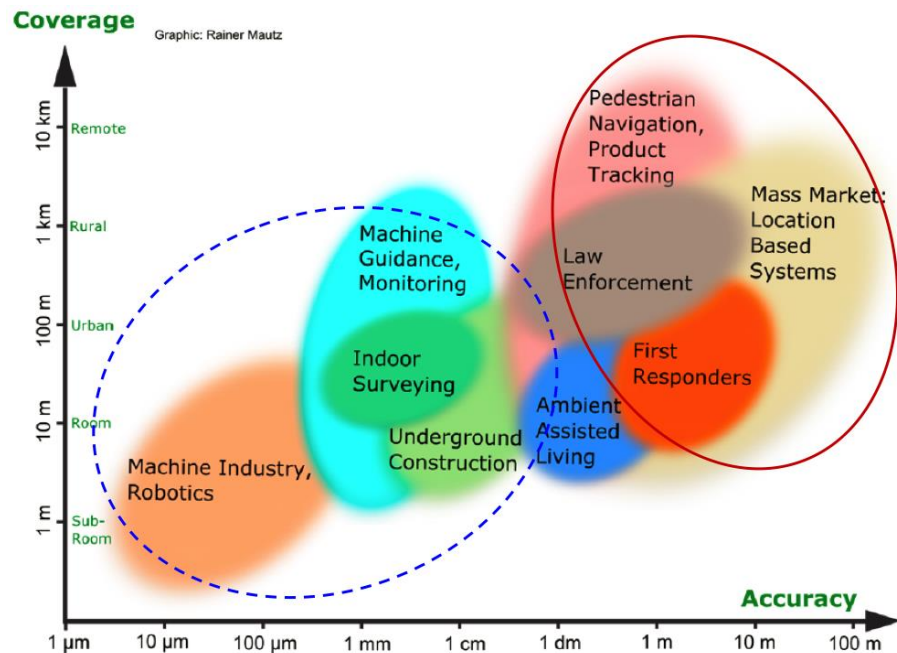


Figure 1-1. Accuracy requirements for indoor positioning (modified on ([Mautz, 2012](#)))

For any navigation application, there is a trade-off between performance and cost. Professional applications (e.g., machine industry and underground construction) commonly require high navigation accuracy and thus need specific devices or networks, and specific manpower. Furthermore, some applications (e.g., robots and automatic vehicles) may also need IntelliSense techniques to sense the environment. On the other hand, many mass-market applications do not

need high navigation accuracy because meter-level accuracy is already within the users' sensing range. However, these applications are usually not affordable for specific devices or manpower which may cost many times more than the services themselves.

Table 1-2. Comparison of professional and mass-market indoor positioning applications

	Professional applications	Mass-market applications
Features	Requires high accuracy; May require IntelliSense; Can use specific devices and networks	Needs medium or less accuracy; Do not need IntelliSense; Not affordable for specific devices or networks.
Accuracy Requirement	Micrometer-level to decimeter-level	Meter-level
Mainstream technologies	Cameras, special signals, pseudolites, UWB, ultrasound, RFID, etc.	WiFi; BLE, sensors, magnetic, Zigbee, RFID, cellular network, etc.

The main application scenarios for this research are the mass-market mobile LBS applications. Therefore, this research only uses the sensors and technologies that are available on consumer portable devices, such as inertial sensors (i.e., gyros and accelerometers), magnetometers, and WiFi. BLE can be used in a similar way to WiFi (either fingerprinting or trilateration); therefore, the utilization of BLE is not discussed in this thesis (sometimes BLE is also used as a landmark to provide position updates, which is straightforward). Although most smartphones are equipped with digital cameras, this thesis does not research vision-based navigation. Besides, this thesis only uses indoor maps to display the navigation results, instead of using maps to constrain the navigation solution.

In January 2015, the Federal Communications Commission (FCC) in the United States has adopted a new standard for the positioning accuracy of E911 services ([Federal Communications](#),

[2015](#)). This new standard requires a 50-meter accuracy for 67 percent of indoor 911 calls within two years, and a 50-meter accuracy for 80 percent of indoor 911 calls within five years. However, for most mass-market applications, it remains difficult to find such a standard because there are numerous specific applications. An accepted classification is that 1-5 m is high accuracy, 6-10 m is medium accuracy, and over 11 m is low accuracy ([Dodge, 2015](#)).

Although a medium accuracy (assuming 6-10 m is the absolute position error, the RMS of errors is 3-5 m) is already acceptable for many mobile LBS applications, to achieve such accuracy indoors with consumer portable devices remains challenging. Specifically, these challenges include low performance of sensors and complexity and unpredictability of indoor environments, as described in the next subsection. The existence of these challenges has limited the achievable accuracy of navigation.

The rest of this chapter first addresses the challenges for indoor pedestrian navigation, followed by a review of the current indoor positioning and navigation approaches, including wireless positioning, DR, and matching techniques, and the hybrid navigation methods. Then, the research objective and innovation points of this research are illustrated. Finally, the thesis structure is outlined.

1.1.3 Challenges for indoor positioning and navigation

While GNSS-based outdoor navigation has achieved great advances over the past decades, positioning and navigation in indoor scenarios and deep urban areas remains an open issue ([Li et al., 2013](#)). Examples of the challenges are:

- The unavailability or degradation of GNSS signals in deep indoor areas ([He, 2013](#)).

- The complexity of environments for wireless signals, such as Non-Line-of-Sight (NLoS) conditions ([Xiao et al., 2015](#)), reflections ([Torres-Solis et al., 2010](#)), and multipath effects ([Bose and Foh, 2007](#)), and even the existence of human bodies ([Schmitt et al., 2014](#)).
- The necessity of using low-grade devices. For example, the errors in the MEMS sensors in consumer devices are several magnitudes higher than those in the traditional sensors. Furthermore, MEMS sensor errors change over time and are significantly dependent on environmental factors such as temperature ([Niu et al., 2013](#)).
- Frequent and severe magnetic disturbance, which is a critical issue when using magnetometers as a compass indoors ([Afzal, 2011](#)).
- The variety and unpredictability of pedestrian motions, such as frequent changes of speed and direction ([Morrison et al., 2012](#)). Moreover, such motions cannot be constrained to predefined paths ([Saeedi, 2013](#)).

The following subsection reviews the current indoor navigation methods, and illustrates why the above issues are difficult to solve. After this, the objective of this research is outlined.

1.2 Literature Review

Based on the mathematical methods used, the current navigation approaches can be classified into three categories: absolute positioning (commonly based on wireless signals), dead-reckoning (DR, mainly based on motion sensors), and database (DB) matching. The typical cases for these categories are GNSS, inertial navigation systems (INS), and map matching, respectively. Based on this classification method, wireless-based trilateration is an absolute positioning approach, while wireless-based fingerprinting is a DB matching approach. This may cause inconvenience when a reader is specially focusing on the wireless positioning technologies. Therefore, this thesis

classifies the positioning and navigation technologies into the following categories: wireless positioning, sensor-based DR, and matching techniques.

1.2.1 Wireless positioning

There are various technologies for indoor environments, such as High-sensitivity GNSS ([He, 2013](#)), RFID ([Ruiz et al., 2012](#)), ZigBee ([Goncalo and Helena, 2009](#)), UWB ([Zampella et al., 2012](#)), and pseudolites ([Barnes et al., 2007](#)). These technologies can provide long-term accurate positions, but require special receivers and the creation and maintenance of a network ([Fallah et al., 2013](#)), which limit their applications on consumer devices. As IEEE 802.11 WiFi chips become ubiquitous, positioning in public buildings with existing WiFi infrastructures becomes feasible ([Talvitie et al., 2015](#)). The common wireless positioning approaches include fingerprinting ([Laoudias et al., 2013a](#), [Lin et al., 2014](#)), trilateration ([Uri Schatzberg, 2014](#)), and their combination ([Kodippili and Dias, 2010](#)). Fingerprinting is commonly achieved by finding the closest match between the features of the received radio signals (RSS) and those stored in the DB (i.e., radio map), while trilateration is a method of determining the relative positions of objects using the geometry of triangles. Fingerprinting can also provide a coarse estimation of orientation ([Xiang et al., 2004](#), [Bahl and Padmanabhan, 2000](#)) based on the fact that the human body affects the propagation of radio signals, which leads to the different fingerprints when the device is placed towards different orientations. Fingerprinting is the most widely used WiFi algorithm in both industrial and academic fields because it can provide position without any knowledge of the access point (AP) location or signal-propagation model. On the other hand, trilateration has its own advantages, such as smaller size of DB, the capability of positioning in the areas beyond the DB, and the feasibility to obtain real-time accuracy of the positioning results through the covariance matrix in the least-square (LS) method. There is literature compares the fingerprinting and

trilateration algorithm, such as ([Zhuang, 2015](#)) and ([Mok and Retscher, 2007](#)). Both fingerprinting and trilateration consist of two phases (steps): off-line pre-survey and on-line positioning. For fingerprinting, the training phase is conducted to build or update a <RSS, location> DB that consists of a set of reference points (RPs) with known coordinates and the RSS from available WiFi APs, while the positioning step is implemented to find the closest match between the features of the measured RSS and those stored in the DB. Although trilateration can be implemented with known AP locations, a pre-survey process is needed to determine the signal-propagation parameters of every specific AP to improve the positioning accuracy.

A key to WiFi fingerprinting is the generation of DB, while the key to generate a DB is obtaining RP coordinates, which is a trade-off between cost and accuracy. Different WiFi DB-training approaches have been researched due to various requirements. The first approach is to survey at every RP and record their fingerprints. This point-by-point method is accurate, and can also improve DB reliability by averaging the RSS at each RP [30] and even provide a coarse estimate of orientation [20, 31]. However, it is time- and labor-consuming when dense RPs are selected to cover an entire area of interest, and a surveyor needs to mark the position of all RPs (labels) manually [32]. The training phase can take up to several hours even for a small building [33]. To minimize the number of labels needed for training, the walk-survey approach is used based on landmarks (i.e., points with known coordinates) or floor plans (i.e., the true position of corners and intersections, and the true orientation of corridors), and constant-speed assumption [24]. The walk-survey approach is significantly more time-effective than measuring the position of all RPs on the digital map; however, it still requires numerous walk trajectories, so as to take average of the RP positions on various trajectories to obtain the estimated RP positions which is close to the true values. The research ([Zhuang, 2015](#)) indicates that more trajectories lead to better accuracy.

There is also literature on the removal of the training process by updating the WiFi DB automatically while navigating based on sensors. WiFi Simultaneous Location and Mapping (SLAM) is an example of such algorithms [34]. The limitation of the SLAM algorithm is that the computational cost increased when the scenarios become larger [35]. There are other approaches based on crowdsourcing. The research [36] estimates the location of WiFi APs or other radio beacons using pedestrian dead-reckoning with high-quality foot-mounted IMUs, while [37, 38] propose similar systems or approaches using handheld smartphones. Based on this idea, it is possible for mobile users to collect WiFi fingerprints automatically in daily life by conducting sensor-based navigation. The key to crowdsourcing is a reliable sensor-based navigation, this is challenging in indoor areas due to the complexity of environments and pedestrian motions. Therefore, this research uses MEMS sensors in consumer portable devices and indoor magnetic features to provide an autonomous navigation solution, which can be potentially used for WiFi crowdsourcing.

The purpose for training the trilateration DB is to obtain AP locations and PPs. The research from PlaceLab ([Cheng et al., 2005](#)) and Skyhook ([Skyhook, 2014](#)) reflect the idea of determining AP locations through a “war-driving” method. However, large estimation errors can result from measurement points with poor geometrical distribution ([Zhuang, 2015](#), [Yu et al., 2012a](#)). The research in ([Yu et al., 2012a](#)) estimates the path loss exponent and a constant parameter of the propagation model through rigorous testing, and then uses a LS method to estimate AP locations. The challenge for this method is that the pre-surveyed parameters are not suitable for the estimation of AP locations when the environment has changed. A method proposed in ([Han et al., 2009](#)) improves the accuracy of the AP location survey by using gradient information derived from RSS variations. Besides the large computation load, another drawback of this algorithm is that the gradient

information derived from RSS variations is not reliable in indoor environments. With MEMS sensors in smartphones, the research ([Zhuang, 2015](#)) presents a crowdsourcing-based system, which estimates AP locations and PPs simultaneously by using a nonlinear iterative LS method for the dynamic environments. In this case, the accuracy of crowdsourcing also depends on the reliability of the sensor-based navigation solution.

The challenges for reaching high WiFi accuracy can be stated as follows: (a) as an absolute positioning system, the performance of wireless positioning systems depends on signal availability and geometry ([Cheng et al., 2013](#)): weak geometry may lead to ambiguity problems ([Zhuang et al., 2015c](#)). (b) RSS fluctuate due to NLoS conditions ([Xiao et al., 2015](#)), reflections ([Torres-Solis et al., 2010](#)), multipath effects ([Bose and Foh, 2007](#)), and even the existence of human bodies ([Schmitt et al., 2014](#)). Additionally, (c) WiFi DBs can be time-variant due to radio signal propagation effects induced by dynamic aspects of the environment such as the presence or absence of people, elevators, moving doors and other environmental changes ([Kushki et al., 2007](#), [Ni et al., 2004](#)).

The effect of (a) may be mitigated by adding access points (APs) at proper places or selecting important APs for positioning ([Fang and Lin, 2010](#)); the consequence of (b) can be alleviated by using enhanced models that considers multipath effects ([Bose and Foh, 2007](#)) or Rayleigh fading effects ([Akyildiz et al., 2009](#)); and the effect of (c) can be mitigated through periodical DB training. However, it is not always affordable to modify the distribution of APs or to investigate on the navigation environment in advance in public places; moreover, most current DB-training methods are tedious and labor-intensive ([Kannan et al., 2013](#)). Furthermore, there are some practical issues when using WiFi for positioning, for example, WiFi chips in smartphones are commonly low-cost and have large signal diversity ([Laoudias et al., 2013b](#)). Moreover, smartphones commonly have

low WiFi update rates (e.g., nearly 0.3 Hz for the tested Samsung Galaxy S3, S4 and Xiaomi 4 smartphones, and 1 Hz for the tested Google Nexus 7 tablet when we used the class “WifiManager” in Android to collect data). Such low update rate may lead to position errors when other techniques (e.g., inertial navigation) are not available, because the history positions are needed for smoothing the RSS and detecting blunders.

In general, most of the above challenges are introduced by navigation environments, instead of the positioning technique itself. To mitigate the effect of these issues, it is preferred to design a self-contained navigation algorithm to bridge short-term WiFi outages and provide continuous navigation results, and to provide smoother and more reliable results when integrating with WiFi. This is one of the main objectives of this research.

1.2.2 Sensor-based DR

Advances in Micro-Electro-Mechanical Systems (MEMS) technology combined with the miniaturization of electronics have made it possible to produce chip-based sensors, such as inertial sensors and magnetometers. MEMS chips are small and lightweight, consume little power, and are extremely low-cost ([El-Sheimy and Niu, 2007](#)). By virtue of these advantages, MEMS sensors have become appropriate candidates for motion tracking and navigation applications. For consumer portable devices, pedestrian dead-reckoning (PDR) is usually the navigation algorithm used to navigate with inertial sensors; thus, inertial sensors are not dependent on the transmission or reception of signals from an external source. Such self-contained MEMS-based sensors are ideal for providing continuous information in indoor/outdoor environments. The shortcoming is that inertial sensors provide only short-term accuracy and suffer from accuracy degradation over time due to the existence of sensor errors ([Titterton and Weston, 2004](#)). In-lab calibration at a room temperature is a useful way to remove many deterministic sensor errors. However, low-cost

MEMS inertial sensors in consumer devices suffer from significant run-to-run biases and thermal drifts ([Niu et al., 2013](#)); thus, the sensors' readings can be very different due to the restart and the difference between the operational and calibration environments. Moreover, it is difficult to compensate for the thermal drifts of MEMS sensor errors. First, it is not affordable for the chip manufacturers to conduct thermal calibration for such low-cost sensors. Second, the research in ([Niu et al., 2013](#)) indicates that MEMS sensor errors can have significant inconsistent curves under different temperature changing profiles, and the real-world temperature changes are complex and unpredictable. Due to the integration process in the inertial navigation mechanization, residual sensor errors will accumulate and lead to attitude errors, and in turn cause position errors. Although the horizontal attitude (i.e., roll and pitch) errors can be bounded by accelerometers ([Lee et al., 2012](#)), the heading error will grow when external updates are not available ([Akeila et al., 2014](#)).

Magnetometers can provide an absolute heading through leveling using accelerometers, magnetic heading calculation, and true heading computation ([Zhang et al., 2013](#)). However, this approach is developed based on the assumption that the local magnetic field (LMF) is simply the geomagnetic field and thus the value of the declination angle can be obtained from the International Geomagnetic Reference Field (IGRF) model ([Chambodut, 2011](#)). When analyzing preliminary results, it was found that the majority of outdoor tests met this assumption; however, the local magnetic field was susceptible to magnetic interferences from man-made infrastructures in indoor environments. Therefore, the existence of magnetic interferences is a critical issue when using magnetometers as a compass indoors.

Scholars have presented several approaches to improve the robustness of the magnetometer-derived heading, for example, using the gyro-derived heading to detect severe magnetic disturbances ([Ladetto et al., 2001](#)), using the magnetometer signals during quasi-static magnetic

periods to provide relative heading changes and calibrate gyros ([Li et al., 2015a](#)), and using magnetometer calibration methods to allow the magnetometer measurements to be consistent with the LMF ([Zhang and Yang, 2014](#)). These approaches can be effective to enhance the DR solution; however, they still need external absolute positioning techniques to integrate with DR and obtain navigation results with long-term accuracy.

Besides, there are vision-based solutions which use camera(s) as a visual gyro ([Ruotsalainen et al., 2013](#)) or a visual odometer ([Qian et al., 2014](#), [Jirawimut et al., 2003](#)). Nevertheless, vision-based technology is sensitive to environmental light conditions and are not scalable because of the computational workload incurred when several targets have to be tracked at the same time ([Colombo et al., 2014](#)). Another challenge is the camera has to be pointed in the appropriate direction, which is not always achieved during the navigation process ([Groves, 2014](#)).

There is also research which has contributed to the enhancement of the DR solution from the algorithm perspective, instead of adding extra hardware. Such software-based approaches are more appropriate for low-cost navigation using consumer devices because they are cost-effective. Examples of these methods include enhancing the quality of sensor data through stochastic modeling ([Georgy et al., 2010](#)) and de-noising ([Nassar and El-Sheemy, 2005](#)); introducing a priori information such as control inputs, vehicle dynamic models, kinematic constraints and the road information ([Skog and Handel, 2009](#)). The approach with a priori information has been used in airborne ([Bryson and Sukkarieh, 2004](#), [Bouadi et al., 2007](#)), land ([Niu et al., 2010](#), [Dissanayake et al., 2001](#), [Shin, 2005b](#)) and submarine ([Hegrenæs and Hallingstad, 2011](#), [Miller et al., 2010](#)) applications. In land-based cases, the so-called Non-Holonomic Constraints (NHC) can improve the heading accuracy significantly when the vehicle moves with enough speed ([Niu et al., 2007a](#), [Dissanayake et al., 2001](#)). The Zero Integrate Heading Rate(ZIHR, also known as Zero Angular

Rate Updates, ZARU) regards the attitudes (especially the heading) change between two epochs should be zero when the vehicle stops ([Shin, 2005b](#)). ZIHR can mitigate the heading drift effectively through updating the vertical gyro bias. When the vehicle moves with little maneuver and with low/zero speed, a steering constraint can be utilized ([Niu et al., 2010](#)). Such constraint stands for the fact that most land vehicles have bounded turning rate under certain speed because of their minimum steering radii. There are also papers use the fact that both the horizontal gyros and the vertical accelerometer provide less important navigation information ([Wu et al., 2010](#), [Niu et al., 2007b](#)). Based on this fact, the former replaces the less important sensor output by constant signals plus noises and thus proposes a universal approach for processing any MEMS inertial sensor configurations for land-based navigation, while the latter directly uses the fact that the roll and the pitch are zeroes as constraints.

In pedestrian navigation cases, the most common a priori information is ZUPT and ZIHR ([Foxlin, 2005](#), [Susi, 2012](#), [Rantakokko et al., 2011](#)). ZUPT is based on the assumption that the device on foot is briefly stationary when the foot is on the ground, while ZIHR can be active when the user stops and there is no heading change. Also, scholars have excavated other a priori information. For example, the kinetic model of human motions (the most typical one is the gait) model can be used as a virtual velocity sensor. To be specific, a step-length model ([Uri Schatzberg, 2014](#)) or a velocity model ([Davidson and Takala, 2013](#)) is used as an update for PDR. Moreover, there are other solutions, such as analyzing the accelerometer and gyro outputs to provide a direction information ([Kourogi et al., 2010](#)), using the floor plan and the assumption of most of the user's movements are constrained to one of four possible directions ([Abdulrahim et al., 2010](#)), etc. Generally speaking, these updates can improve the system when used properly (i.e., when the practical navigation condition meets the assumptions). ZUPT and ZIHR are reliable when the

inertial measurement unit (IMU) is mounted on foot because there are reliable quasi-static periods; however, when the device is not fixed (i.e., mounted on foot or on the body, hold stably in hand, etc.), both updates will contribute less to, or even destroy the navigation algorithm under extreme conditions. The extent of their contribution and the risk depends on actual human motion and the setting of the algorithm parameters (e.g., parameters in the R matrix). Also, the human motion models need to be trained before use ([Hoseini-Tabatabaei et al., 2013](#)). The motion parameters are different from person to person, and can be different with various device locations or attitudes. Furthermore, motion models may be influenced by navigation environment. For instance, the step-length model is susceptible to the ramps on the ground.

1.2.3 Matching techniques

There are various matching approaches for pedestrian navigation applications, such as the methods using floor plans to ensure that the position estimation do not pass through walls ([Klepal and Beauregard, 2008](#)), using map-based angular probability density functions ([Kaiser et al., 2013](#)), using a vision-based technology and a DB to offer the absolute position ([Turcot and Lowe, 2009](#)), using shadows from the buildings ([Wang et al., 2013](#)), using landmark matching ([Dawadee et al., 2013, Riseman et al., 2013](#)), using light matching ([Jiménez et al., 2013](#)), using magnetic matching (MM) ([Xie et al., 2014, Zhang et al., 2014](#)), and using ramp model matching ([Jiménez et al., 2011](#)). Also, there are other matching solutions utilizing the user activities such as going up the stairs and turning around a corner ([S. Jeon, 2014](#)). Although conventional outdoor map matching algorithm is straightforward as the position is projected to the nearest path, it is hard to use it for indoor map matching without any change, since many commercial GNSS receivers provide better accuracy than indoor positioning technologies such as Wi-Fi. Besides, to distinguish the indoor obstacles such as machines, walls, corridors, open areas and metals, more accurate map resolution is required

indoor than outdoor. Other technologies, i.e., shadow matching, light matching, activity matching, etc., work in limited environments, and thus can only be used selectively to improve the navigation. Although the magnetic field is omnipresent, the performance of MM is highly dependent on the LMF ([Pritt, 2014](#), [Li et al., 2015b](#)): MM solutions may be accurate in some areas but suffered from mismatches (e.g., matching to a point that is over 20 m away from the true value) in other areas.

Matching techniques have been widely used in high-end navigation applications such as military terrain ([Golden, 1980](#)), gravity ([Yan and Cui, 2007](#)), and magnetic referenced navigation systems ([Liu et al., 2007](#)); also, there are well-developed profile-matching approaches such as terrain contour matching (TERCOM) ([Golden, 1980](#)) and iterative closest contour point (ICCP) ([Yan and Cui, 2007](#)). The basic idea of profile-matching is to save a profile (i.e., a sequence of observations) in the memory and then compared it with the candidate profiles stored in a DB ([Golden, 1980](#)). To obtain the optimal match, the profile length should be long enough to show the profile feature; moreover, it is preferred that the length of the measured profile is the same as that of the candidate profiles. Thus, traditional profile-matching vehicles (e.g., cruise missiles and submarines) are equipped with a high-end INS, and utilize constraints, such as NHC ([Yu et al., 2012b](#)) and ZUPT ([Bloch et al., 2005](#)), to correct DR solutions and obtain accurate short-term trajectories. However, in indoor pedestrian navigation applications, sensors are low-end and there is no effective constraint when the device is not fixed on the body (e.g., on-foot or in-belt). Thus, the sensor-based navigation errors may accumulate quickly, which makes it difficult to measure the accurate moving distance.

Therefore, DB matching is commonly an optional navigation technique, which can provide accurate update information on certain occasions but cannot work under all scenarios. Considering

the popularization of MEMS sensors and the omnipresence of magnetic field, this thesis combines sensor-based DR and MM to obtain a self-contained navigation solution.

1.2.4 Hybrid navigation

As a summary of previous subsections, Table 1-3 lists some limitations for WiFi positioning, DR, and DB matching. All the existing technologies have their advantages and limitations ([Khaleghi et al., 2013](#)). Therefore, it is commonly challenging to provide a low-cost and high-performance navigation solution by using a stand-alone technology. Considering the complementary characteristics of different technologies, their combination is a key factor of success for reliable, continuous and accurate outdoor/indoor seamless navigation.

Table 1-3. Limitations for indoor navigation technologies

Technology	Limitations
Wireless positioning	Dependency on signal availability and geometry (Cheng et al., 2013); RSS fluctuations due to NLoS conditions (Xiao et al., 2015), reflections (Torres-Solis et al., 2010), and multipath effects (Bose and Foh, 2007), and even the existence of human bodies (Schmitt et al., 2014); Time-variant nature of radio map (Bahl and Padmanabhan, 2000 , Kushki et al., 2007 , Ni et al., 2004).
Dead-reckoning	Significant sensor errors, especially run-to-run biases and thermal drifts (Niu et al., 2013); Variety and unpredictability of pedestrian motions, such as frequent changes of speed and direction (Morrison et al., 2012); Frequent and severe magnetic disturbance (Afzal, 2011).
DB Matching	Performance depends on operating environment (i.e., Work in limited environments).

“Multi-sensor fusion deals with the combination of complementary and sometimes competing sensor data into a reliable estimate of the environment to achieve a sum which is better than the parts” ([Hackett and Shah, 1990](#)). Over the last few years, scholars from different institution developed pedestrian navigation platforms ([Kannan et al., 2013](#), [Morrison et al., 2012](#), [Rantakokko et al., 2011](#), [Chen et al., 2011](#), [Monteserin, 2014](#), [Grejner-Brzezinska et al., 2012](#), [S. Jeon, 2014](#), [Leppäkoski et al., 2013](#), [Colombo et al., 2014](#)). A common view in most of research systems is that the information from the inertial sensors can be used to build the system model and provide a short-term prediction, while other technologies provide the update information. On the other hand, in industry, most of the current indoor solutions focus on wireless technologies including Wi-Fi, BLE, etc., while only two companies in Table 2 focus on the independent use of sensors. This phenomenon is mainly caused by the difficulties of using DR for indoor pedestrian applications. However, due to the self-contained characteristics of inertial sensors and their popularization, it is worthwhile to make effort to utilize them.

DR and MM are technologies that are available by using off-the-shelf sensors in consumer devices. There is literature that focuses on enhancing navigation results through better fusion of inertial sensors and magnetometers. For example, the research ([Ladetto et al., 2001](#)) utilizes the gyro-derived heading to detect and remove severe magnetic disturbances, and the research ([Li et al., 2015a](#)) use the magnetometer measurements during quasi-static magnetic field periods to calibrate gyros. These approaches are effective on improving the robustness of using magnetometers indoors, but still suffer from the issue inherent in DR – the drift of position. To provide long-term accuracy, a common way is to integrate DR with WiFi. Different estimation techniques, such as Kalman filter (KF) ([Tian et al., 2015](#)) and particle filter (PF) ([Evennou and Marx, 2006](#)), have been used for the fusion. The majority of literature integrates MEMS sensors

with RSS through a loosely-coupled way ([Tian et al., 2015](#)), while others apply a tightly-coupled approach ([Ruiz et al., 2012](#)). Compared with WiFi and sensor-based navigation, the research of indoor MM started later, and most of related works use MM by itself ([Li et al., 2012a](#)) or integrate it with DR ([Xie et al., 2014](#)). Other than DR, the research ([Ezani et al., 2014](#)) and ([Shu et al.](#)) integrate WiFi with MM for indoor pedestrian navigation. The former uses a region-point indoor localization approach via RSS-magnetic fingerprinting, while the latter applies a two-pass particle filter to fuse magnetic and WiFi signals. Besides, the literature ([Pritt, 2014](#)) compares the region-point indoor localization approach and the approach that regards the magnetic intensity and inclination as pseudo WiFi APs.

For the integration of DR, WiFi, and MM, there are relatively less publications. The literature ([Ban et al., 2015](#)) uses a KF to fuse the information from different sensors, while the research ([Mirowski et al., 2013](#)) utilizes a bundle adjustment approach to implement SLAM. The hybrid navigation structure behind these works is to feed all sensor data into a fusion module. Furthermore, scholars have noticed that MM results have small fluctuations ([Ezani et al., 2014](#)), but have a risk of mismatching due to low magnetic fingerprint dimension ([Li et al., 2012a](#)); in contrast, WiFi results have a low mismatch rate but suffer from larger fluctuations ([Pritt, 2014](#)). Therefore, there is a potential to use WiFi for a rough positioning, and then use MM for a more precise localization ([Ezani et al., 2014](#)). For example, WiFi can be used to determine the region where the target device resides while MM narrows down further to determine the location of the device. Based on this WiFi/MM strategy, an improved structure is developed, in which WiFi results are used to limit the MM search space to reduce both mismatch rate and computational load. After this, both WiFi and MM (WiFi aided) results are utilized as updates to integrate with DR. Tests in this research supported that by using WiFi solutions to limit the search space, MM errors were reduced

significantly. However, although MM (WiFi-aided) could provide better results than either the independent use of WiFi or MM, it still suffered from mismatches. The main reason for this outcome is that WiFi results suffer from fluctuations, which is the issue inherent in any approach based on RSS. Therefore, another improved structure is presented to further improve the reliability of hybrid PDR/WiFi/MM navigation. The improved structure is more effective on detecting MM mismatches, especially in areas with limited WiFi RSS or weak RSS distribution.

1.3 Research Objective

The main objective of this research is to develop a reliable indoor pedestrian navigation algorithm platform with off-the-self sensors in consumer portable devices. For mass-market applications, user experience and reliability are even more important than the navigation accuracy. Therefore, the positioning results should be continuous and not have any “jump point”, as well as have acceptable accuracy. As described before, if the RMS of position errors is 3-5 m (nearly room-level), the navigation accuracy will be enough for many public applications because the position error is within the users’ sensing range. Therefore, compared with accuracy, this research makes more efforts to improve the robustness of the navigation solution. In general, the proposed algorithm platform can achieve the following performance:

- Devices: the algorithm only needed consumer devices and existing WiFi infrastructures in public buildings;
- Availability: the algorithm can provide a ubiquitous navigation solution indoors/outdoors (outdoor navigation is not researched because it is well-developed by using GNSS);
- Reliability: the navigation solution does not have failure or jump point;
- Accuracy: the RMS value of position errors reaches 3 - 5 m;
- Expandability: combining the algorithm with other technologies is straightforward;

- Real-time: the algorithm can run on consumer devices without any time delay.

Furthermore, by taking better advantage of the merits of DR, WiFi, and MM, the proposed algorithm has the following features:

- 1) The algorithm can significantly improve the attitude-determination and DR results with commercial-grade MEMS gyros (typically have biases of up to several deg/s) without the need for any external calibration equipment or user intervention.
- 2) The algorithm can provide reliable and continuous indoor navigation results when external positioning technologies (e.g., WiFi and BLE) are not available; also, it can achieve optimal system performance when an external technology is available.
- 3) The algorithm can reduce dependency on navigation environments. For example, the algorithm works in indoor environments that have weak WiFi signal distribution, or in environments with frequent magnetic interferences.
- 4) The algorithm can reduce dependency on device motion conditions. Specifically, the algorithm can work under natural motion conditions such as handheld, phoning (i.e., close to the ear), dangling (i.e., walking with phone in hand), and in pants pockets.

Due to the above advantages, there are various potential applications for the outcomes of this research, for example:

- Mobile LBS that use consumer portable devices;
- Indoor photogrammetry and mapping;
- Crowdsourcing of WiFi/magnetic DBs by using daily-life data from users;
- To augment smartphone-based GNSS positioning (e.g., precise point positioning);
- Integration with other available technologies (e.g., BLE, LED, and map matching).

1.4 Innovation Points

Compared with previous hybrid navigation algorithms, the main innovation points of this research are:

- 1) This research presents a real-time calibration method for gyro sensors in consumer portable devices. The calibration happens automatically without the need for external equipment or user intervention. Multi-level constraints (i.e., the pseudo-observations, the accelerometer and magnetometer measurements, the norm vector of the accelerometer and magnetometer measurements, and the quasi-static attitude updates) are used to ensure the method is reliable and accurate under natural user motions. This method provided promising calibration results, even under challenging motion modes such as dangling and pocket, and in challenging indoor environments with frequent magnetic interferences.
- 2) This research proposes an autonomous navigation algorithm for challenging indoor environments that do not have any WiFi signal or have WiFi signals with a weak distribution. This algorithm integrates DR and MM, and uses several approaches to improve the DR and MM performance. Furthermore, realizing that the key to enhancing the DR/MM performance is to mitigate the impact of MM mismatches, this research introduces and evaluates two mismatch-detection approaches, including a threshold-based method that sets the measurement noises of MM positions based on their distances to the historical DR/MM position solutions, and an adaptive Kalman filter (AKF) based method that introduces the estimation of the innovation sequence covariance into the calculation of the KF gain matrix.
- 3) This research presents a profile-based WiFi fingerprinting algorithm by using the short-term trajectories from DR and geometrical relationships of various RPs in the space. The Multi-Dimensional Dynamic Time Warping (MD-DTW) algorithm is introduced to match with

inaccurate profile length for such a multi-dimensional system. The use of the profile-based approach can reduce the probability of mismatches. Furthermore, the profile-based approach is especially useful to provide a more accurate initialization for position as soon as a user starts navigating.

- 4) This research proposes a WiFi-aided MM algorithm, which uses the WiFi results to limit the MM search space to reduce both the mismatch rate and computational load. The complementary characteristics of WiFi and MM are especially useful for improving the navigation applications that use consumer devices not equipped with gyros (e.g., many medium- and low-end smartphones contain accelerometers and magnetometers but do not have gyros). Furthermore, when aided by WiFi (or DR/WiFi) to remove mismatches, MM results can be used as reliable updates in the position-tracking KF.
- 5) This research provides designs for and evaluates two hybrid integration structures that uses off-the-shelf sensors in consumer portable devices and existing WiFi infrastructures. Structure #1 utilizes the WiFi-aided MM algorithm, while Structure #2 uses both DR and WiFi results (i.e., the integrated DR/WiFi solutions) to limit the MM search space. Furthermore, a multi-level quality control mechanism is designed based on the interaction between different techniques and utilized in Structure #2. This mechanism has at least one more level than those in previous DR/WiFi/MM structures. Therefore, Structure #2 is more effective than previous structures at detecting MM mismatches, even in areas with limited WiFi RSS or weak RSS distribution. This structure reduced dependency on both navigation environments and motion condition. It provided consistent positioning accuracy in indoor environments with frequent magnetic interferences, and under different motion conditions.

1.5 Thesis Outline

The balance of this thesis is organized as follows.

Chapter 2 covers the necessary fundamental knowledge for multi-sensor navigation, including that of each separate technology, and the information-fusion technique.

Chapter 3 focuses on improving sensor-based DR, and answers the question:

- *How can we mitigate the significant gyro biases in real time without any equipment or user intervention, so as to improve the attitude and position results from DR under natural phone motion conditions?*

Chapter 4 provides an autonomous navigation solution with DR and local magnetic features. It provides a solution for the issue:

- *How can we obtain long-term navigation accuracy in indoor areas that do not have WiFi signals or only have WiFi signals with a weak distribution?*

Chapter 5 is on the DR/WiFi/MM integration level, and answers the question:

- *How can we achieve optimal system performance when an external absolute positioning technique (e.g., WiFi) is available?*

Chapter 6 discusses the conclusions and recommends future works based on this research.

Figure 1-2 shows the outline of the thesis and the detailed issues corresponding to each topic.

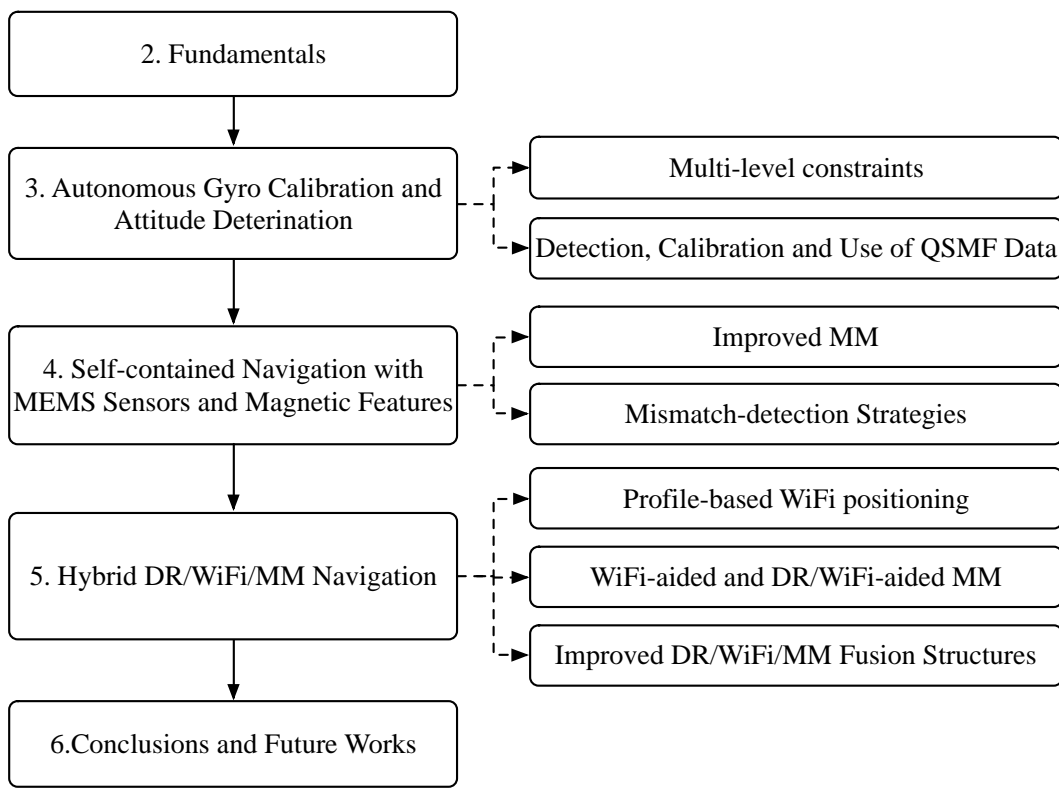


Figure 1-2. Thesis outline and detailed issues

CHAPTER 2: FUNDAMENTALS FOR NAVIGATION

This chapter covers the basic knowledge for the hybrid DR/WiFi/MM navigation system. Section 2.1 describes the necessary coordinate frames; Sections 2.1 - 2.3 introduce the fundamentals for WiFi fingerprinting, sensor-based DR, and MM, respectively; Finally, Section 2.5 describes the KF algorithm.

2.1 Reference Systems

The most commonly used reference frames in navigation is the inertial frame, the Earth-Centered Earth-Fixed (ECEF) frame, the navigation frame (or local-level frame), the vehicle frame, and the body frame. For pedestrian navigation applications, the vehicle frame represents the reference frame for the human body, while the body frame is the reference frame for the sensors on the consumer portable devices.

The inertial frame (i.e., i-frame) is an ideal frame of the reference which directly follows Newton's 1st and 2nd laws of motion and has no rotation or acceleration. Since the ideal frame is not possible in reality, a common version of the i-frame has its origin at the center of the Earth and axes with non-rotating/accelerating axes with respect to distant galaxies. The i-frame has its z-axis parallels to the spin axis of the Earth (polar axis), its x-axis points toward the mean vernal equinox, and its y-axis that completes a right-handed orthogonal frame.

The ECEF frame (i.e., e-frame) is a reference frame used for navigation applications with both GNSS and INS. As an example, the World Geodetic System (WGS) - 84 frame has its origin at the center of the Earth and axes that are fixed with respect to the earth. This frame has its x-axis in the equatorial plane points toward the Greenwich meridian, its z-axis along the Earth's polar axis and its y-axis completes a right-handed orthogonal frame.

The navigation frame (i.e., n-frame) is a local geodetic frame, which can also be referred as the local-level frame (i.e., l-frame). The north-east-down (NED) frame is used as the n-frame in this thesis. This frame has its origin coinciding with the measurement center of the sensors, its x-axis points toward geodetic north, its z-axis orthogonal to the reference ellipsoid pointing down, and its y-axis completes a right-handed orthogonal frame.

The vehicle frame (i.e. v-frame) is the frame fixed with the vehicle, which has its origin coinciding with the measurement center of the sensors, its x-axis points toward the forward direction of the vehicle, its y-axis points toward the horizontal right of the vehicle and its z-axis points downwards of the vehicle. The v-frame is useful when some curtain constraints on the vehicle motion, such as NHC, are used.

The body frame (b-frame) is the same as the IMU's body axes. Its original is at the center of the measurement center of the sensors, and its axes are aligned with the roll, pitch and heading axes of the inertial hardware assembly. The b-frame is commonly used since most civilian applications use strap-down sensors.

Figure 2-1 illustrates the e-, n-, v-, and b-frames, in which X, Y, and Z represent different axes and the superscripts denote for the frames. λ and φ are the latitude and longitude of the device.

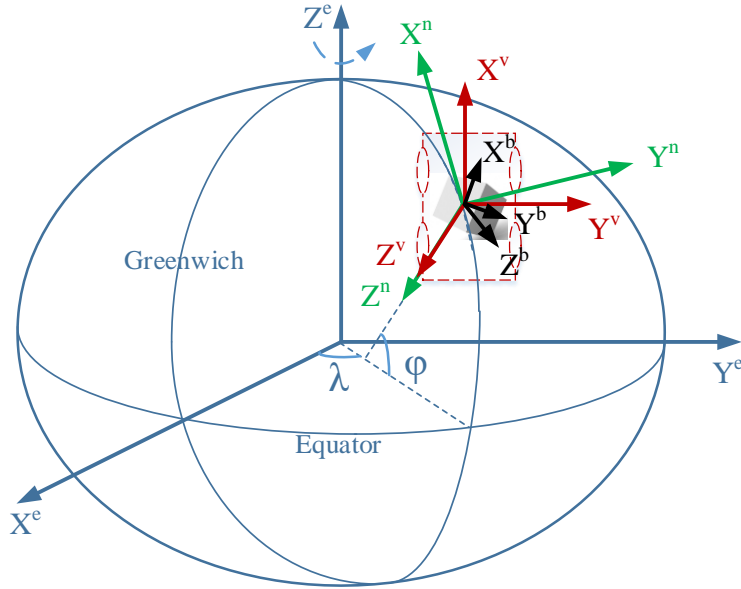


Figure 2-1. Coordinate systems used in navigation

2.2 WiFi Fingerprinting

As described in Chapter 1, the common wireless positioning techniques include fingerprinting, trilateration, and their combination. Both fingerprinting and trilateration have their advantages and disadvantages ([Zhuang, 2015](#)). This thesis only uses fingerprinting because it can provide position without any knowledge of AP location or signal-propagation model.

Fingerprinting consists of two phases: off-line pre-survey (training) and on-line positioning. The training phase is conducted to build or update a <RSS, location> DB that consists of a set of RPs with known coordinates and the RSS from available WiFi Aps, while The positioning phase is implemented to find the closest match between the features of the measured RSS and those stored in the DB. Figure 2-2 illustrates the procedure of training and positioning. The blue and red boxes indicates the training and positioning phases.

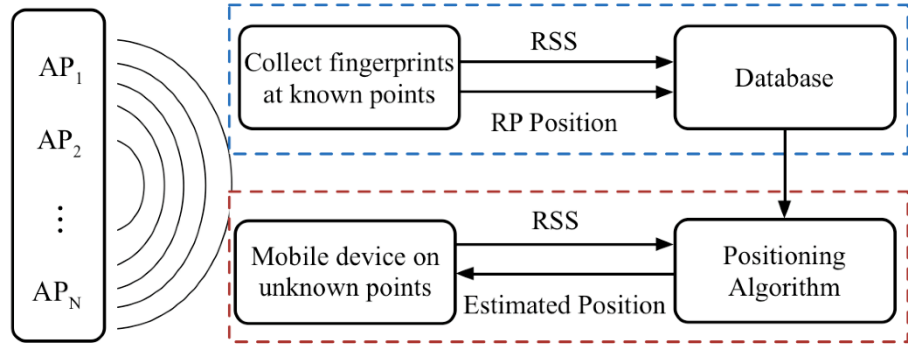


Figure 2-2. Procedure of training and positioning

In the training phase, the RSS vectors at all RPs and the RP coordinates are measured and saved into the DB. The WiFi fingerprint at the i -th RP is recorded as

$$\mathbf{FW}_i = \{\mathbf{pos}_i, (mac_{i,1}, RSS_{i,1}), (mac_{i,2}, RSS_{i,2}), \dots, (mac_{i,m_i}, RSS_{i,m_i})\} \quad (2-1)$$

where \mathbf{pos}_i is the coordinate of RP_i , $mac_{i,j}$ and $RSS_{i,j}$ are the MAC address and RSS value of the j -th AP received at RP_i , and m_i is the number of available APs at RP_i .

In the positioning phase, a mobile device measures the RSS vector at an unknown point, and compares this RSS vector with those stored in the DB to estimate its current location. The hypothesis behind WiFi fingerprinting is that the RSS values stable over time and non-uniform (i.e., changes significantly) with location. The optimal match of WiFi fingerprinting can be found by the minimum value of a certain criterion, for example, the two-dimensional Euclidean distance

$$d_i = |S - M_i| \quad (2-2)$$

where S and M_i are the measured WiFi fingerprint and the i -th candidate fingerprint in the DB, and d_i is the the two-dimensional Euclidean distance between S and M_i .

To mitigate the impact of blunders, the KNN method can be considered ([Peng et al., 2011](#)).

This method estimates the position by a weighed sum of the position of the k selected RPs that have the smallest differences

$$\hat{\mathbf{r}} = \sum_{i=1}^k \left(\frac{c_i}{C} \mathbf{r}_i \right) \quad (2-3)$$

where $c_i = 1/d_i$, $C = \sum_{i=1}^k c_i$, \mathbf{r}_i is the position of the i-th selected RP, and $\hat{\mathbf{r}}$ is the estimated

position. A special case is that when a certain d_i is zero, the estimation of \mathbf{r}_i can be taken as the estimated position.

Fingerprinting can also provide a coarse estimation of orientation ([Xiang et al., 2004](#), [Bahl and Padmanabhan, 2000](#)) based on the fact that the human body affects the propagation of radio signals, which leads to the different fingerprints when the device is placed towards different orientations. Also, device rotation can level out or equalize the impact of its orientation to measure more reliable fingerprints compared to the fingerprint that is measured only for one direction ([Jekabsons et al., 2011](#)). The research in ([Liao and Kao, 2008](#)) records the RSS values in four orientations during the training phase to obtain a more accurate positioning. The positioning accuracy was improved when the user moved straightforward; however, the positioning accuracy was degraded if the orientation of the device is estimated incorrectly.

2.3 Sensor-based Navigation

There are mainly two types of DR algorithms that use inertial sensors, the INS mechanization and PDR. INS can provide 3-D navigation solution while PDR is a 2-D approach. The former is widely used in traditional land-based, marine, and airborne navigation applications, while the latter is the common pedestrian navigation algorithm. These methods are described separately.

2.3.1 Inertial Navigation

Inertial navigation is a dead-reckoning technique in which an IMU is tracked relative to its initial position, velocity, and attitude (i.e., the orientation from the b-frame to the n-frame). An IMU usually consists of a gyro triad and an accelerometer triad which are aligned with one another. The gyros and accelerometers are used to measure angular rates (or velocity increments and angular increments) and specific forces (acceleration due to all forces except for gravity), respectively. An INS consists of an IMU together with a navigation processor, which uses measurements from the IMU and the INS mechanization to track its position, velocity, and attitude.

In the INS mechanization, the gyro-derived angular rates are first used to track the attitude of the IMU. The known attitude is then used to transform the specific forces from the b-frame to the n-frame. After that, the gravity vector is added to the specific force in the n-frame to obtain the acceleration of the device. Finally, the acceleration is integrated once to determine the velocity and twice to track the position of the IMU in the n-frame ([Titterton and Weston, 2004](#)). The continuous-time INS mechanization algorithm in the n-frame is

$$\begin{bmatrix} \dot{\mathbf{r}}^n \\ \dot{\mathbf{v}}^n \\ \dot{\mathbf{C}}_b^n \end{bmatrix} = \begin{bmatrix} \mathbf{D}^{-1}\mathbf{v}^n \\ \mathbf{C}_b^n \mathbf{f}^b - (2\boldsymbol{\omega}_{ie}^n + \boldsymbol{\omega}_{en}^n) \times \mathbf{v}^n + \mathbf{g}^n \\ \mathbf{C}_b^n (\boldsymbol{\omega}_{ib}^b \times) - (\boldsymbol{\omega}_{in}^n \times) \mathbf{C}_b^n \end{bmatrix} \quad (2-4)$$

where

$$\mathbf{D} = \text{diag}([R_m + h \quad (R_n + h) \cos \varphi \quad -1]) \quad (2-5)$$

$\mathbf{r}^n = [\varphi \quad \lambda \quad h]^T$ represents the position vector (latitude, longitude, and height);

$\mathbf{v}^n = [v_N \quad v_E \quad v_D]^T$ denotes the velocity vector in the n-frame; \mathbf{C}_b^n is the Direction Cosine Matrix (DCM) from the b-frame to the n-frame; \mathbf{f}^b is the specific force vector, and $\boldsymbol{\omega}_{ib}^b$ is the angular rate

of the b-frame with respect to the i-frame, both projected to n-frame; ω_{ie}^n and ω_{en}^n represent the angular rate of the Earth and that of the n-frame with respect to the e-frame; \mathbf{g}^n is the local gravity vector; R_m and R_N are the radius of curvature of meridian and curvature in the prime vertical, respectively, and h is the altitude. The symbol “ $(\mathbf{s}\times)$ ” denotes the skew-symmetry matrix of the vector “ \mathbf{s} ”, and the symbol “ $diag(\mathbf{s})$ ” indicates the diagonal matrix form of the vector “ \mathbf{s} ”. The symbol “ \times ” denotes the cross product of two vectors.

Figure 2-3 shows the diagram of the INS mechanization, where the symbol “ $\omega_{\alpha\beta}^\chi$ ” represents the angular rate of the “ β ”-frame with respect to the “ α ”-frame, projected to the “ χ ”-frame.

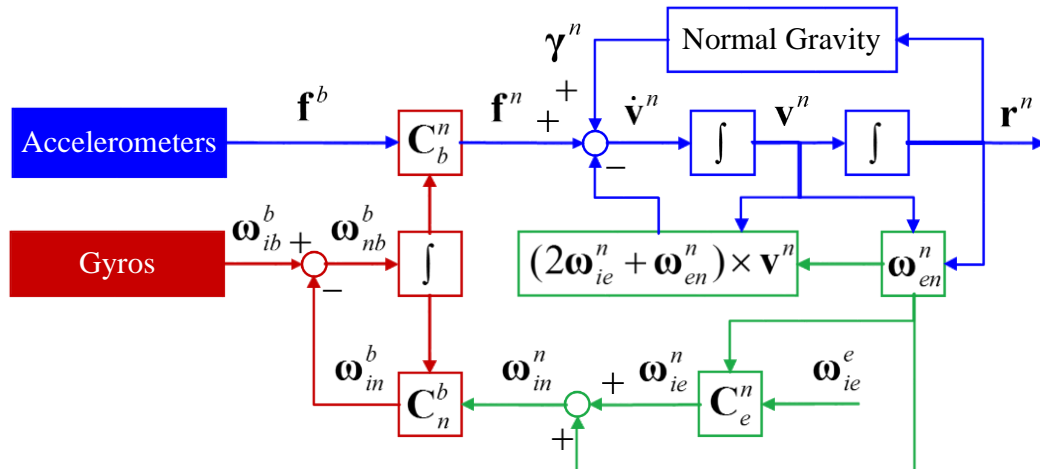


Figure 2-3. Diagram of the INS mechanization (Shin, 2005a)

2.3.2 Pedestrian Dead-Reckoning

PDR is used as the pedestrian position-tracking algorithm. It is the relative means of determining of a new position $(\varphi_{k+1}, \lambda_{k+1})$ from a previous known position (φ_k, λ_k) using the latest heading and step length by:

$$\begin{bmatrix} \varphi_{k+1} \\ \lambda_{k+1} \end{bmatrix} = \begin{bmatrix} \varphi_k + s_k \cos \psi_{k-1} / (R_m + h) \\ \lambda_k + s_k \sin \psi_{k-1} / [(R_n + h) \cos \varphi_k] \end{bmatrix} \quad (2-6)$$

where ψ , and s are heading and step length, and the subscript k and $k+1$ indicate the count of steps.

Therefore, a PDR algorithm consists of three parts: step detection, step-length estimation, and step heading estimation. Figure 2-4 demonstrates the process of PDR.

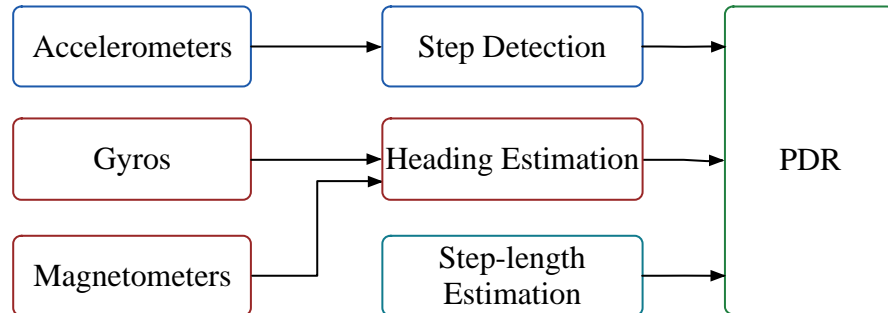


Figure 2-4. Diagram of PDR

The steps of a pedestrian can be detected by using the accelerometer and gyro signals. Details of step detection methods (e.g., peak detection, zero crossing, and spectral analysis) are described in ([Harle, 2013](#)). There is also research on step-detection using devices on different places of a body, for example, foot, backpack, and waist ([Alvarez et al., 2006](#), [Cho and Park, 2006](#)).

For step-length estimation, there are various approaches. The INS mechanization can be used to calculate the step length when the device is fixed on the human body (e.g., on-foot or in-belt) and constraints such as ZUPT and ZIHR are available ([Alvarez et al., 2006](#), [Seco et al., 2009](#)). When the device is not fixed, the common method is to train the step-length model when an external positioning technique such as GNSS is available. The research ([Shin et al., 2007](#)) provides a linear step-length model that considers both the walking frequency and the variance of the accelerometer signals. The step length model is

$$SL_k = \alpha \cdot f_k + \beta \cdot v_k + \gamma \quad (2-7)$$

where

$$f_k = 1 / (t_k - t_{k-1}) \text{ and } v_k = \sum_{t=t_{k-1}}^{t_k} \frac{(a_t - \bar{a}_k)^2}{N} \quad (2-8)$$

f_k and v_k are the walking frequency and acceleration variance, respectively; a is acceleration, \bar{a}_k and N are the mean value and the number of accelerations during the time period $[t_{k-1}, t_k]$, respectively; α , β and γ are the parameters pre-learned during a pre-calibration stage.

In practical uses, accurate estimation of step-length in real time is still challenging because it needs sufficient experimental data for each separate pedestrian. Different step-length models may be used accordingly to the detection of motion types, for example, walking and running.

2.3.3 Heading estimation using magnetometers

Magnetometers can provide an absolute heading through the following steps ([Zhang et al., 2013](#)): a) leveling the magnetometer measurements by using accelerometer-derived roll and pitch angles; b) using the levelled magnetometer measurements to calculate the magnetic heading (i.e., the heading angle from the Earth's magnetic north); and c) calculating the true heading (i.e., the heading angle from the Earth's geographic north) by adding a declination angle to the magnetic heading.

The process of levelling is using accelerometer measurements to calculate the horizontal angles (i.e., roll and pitch). The DCM from the b-frame to the n-frame can be expressed as ([Shin, 2005a](#)):

$$\mathbf{C}_b^n = \begin{bmatrix} \cos \theta & 0 & \sin \theta \\ 0 & 1 & 0 \\ -\sin \theta & 0 & \cos \theta \end{bmatrix} \begin{bmatrix} 1 & 0 & 0 \\ 0 & \cos \phi & -\sin \phi \\ 0 & \sin \phi & \cos \phi \end{bmatrix} = \begin{bmatrix} \cos \theta & \sin \phi \sin \theta & \cos \phi \sin \theta \\ 0 & \cos \phi & -\sin \phi \\ -\sin \theta & \sin \phi \cos \theta & \cos \phi \cos \theta \end{bmatrix} \quad (2-9)$$

Therefore, the X, Y and Z magnetometer readings can be transformed to the horizontal plane (X_H, Y_H) by

$$\begin{aligned} X_H &= X \cos \theta + Y \sin \phi \sin \theta + Z \cos \phi \sin \theta \\ Y_H &= Y \cos \phi - Z \sin \phi \end{aligned} \quad (2-10)$$

The true heading is calculated by adding a declination angle to the magnetic heading, which is determined by using the transformed magnetometer readings in the horizontal plane (X_H, Y_H). The true heading can be computed as

$$\begin{aligned} Azimuth_true &= Azimuth_mag + \varnothing \\ &= \arctan(Y_H / X_H) + \varnothing \end{aligned} \quad (2-11)$$

where \varnothing is the declination angle.

This approach is developed based on the assumption that the LMF is the GF and thus the value of the declination angle can be obtained from the IGRF model. However, the LMF was susceptible to magnetic interferences from man-made infrastructures in indoor or urban environments. Hence, the existence of magnetic interferences is a critical issue when using magnetometers as a compass indoors because it is difficult to obtain the accurate value of the declination angle in real time.

Scholars have presented various approaches to improve the robustness of the magnetometer-derived heading. For example, the gyro-derived heading is utilized to detect severe magnetic disturbances by ([Ladetto et al., 2001](#))

$$|\omega_G - \omega_M| > T \quad (2-12)$$

where ω_G is the angle rate measured by gyros, T is the threshold, and $\omega_M = (\alpha_{t_{k+1}} - \alpha_{t_k}) / (t_{k+1} - t_k)$, where α_{t_k} and $\alpha_{t_{k+1}}$ are the true heading angles calculated from the magnetometer measurements at time t_k and t_{k+1} , respectively.

2.4 Magnetic Matching

The Earth's is often viewed as a large dipole magnet that has two opposing poles (generally termed north and south poles) at each end ([Campbell, 2001](#)), as shown in Figure 2-5. Although there are a number of naturally occurring variations that may cause variation in the intensity of the magnetic field, the main field of the Earth's magnetic field is fairly constant ([Storms, 2009](#)). The parameters for the geomagnetic field (i.e., intensity, declination angle, inclination angle, etc.) can be obtained from the IGRF model ([Chambodut, 2011](#)).

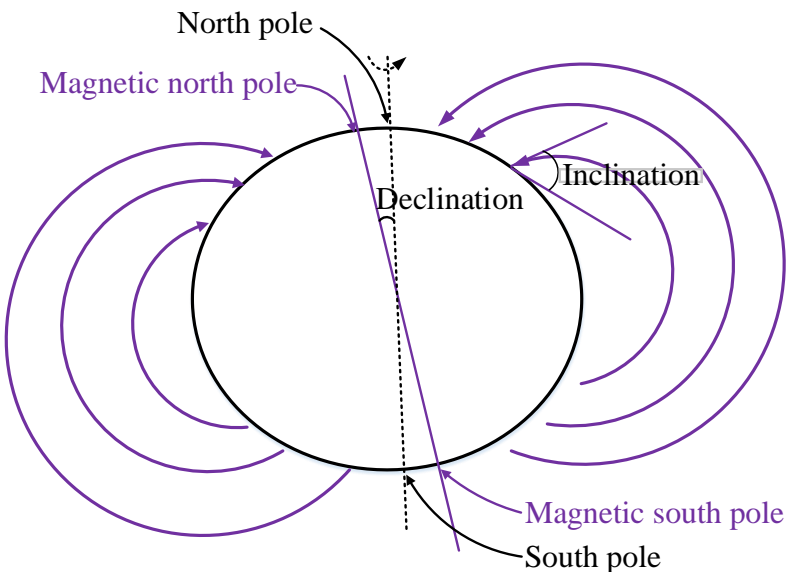


Figure 2-5: Earth's main dipole magnetic field, modified on ([Simanek et al., 2015](#))

Plenty of evidence has implied that animals such as pigeons and sea turtles utilize the geomagnetic field (GF) information for long-distance migration and homing ([Zhao et al., 2014](#)). By sensing the GF, these animals are able to perceive orientations, altitudes, and positions ([Winklhofer, 2009](#)). The experiment in ([Dennis et al., 2007](#)) indicated that a homing pigeon flew a trajectory according to the gradient of the GF intensity. For humans, magnetic fields have also been observed and used for centuries. The Chinese developed a magnetic compass between 300 and 200 BC that was used to align construction with the Earth's magnetic fields ([Campbell, 2001](#)).

This was the start of compass navigation. Compasses use the magnetic properties of repulsion and attraction to determine which direction is north relative to the users' current position. Other than compasses, there are MM techniques that use the gradient of GF for matching ([Liu et al., 2007](#)). As described in Chapter 1, both techniques are used in modern navigation applications.

The approach that uses magnetometer measurements to calculate the heading has been illustrated in Subsection 2.3.3. Thus, only the MM approach is described here. There are well-developed profile-matching approaches such as terrain contour matching (TERCOM) ([Golden, 1980](#)) and iterative closest contour point (ICCP)([Behzad and Behrooz, 1999](#)). Although these methods were first introduced for terrain- and gravity-based navigation systems, they can also be applied on MM. The basic idea of profile-matching is to save a profile (i.e., a sequence of observations) in the memory and then compared it with the candidate profiles stored in a DB ([Golden, 1980](#)). Thus, traditional profile-matching vehicles are equipped with a high-end INS to obtain accurate short-term trajectories.

The TERCOM algorithm was originally conceived in late 1950s and a well-known literature for this method is ([Golden, 1980](#)). The basic principle for TERCOM algorithm is correlative analysis. There are several algorithms to be used for correlative analysis, for example, the cross-correlation (COR) algorithm, the mean absolute difference (MAD) algorithm, and the mean squared difference (MSD) algorithm. These algorithms can be depicted as follows ([Zhao et al., 2009](#)).

$$COR(\tau_x, \tau_y) = \frac{1}{L} \int_{-L/2}^{L/2} T_{ACQ}(x, y) * T_{ST}(x + \tau_x, y + \tau_y) dx \quad (2-13)$$

$$MAD(\tau_x, \tau_y) = \frac{1}{L} \int_{-L/2}^{L/2} |T_{ACQ}(x, y) - T_{ST}(x + \tau_x, y + \tau_y)| dx \quad (2-14)$$

$$MSD(\tau_x, \tau_y) = \frac{1}{L} \int_{-L/2}^{L/2} [T_{ACQ}(x, y) - T_{ST}(x + \tau_x, y + \tau_y)]^2 dx \quad (2-15)$$

where τ_x and τ_y are the offset values in the direction parallel to the x- and y-axes, respectively; T_{ACQ} and T_{ST} are respectively the magnetic intensity value measured by magnetometers and that stored in the DB at the point $(x + \tau_x, y + \tau_y)$; and L is the length of the matching profile. The optimal match can be selected when the COR value becomes maximum, or when the MAD or MSD value becomes minimum.

The ICCP algorithm was first presented by ([Kamgar-Parsi and Kamgar-Parsi, 1999](#)) for gravity-based navigation. It is derived from iterated closest point (ICP) ([Besl and McKay, 1992](#)) that is widely used in image registration. ICP is an algorithm employed to minimize the difference between two clouds of points. In the algorithm, one point cloud is kept fixed, while the other one is transformed to best match the reference. The algorithm iteratively revises the transformation (combination of translation and rotation) needed to minimize the distance from the source to the reference point cloud.

To implement MM based on ICCP, it is straightforward to find the contour of the magnetic intensity observation, but difficult to determine the actual location along the profile. To acquire the actual location, a rigid transformation, including a rotation transformation and a translation transformation, is performed on the INS-derived short-term trajectory. After that, the optimal matching can be achieved through finding the smallest distance from the INS-derived position to the corresponding point at the profile by using a certain criterion (e.g., the Euclidean distance) ([Zhao et al., 2009](#)).

In indoor or urban areas, there are artificial infrastructures may perturb the Earth's magnetic field. These artificial disturbances are caused by electrical currents running through any type of metal or conducting structure ([Storms, 2009](#)). In buildings, walls are often reinforced with steel rebar, newer construction projects use steel studs in interior walls. Steel beams used to support the floors of buildings add to the problem, as well as pipes, wires, and electric motors or equipment. The existence of these indoor magnetic interference can be exploited as an advantage by leveraging the magnetic abnormalities as fingerprints or landmarks ([Xie et al., 2014](#), [Subbu et al., 2013](#)). This fact provides the possibility for indoor MM.

2.5 Kalman Filter

Filtering is a process of estimating and tracking the state of a linear or nonlinear stochastic system from Gaussian or non-Gaussian noisy observation data ([Haug, 2005](#), [Gordon et al., 2004](#)). Since R.E. Kalman published his well-known paper introducing a recursive approach for the discrete linear filtering issue ([Kalman, 1960](#)), KF has been used in extensive research and applications, especially in the field of guidance, navigation, and control. KF is a “prediction-correction” algorithm that can be derived based on the optimal criterion of unbiased estimation of the state vector of the state vector with the optimal weight. There are several assumptions behind KF ([Welch and Bishop, 1995](#)). The first assumption is that the state vector \mathbf{x} is a random process that can be described with a discrete-time system model (2-16), and the measurements can be described with a discrete-time measurement model (2-17).

$$\mathbf{x}_k = \Phi_{k/k-1} \mathbf{x}_{k-1} + \mathbf{w}_{k-1} \quad (2-16)$$

$$\mathbf{z}_k = \mathbf{H}_k \mathbf{x}_k + \mathbf{n}_k \quad (2-17)$$

where \mathbf{x}_{k-1} and \mathbf{x}_k represent the state vectors at the epochs $k-1$ and k ; $\Phi_{k/k-1}$ is the system transformation matrix from $k-1$ to k ; \mathbf{z}_k denotes the measurement vector at k ; and \mathbf{w}_{k-1} and \mathbf{n}_k represent the system and measurement noise vectors.

Additionally, it is assumed that the process and measurement noises are both white and uncorrelated with one another, as well as uncorrelated with the state vector, specifically,

$$\mathbf{E}\{\mathbf{w}_l\} = \mathbf{0}, \quad \mathbf{E}\{\mathbf{w}_l \mathbf{w}_p\} = \begin{cases} \mathbf{Q}_l & l = p \\ \mathbf{0} & l \neq p \end{cases} \quad (2-18)$$

$$\mathbf{E}\{\mathbf{n}_l\} = \mathbf{0}, \quad \mathbf{E}\{\mathbf{n}_l \mathbf{n}_p\} = \begin{cases} \mathbf{R}_l & l = p \\ \mathbf{0} & l \neq p \end{cases} \quad (2-19)$$

$$\mathbf{E}\{\mathbf{w}_l \mathbf{n}_p\} = \mathbf{0} \quad \text{for all } l \text{ and } p \quad (2-20)$$

where \mathbf{Q} and \mathbf{R} are the system and measurement noise matrices, respectively. The final assumption is that an *a priori* unbiased estimation, $\mathbf{x}(t_0)$, of the state is available, along with its corresponding covariance matrix \mathbf{P}_0 , that is

$$\mathbf{E}\{\hat{\mathbf{x}}_0\} = \mathbf{x}(t_0), \quad \mathbf{E}\{\hat{\mathbf{x}}_0 \hat{\mathbf{x}}_0^T\} = \mathbf{P}_0 \quad (2-21)$$

KF works based on a close-loop feedback mechanism: the filter estimates the process state and then obtains feedbacks from noisy measurements. Therefore, the process for KF can be divided into two steps: prediction (or time update) and update (or measurement update). The diagram of the KF algorithm is shown in Figure 2-6.

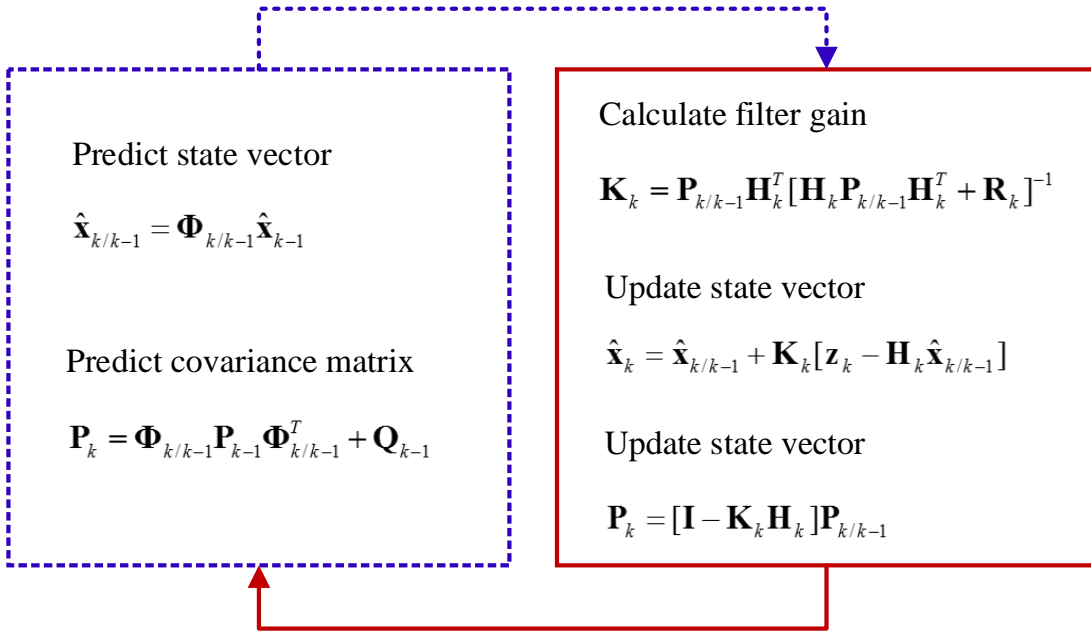


Figure 2-6. Diagram of Kalman filter

where $\hat{x}_{k/k-1}$ and $P_{k/k-1}$ represent the a priori state estimation and covariance matrix at the epoch k ; \hat{x}_{k-1} and \hat{x}_k are a posteriori state estimation at the epochs $k-1$ and k , and P_{k-1} and P_k are a posteriori error covariance matrices; K_k is the filter gain; and I is the unit matrix.

In the prediction step, the KF produces estimates of the current state variables, along with their uncertainties. Once the outcome of the next measurement (necessarily corrupted with some amount of error, including random noise) is observed, these estimates are updated using a weighted average, with more weight being given to estimates with higher certainty. The algorithm is recursive, which can run in real time, using only the present input measurements as well as the previously calculated states and their uncertainties; no additional past information is required.

The most widely used KF approach, due to its simplicity, is the extended Kalman Filter (EKF) ([St-Pierre and Gingras, 2004](#)). The idea behind the EKF is to linearize both the process and measurement models around the current navigation solution and turn the nonlinear filtering

problem into a linear problem. Assuming Gaussian distributed noise sources, the minimum mean square error (MMSE) solution to the linear problem can be obtained ([Kailath et al., 2000](#)).

For systems that have a highly nonlinear nature and non-Gaussian noise sources, nonlinear KF approaches have been presented. The most widely used nonlinear KF methods are sigma-point filters (Unscented Kalman Filters, UKF) and PF (sequential Monte Carlo methods) ([Georgy, 2010](#), [Aggarwal et al., 2008](#), [Crassidis, 2006](#), [Van Der Merwe et al., 2000](#), [Julier et al., 1995](#)). UKF is based on the principle that it is easier to approximate a Gaussian distribution than to approximate an arbitrary nonlinear function ([Crassidis, 2006](#), [Van Der Merwe et al., 2000](#), [Julier et al., 1995](#)). It approximates the Gaussian distribution by a set of deterministically selected samples called the sigma points. The sigma points are then propagated through the true nonlinear models to capture the true mean and covariance of transformed distribution. Unlike EKF or UKF, PF is designed particularly for highly nonlinear and non-Gaussian systems. It is a sequential Monte Carlo based method that allows for a complete representation of the state distribution using sequential importance sampling and re-sampling ([Georgy, 2010](#)). PF gives an approximate solution to an exact model, rather than the optimal solution to an approximate model which is the basics for KF ([Gustafsson et al., 2002](#)). The inherent weakness of PF is its computational complexity usually grows exponentially with the dimension of the state vector being estimated. Therefore, since the navigation equations in many navigation systems are only partial nonlinear, the filtering problem can be divided into a linear part and a nonlinear part, where the linear part, under the assumption of Gaussian-distributed noise entries, may be solved using a Kalman filter, hence, reducing the computational complexity of the system ([Schön et al., 2005](#), [Karlsson et al., 2004](#)).

CHAPTER 3: AUTONOMOUS GYRO CALIBRATION AND ATTITUDE

DETERMINATION

3.1 Introduction

As described in Chapters 1 and 2, wireless positioning techniques can provide long-term absolute positions, but require special receivers and the creation and maintenance of a network, which limit their applications on consumer devices. Although it is becoming feasible to determine the user position by using existing WiFi infrastructures in public buildings, there are several challenges for achieving high position accuracy. These challenges include dependency on signal availability and distribution ([Cheng et al., 2013](#)), fluctuation of RSS ([Xiao et al., 2015](#), [Bose and Foh, 2007](#), [Schmitt et al., 2014](#)), and time-variant nature of DBs ([Bahl and Padmanabhan, 2000](#), [Kushki et al., 2007](#), [Ni et al., 2004](#)). Because it is difficult to solve these issues inherent to wireless techniques through improving the WiFi positioning approaches, it is preferred to use other technologies to provide an augment in environments that have weak WiFi distribution.

MEMS sensors should be the first choice because of their popularization in the latest consumer devices and their independency on the transmission or reception of signals from an external source ([Huang et al., 2010](#)). A reliable sensor-based DR algorithm can bring several benefits: (a) It can provide short-term navigation solutions when external positioning techniques (e.g., GNSS, WiFi, and Bluetooth) are not available; (b) When other positioning techniques are available, it is straightforward to use these information to update the DR solution and obtain a navigation solution with long-term accuracy. Also, such integrated navigation can provide more reliable navigation results than the independent use of wireless positioning techniques, especially when the distribution of the wireless signals is weak. Additionally, (c) With a robust self-contained

navigation solution, it is possible to update WiFi DBs through a crowdsourcing approach by using daily-life navigation solutions ([Kim et al., 2012](#), [Zhuang et al., 2015a](#)).

Current INS mechanization algorithm is accurate enough in a short term even when using in high-end navigation applications such as those for spacecrafts and missiles ([Lawrence, 2012](#)). Therefore, one main fact that restricts the accuracy of DR with the MEMS sensors in consumer portable devices is the tremendous sensor errors, especially run-to-run biases and thermal drifts ([Niu et al., 2013](#)). Table 3-1 compares the performance of typical MEMS sensors ([InvenSense, 2014](#)) that used in smartphones and that of a typical tactical-grade IMU ([NovAtel, 2015](#)) that can be used in mobile mapping applications.

Table 3-1. Performance of MEMS sensors in smartphones and that in tactical IMU

Parameter	MPU-6500 (InvenSense, 2014)	FSAS-IMU (NovAtel, 2015)
Grade	Low-cost MEMS	High-end tactical
Gyro Biases	Initial biases at 25 °C: 18000 deg/h Thermal drifts: 864 deg/h/°C (From -40 to +85 °C)	0.75 deg/h
Angular Random Walk	0.6 deg/sqrt(h)	0.1 deg/sqrt(h)
Accelerometer Biases	Initial biases at 25 °C: 60 mg Thermal drifts: 0.64 mg/°C (From -40 to +85 °C)	1 mg
Velocity Random Walk	0.18 m/s/sqrt(h)	—

Although lab calibration at room temperature is a useful way to remove many deterministic sensor errors ([Titterton and Weston, 2004](#)), the MEMS sensors' readings can be very different due to the restart and the difference between the operational and calibration environments. Also, it is

not affordable for chip manufacturers to conduct thermal calibration of low-cost sensors. Due to the integration process in the DR mechanization, any sensor errors will accumulate, resulting in increasing navigation errors. For indoor environments, position or velocity updates from GNSS are not always available. If this is the case, the navigation accuracy will degrade faster over time.

Therefore, a real-time calibration process is needed to mitigate the drift of the inertial sensor errors, especially gyro biases. The calibration process should happen automatically in the background without the need for user intervention. This is because mainstream consumer and non-professional users should be able to benefit from the calibration and from a better navigation solution using the calibrated sensors without any specific requirement from them. Achieving such a calibration is not easy, especially when working with consumer-grade inertial sensors. Most calibration methods require external equipment or tools to provide a reference for calibration. It is not realistic to expect the users of the electronic products to use a separate tool to calibrate the sensors. Furthermore, current traditional methods to calibrate the inertial sensors without an external tool involve: a) using static periods for gyroscopes calibration when the sensors are fully static; and b) using the gravity vector for accelerometer calibration while ensuring that the IMU covers various attitudes to make sure that the system is observable ([Syed et al., 2007](#)). The need for static periods limits the scenarios where calibration can happen; the need for various attitudes increases the operation complexity. Furthermore, when the calibration is done automatically in the background, the need for various attitudes will delay having a full calibration without the user involvement to do specific motions.

Therefore, this chapter aims to answer the following question:

- How to mitigate the significant gyro biases in real time without any equipment or user intervention, so as to improve the attitude and position solution from DR under natural phone motion conditions?

This research focuses on calibrating gyros, instead of accelerometers or magnetometers because of the following facts:

- Gyros are more important than accelerometers in pedestrian navigation applications. Most pedestrian navigation algorithms use gyros to predict attitudes; thus, any gyro errors may directly lead to heading errors and in turn cause position errors. On the other hand, accelerometer measurements are utilized to detect steps or provide updates for horizontal attitude angles; therefore, accelerometers do not participate in the PDR algorithm directly. Assuming that an uncompensated gyro bias is 1 deg/s, it might cause an attitude error that increases over time, for example, 30 deg after 30 second and 100 deg after 100 sec. Also assuming that an uncompensated accelerometer bias is 20 mg, it may cause an attitude error of 1.14 deg, and this attitude error does not increase over time. Furthermore, the current technological level for MEMS accelerometers is more advanced than that of MEMS gyros. This fact can also explain why there are gyro-free navigation solutions that use multiple accelerometer triads ([Kodippili and Dias, 2010](#)).
- There are already researches about magnetometer calibration. Examples of magnetometer calibration approaches include “compass swinging” ([Bowditch and Bowditch, 1802](#)), ellipse fitting ([Camps et al., 2009](#), [Zhang and Yang, 2014](#)), iteration ([Tabatabaei et al., 2013](#)), real-time calibration ([Wahdan et al., 2015](#)), etc. These calibration methods can be effective ([Wahdan et al., Tabatabaei et al., 2013](#)); however, the main challenge for using magnetometers indoors is the change of LMF when the user moves. This phenomenon may

degrades the effect of calibration. Nevertheless, these methods require the user to get involved: the user has to either rotate the device by a “8”-shape or rotate the devices around each axis for a given angle (e.g., 360 degrees). Due to these facts, this thesis does not have research on magnetometer calibration.

This chapter propose an autonomous calibration method to calculate the gyros in consumer electronics. This method uses a KF algorithm and utilizes multiple constraints, including the pseudo-observations, the accelerometer and magnetometer measurements, the norm vector of the accelerometer and magnetometer measurements, and the quasi-static attitude updates. The advantages of the proposed calibration algorithm includes:

- The calibration happens automatically without the need for external equipment or user intervention;
- The algorithm works under natural user motions such as handheld, phoning, dangling, and pocket. Also, there is no singularity problem when the pitch angle reaches $\pm 90^\circ$;
- The algorithm works even in indoor environments with frequent magnetic interferences.

This chapter is organized as follows. Section 3.2 reviews the previous relevant works; Section 3.3 explains the methodology of the calibration algorithm, including the details of multiple constraints; Section 3.4 shows some results with analysis and Section 3.5 provides a summary.

3.2 Calibration Approaches

“Calibration is the process of comparing instrument outputs with known reference information and determining the coefficients that force the output to agree with the reference information over a range of output values” (Chatfield 1997). The commonly used calibration methods include the standard calibration methods ([Titterton and Weston, 2004](#), [Xiao et al., 2008](#)) and the multi-position calibration methods ([Lötters et al., 1998](#), [Skog and Hänel, 2006](#), [Syed et al., 2007](#), [Zhang et al.,](#)

[2010, Nieminen et al., 2010](#)). Standard calibration methods determine sensor errors by comparing the sensor outputs with known reference inputs. The six-position static method and rate tests are normally used for this purpose. These tests often require the use of specialized equipments or special references such as alignment to a given frame. With these references, each sensitive axis of every sensor can point alternately up and down precisely, and the IMU can be rotated around each gyro axis both clockwise and counter-clockwise with accurately known angles (Titterton and Weston 1997, El-Sheimy 2006). Based on the idea of six-position method, there are also twelve-position method and twenty-four-position method, etc (Xiao *et al* 2008). Compared with the six-position method, the improvement of these methods lies in that the effects of some error sources can be effectively eliminated or mitigated through adding a number of specific position arrangements. The accuracy of standard calibration methods depends on how well the axes are aligned with the reference frame. In order to obtain accurate results, specialized equipments (i.e. a turntable or a perfect cube) are always required so as to make IMU attitude and rotations precisely known. Due to the dependence on specialized equipment, the standard methods are always designed for in-lab tests, factory calibration and relatively high-grade IMUs.

For medium or low grade IMU, it is not economical to utilize the expensive specialized equipments and manpower that would make the calibration costs even more than the value of sensor or IMU itself. To calibrate an IMU just with simple devices or even without any specific tool, multi-position methods are developed. The basic idea of a multi-position method can be stated as follows: the norms of the measured outputs of the accelerometer and gyro cluster are equal to the magnitudes of the given specific force (i.e., gravity) and rotational velocity inputs (i.e., the Earth rotation), respectively ([Shin and El-Sheimy, 2002](#)). A major and vital improvement to the standard calibration methods mentioned above is that the multi-position method can be performed

without special aligned mounting to the local level frame (e.g. North-East-Down). However, the main drawback in using multi-position calibration method is that the gyro reference (the Earth rotation rate) is a weak signal (15 deg/h) which can result in observability problems. Therefore, a single axis turntable is required to provide a strong rotation rate signal ([Skog and Händel, 2006](#), [Syed et al., 2007](#), [Zhang et al., 2010](#), [Nieminen et al., 2010](#)), which limits the multi-position method to laboratories.

To estimate gyro errors without any external equipment, an in-field calibration method has been developed ([Fong et al., 2008](#)). The accelerometer triad is first calibrated by the multi-position method through multiple quasi-static states generated by hand holding. Then, the outputs from the calibrated accelerometers can be used to calibrate gyros. To avoid the requirement of being static/quasi-static, researches have presented gyro calibration methods such as the vertical gyro (VG) method ([InertialLabs, 2014](#)) and the approach that uses accelerometers to estimate the horizontal gyro errors ([Li et al., 2012b](#)). These methods are efficient in calibrating the horizontal gyros but have limited effect on the vertical gyro ([Li et al., 2012b](#)). To make all sensor errors observable, user intervention is still required: the user needs to rotate the device to different attitudes to make sure that every gyro axis has the chance to experience the horizontal direction. It takes several minutes to complete the whole calibration process.

In this chapter, we remove both the inconvenient user intervention process and the quasi-static assumption by using constraints from multiple sensors and a priori information. The features of the referred previous works and the proposed method are listed in Table 3-2.

Table 3-2. Comprehensive characteristics of previous works and proposed method

Method and author(s)	Required equipment	Calibration accuracy	Features
Standard methods (e.g. six-position method)	Specialized equipment	High	High precision and reliable
Multi-position method (<i>Lötters et al 1998</i>)	None (quasi-static required)	Low	Calibrate biases and scale factors of the tri-axial accelerometer under quasi-static conditions without any equipment
Improved multi-position methods (<i>Syed et al 2007, Skog and Händel 2006</i>)	A single axis angle turntable	High	Calibrate accelerometer non-orthogonalities as well; calibrate gyros using a single axis turntable
Improved multi-position method (<i>Zhang et al 2010</i>)	A single axis angle turntable	High	Detect the inter-triad misalignment between the accelerometer and gyro triads; Relax the requirement of precise orientation control.
Improved multi-position method (<i>Nieminen et al 2010</i>)	A single axis rate turntable	High	Exploiting the centripetal accelerations caused by the rotation of the turntable
Improved multi-position method (<i>Fong et al 2008</i>)	None (quasi-static required)	Low	Calibrate the low-cost gyro triad as well as accelerometers without any equipment
In-situ method (<i>Li et al 2012</i>)	None (in-situ required)	Low	Calibrate gyros and accelerometers biases and scale factors without any equipment in a short period (about 30 seconds)
Proposed method	None	Low	Using KF with multi-level constraints to conduct calibration under natural user motions.

3.3 Algorithm Description

When compared with previous works, the main advantage of the proposed method is the removing of the requirement of equipment and user intervention. In addition, the proposed method can work in real time under natural human motions in both indoor and outdoor environments. In this chapter, the details of the proposed method will be given. This chapter will also answer the following questions: a) how can the algorithm work under various human motions? and b) how can the algorithm work in indoor environments with frequent magnetic interferences?

Multi-level constraints are utilized to improve the calibration efficiency and accuracy, as demonstrated in Figure 3-1. The first level is called pseudo-observation updates. This constraint is activated when the change in position between two time epochs is within a limited range. In this case, the constraints $\tilde{r} = \text{constant}$ and $\tilde{v} = 0$ are regarded as an observation of pseudo-position and pseudo-velocity ([Li et al., 2012b](#)). The uncertainty of position and velocity changes during the calibration process are embodied in the covariance matrix of measurement noise (R) in the KF. The R matrix is tuned adaptively according to the IMU outputs. The use of the pseudo-observation updates makes it possible to calculate the gyro errors without external equipment or tools; also, the pseudo-observation updates can be used under natural human motions without special training. Therefore, it is feasible to run the calibration algorithm in the background without user interaction.

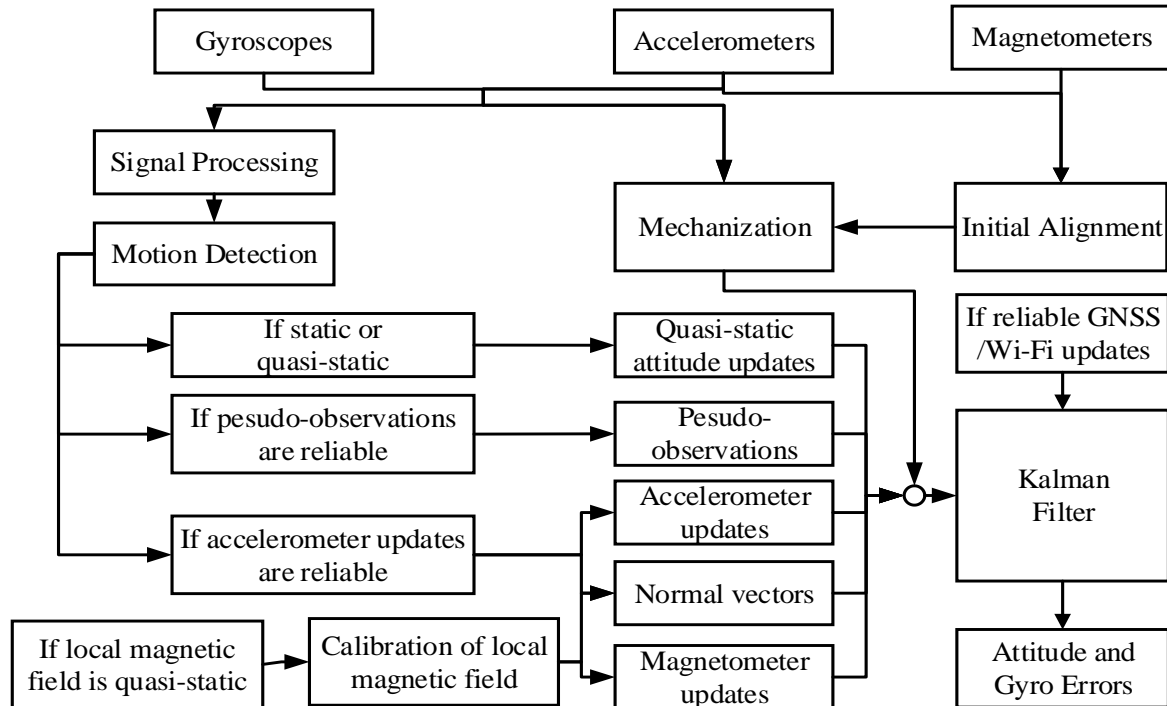


Figure 3-1. Structure of proposed calibration algorithm

The second level of constraints is from accelerometers and magnetometers. This research uses the accelerometer and magnetometer measurements in a tightly-coupled way, which brings several benefits for the pedestrian navigation applications with various phone displacements. Also, the norm vectors of the accelerometer and magnetometer measurements are used as updates. When there is a strong acceleration, the magnetometer measurement as well as the normal vector can be used. On the other hand, if the magnetometer measurement is perturbed, the accelerometer measurement as well as the normal vector can be used.

Another advantage of the proposed method is that it maximizes the contribution from magnetometers in environments with frequent magnetic perturbations. This method makes the magnetometer measurements reliable based on the following fact: to aid gyro calibration, what we need is attitude changes, instead of the absolute attitude. The proposed method can use the magnetometer measurements without knowing the absolute values of the local magnetic field (LMF) parameters (i.e., declination, inclination, and magnitude).

Moreover, the proposed calibration method is different from the traditional method which adds sensor errors into the navigation KF. The main objective of the navigation algorithm is to estimate the navigation states (i.e., position, velocity, and attitude) instead of sensor errors. Therefore, when using extra apriori information or setting parameters, it is preferable to assure that any inaccurate estimate of sensor errors will not destroy the navigation algorithm rather than to estimate residual sensor errors with a higher accuracy. However, the proposed calibration method uses specific updates, such as the pseudo-observations, and set the KF parameters with the aim of maximizing the calibration accuracy. Also, the calibration results can be evaluated before feedback to avoid the degradation of the whole navigation system under extreme navigation conditions.

The algorithm is comprised of the IMU sensor error models, the INS mechanization, and the KF models. The INS mechanization follows ([Shin, 2005b](#)) and will not be described in detail. For details about KF the reader can refer to ([Brown and Hwang, 1992](#)). The following sub-sections will introduce the algorithm, including system error models, the system model and the measurement model (for updates from multiple sensors and apriori information).

3.3.1 Sensor Error Models

A major problem of applying MEMS sensors is the changes of the biases and the scale factors ([Niu et al., 2013](#)). With the current MEMS manufacturing technology, non-orthogonality errors are relatively smaller compared to the biases and scale factor errors. Therefore, only biases and scale factor errors are taken into account. The output error equations of accelerometers and gyros can be described respectively as below:

$$\delta \mathbf{f}^b = \mathbf{b}_a + \text{diag}(\tilde{\mathbf{f}}^b) \delta \mathbf{s}_a + \mathbf{w}_a \quad (3-1)$$

$$\delta \boldsymbol{\omega}_{ib}^b = \mathbf{b}_g + \text{diag}(\tilde{\boldsymbol{\omega}}_{ib}^b) \delta \mathbf{s}_g + \mathbf{w}_g \quad (3-2)$$

where $\delta \mathbf{f}^b$ and $\delta \boldsymbol{\omega}_{ib}^b$ are the error vectors of specific force and angular rate, respectively. \mathbf{b}_a and \mathbf{b}_g are the accelerometer and gyro biases. $\delta \mathbf{s}_a$ and $\delta \mathbf{s}_g$ are the linear scale factor error vectors, \mathbf{w}_a and \mathbf{w}_g represent the sensor noises, and $\tilde{\mathbf{f}}^b$ and $\tilde{\boldsymbol{\omega}}_{ib}^b$ are the measured specific force and angular rate, respectively.

The sensor biases and scale factor errors are modeled as first-order Gauss-Markov processes ([Maybeck, 1982](#)). Take the gyro biases as an example:

$$\dot{\mathbf{b}}_g = -(1/\tau_{bg})\mathbf{b}_g + \mathbf{w}_{bg} \quad (3-3)$$

where τ_{bg} denotes for the correlation time of the gyro biases and \mathbf{w}_{bg} is the driving noise vector.

3.3.2 Kalman Filter - System Model

A simplified form of the psi-angle error model ([Shin, 2005b](#)) is applied as the continuous-time state equations in the KF ([Li et al., 2012b](#)).

$$\begin{bmatrix} \delta\dot{\mathbf{r}}^n \\ \delta\dot{\mathbf{v}}^n \\ \dot{\psi} \end{bmatrix} = \begin{bmatrix} -\boldsymbol{\omega}_{en}^n \times \delta\mathbf{r}^n + \delta\mathbf{v}^n \\ -(2\boldsymbol{\omega}_{ie}^n + \boldsymbol{\omega}_{en}^n) \times \delta\mathbf{v}^n + \mathbf{f}^n \times \boldsymbol{\psi} + \mathbf{C}_b^n \delta\mathbf{f}^b \\ -(\boldsymbol{\omega}_{ie}^n + \boldsymbol{\omega}_{ec}^n) \times \boldsymbol{\psi} - \mathbf{C}_b^n \delta\boldsymbol{\omega}_{ib}^b \end{bmatrix} \quad (3-4)$$

where $\delta\mathbf{r}^n$, $\delta\mathbf{v}^n$ and $\boldsymbol{\psi}$ are the errors of position, velocity, and attitude. \mathbf{C}_b^n is the DCM from the b-frame to the n-frame. \mathbf{f}^n is the specific force vector projected to the n-frame, and $\boldsymbol{\omega}_{ie}^n$ and $\boldsymbol{\omega}_{en}^n$ represent the angular rate of the Earth and that of the n-frame with respect to the e-frame, both projected to n-frame. $\delta\mathbf{f}^b$ and $\delta\boldsymbol{\omega}_{ib}^b$ are the output errors of accelerometers and gyros, as explained in (3-1) and (3-2).

3.3.3 Kalman Filter - Measurement Model

Different kinds of constraints are used to build the measurement model, including the pseudo-observations, the accelerometer and magnetometer measurements, the norm vector of the accelerometer and magnetometer measurements, and the quasi-static attitude updates. The details are introduced in this section.

1) Pseudo-observations

The pseudo-position and pseudo-velocity observations are proposed based on the fact that the range of the position and linear velocity of the IMU are within a limited scope ([Li et al., 2012b](#)). This research uses the pseudo-position updates while walking with natural human motions. The actual position and velocity changes during the calibration process can be embodied in the

covariance matrix of measurement noise (\mathbf{R}) in the KF. The measurement model of pseudo-position is

$$\hat{\mathbf{r}}^n - \tilde{\mathbf{r}}^n = \delta \mathbf{r}^n + \mathbf{n}_r \quad (3-5)$$

with $\tilde{\mathbf{r}}^n = \text{constant}$, or

$$\hat{\mathbf{v}}^n = \delta \mathbf{v}^n + \mathbf{n}_v \quad (3-6)$$

where $\hat{\mathbf{r}}^n$ and $\hat{\mathbf{v}}^n$ are position and velocity vectors predicted by the INS mechanization; $\tilde{\mathbf{r}}^n$ is the observation vectors of the proposed pseudo-position and pseudo-velocity, respectively; $\delta \mathbf{r}^n$ and $\delta \mathbf{v}^n$ are the position errors and velocity errors. \mathbf{n}_r and \mathbf{n}_v are the measurement noises (i.e. the inaccuracy) of the pseudo-position and pseudo-velocity. The measurement noises are manifested in the measurement noise covariance matrix \mathbf{R} .

Either pseudo-position or pseudo-velocity can be used as the observations, as well as both of them. The elements in the \mathbf{R} matrix should be determined according to the actual IMU motions by hands, i.e. how much is the position or velocity variation of the IMU in practice (i.e. $\text{var}(\mathbf{r})$ or $\text{var}(\mathbf{v})$). Here a feasible method of setting \mathbf{R} is provided. First a set of initial position or velocity noises can be given empirically; then, the position or velocity changes during the whole calibration process could be calculated; based on this result, the elements in \mathbf{R} can be further adjusted.

2) Accelerometer measurement model

This research builds the measurement model by using the accelerometer readings directly, instead of using the accelerometers-derived roll and pitch angles. This is important for the pedestrian navigation applications with arbitrary phone displacements, since it avoids the

singularity problem when the pitch angle reaches $\pm 90^\circ$. The tightly-coupled accelerometer measurement model is ([Wang et al., 2004](#))

$$\delta \mathbf{f}^n = \mathbf{f}^n - \hat{\mathbf{f}}^n = \mathbf{f}^n - \mathbf{C}_b^n \tilde{\mathbf{f}}^b \quad (3-7)$$

When neglecting the accelerometer deterministic errors,

$$\begin{aligned} \delta \mathbf{f}^n &= \mathbf{f}^n - (\mathbf{I} - [\boldsymbol{\psi} \times]) \mathbf{C}_b^n \mathbf{f}^b + \mathbf{C}_b^n \mathbf{n}_2 \\ &= -[\boldsymbol{\psi} \times] \mathbf{g}^n + \mathbf{C}_b^n \mathbf{n}_2 \\ &= [\mathbf{g}^n \times] \boldsymbol{\psi} + \mathbf{C}_b^n \mathbf{n}_2 \end{aligned} \quad (3-8)$$

where, $\mathbf{f}^n = -\mathbf{g}^n = [0 \ 0 \ -g]^T$, g is the local gravity value, $\boldsymbol{\psi}$ is the attitude error, and \mathbf{n}_2 is the noise.

For pedestrian applications, the acceleration are commonly high-frequency and alternating. Thus, it is reasonable to model the actual accelerations as measurement noises. The components in \mathbf{R} related to the accelerometer measurements are set based on the value of the actual linear acceleration A .

$$A = |norm(\mathbf{f}^b) - g| \quad (3-9)$$

When $A \leq |Th_{acc1}|$ (i.e., in non-acceleration mode), the corresponding components in \mathbf{R} are set as σ_a^2 , where σ_a^2 is set according to the specifications of the accelerometer used.

When $|Th_{acc1}| \leq A \leq |Th_{acc2}|$ (i.e., in low-acceleration mode), the acceleration uncertainties is set as $s(A^2 / P)\sigma_a^2$, where P is the corresponding components of attitudes in the covariance matrix and s is a scalar.

When $A \geq |Th_{acc_2}|$ (i.e., in high-acceleration mode), the accelerometer is far away from the truth.

Accordingly, the components in \mathbf{R} are set as a large number σ_{aMax}^2 . In this situation, the accelerometer measurements will not contribute to the solution.

3) Magnetometer measurement model

The main challenge for using the magnetometer measurements indoors is that there may be frequent magnetic perturbations indoors. The perturbations in the magnetometer measurements are different from that in the accelerometers. The latter is commonly high-frequency and alternating; however, the magnetic perturbations are caused by external magnetic bodies such as man-made infrastructures. Among various kinds of magnetic perturbations, a typical type of magnetic perturbation is that both the direction and strength of the LMF are changed, but the change is stable within a limited space (or periods). The period during which the LMF is stable can be called as quasi-static magnetic field (QSMF) period, and can be detected by using the magnitude of magnetometer readings ([Afzal et al., 2011](#)).

The proposed algorithm uses magnetometer measurements to improve the gyro calibration during QSMF periods. It is assumed that there is totally no idea about the LMF parameters. Instead, the proposed algorithm calibrate the LMF at the beginning of each QSMF period. The flowchart of using magnetometers under QSMF periods is shown in Figure 3-2.

The LMF vector during the k-th QSMF period is calibrated by:

$$\mathbf{m}_k^n = (\mathbf{C}_n^b)^T \tilde{\mathbf{m}}_{k,1}^b \quad (3-10)$$

where $\tilde{\mathbf{m}}_{k,1}^b$ is the magnetometer reading at the beginning of the first epoch(s) of k-th QSMF period.

The computed \mathbf{m}_k^n is then used as the reference during the k-th QSMF period.

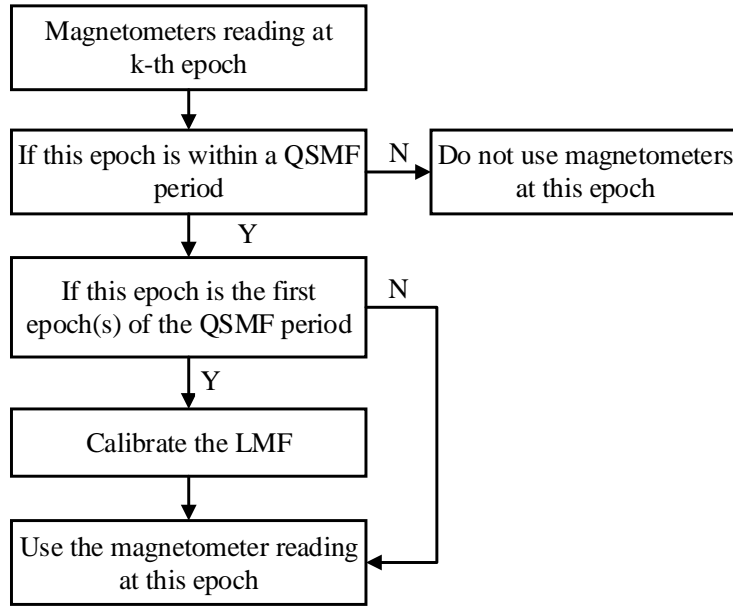


Figure 3-2. The flowchart of using magnetometer data during QSMF periods

The measurement model is built by using the magnetometer readings directly, which avoid the leveling (i.e., using the accelerometer readings to calculate the roll and pitch angles) step. Therefore, the measurement model, as shown in (10), is independent from the accelerometer measurements.

$$\delta\mathbf{m}^n = [\mathbf{m}^n \times] \boldsymbol{\psi} + \mathbf{C}_b^n \mathbf{n}_3 \quad (3-11)$$

where, $\delta\mathbf{m}^n = \mathbf{C}_b^n \tilde{\mathbf{m}}^b - \mathbf{m}^n$, $\tilde{\mathbf{m}}^b$ is the magnetometer measurement, \mathbf{m}^n is the calibrated LMF vector, $\boldsymbol{\psi}$ is the attitude error, and \mathbf{n}_3 is the measurement noise.

4) Norm vector of magnetometer and accelerometer measurements

The norm vector of two non-parallel vectors is orthogonal to both vectors ([Besl and McKay, 1992](#)). Therefore, the norm vector of the accelerometer and magnetometer measurement vectors will be independent from both vectors, since accelerometers and magnetometers sense different signals ([Niu, 2002](#)). When there is a strong acceleration, the magnetometer measurement as well as the

normal vector can be used. On the other hand, if the magnetometer measurement is perturbed, the accelerometer measurement as well as the normal vector can be used.

The measurement model for the normal vector is

$$\delta \mathbf{I}^n = [\mathbf{I}^n \times] \boldsymbol{\Psi} + \mathbf{C}_b^n \mathbf{n}_4 \quad (3-12)$$

where $\delta \mathbf{I}^n = \mathbf{C}_b^n \tilde{\mathbf{I}}^b - \mathbf{I}^n$, $\mathbf{I}^n = \mathbf{f}^n \times \mathbf{m}^n$, and \mathbf{n}_4 is the noise. The related \mathbf{R} matrix is set based on the accuracy of both the accelerometer and magnetometer measurements.

The norm vector of the accelerometer and magnetometer measurements is also used for the initial alignment process of the INS mechanization. Denoting that $\tilde{\mathbf{f}}^b = \mathbf{C}_n^b \mathbf{f}^n$, $\tilde{\mathbf{m}}^b = \mathbf{C}_n^b \mathbf{m}^n$, and $\tilde{\mathbf{r}}^b = \mathbf{C}_n^b \mathbf{r}^n$, then

$$[\tilde{\mathbf{f}}^b \quad \tilde{\mathbf{m}}^b \quad \tilde{\mathbf{r}}^b]^T = [\mathbf{f}^n \quad \mathbf{m}^n \quad \mathbf{r}^n]^T \mathbf{C}_b^n \quad (3-13)$$

The initial DCM from the b-frame to the n-frame can be computed by

$$\mathbf{C}_b^n = \left([\mathbf{f}^n \quad \mathbf{m}^n \quad \mathbf{r}^n]^T \right)^{-1} [\tilde{\mathbf{f}}^b \quad \tilde{\mathbf{m}}^b \quad \tilde{\mathbf{r}}^b]^T \quad (3-14)$$

5) Quasi-static attitude updates

Quasi-Static periods were first used in the surgery to determine the attitude of the patient and calibrate the accelerometers (Lötters et al. 1998). In the latest decade, as pedestrian navigation is becoming a hot topic, the detection and use of quasi-static data is commonly used, especially for the foot-mounted IMUs. Refer to ([Saxena et al., 2005](#)) for details about quasi-static detection.

The assumption for this constraint is that any rotation sensed by the gyros should be caused by the gyro biases when the device is quasi-static. Therefore, it is feasible to improve the gyro calibration during not only strict static periods, but also any quasi-static periods such as the periods

when the user stands in-situ and the phone is handheld, phoning, or putting in pocket. The detection of quasi-static periods has been detailed in ([Saxena et al., 2005](#)). The quasi-static attitude updates (QSAU) can be written as

$$\tilde{\omega}_{ib}^b = \mathbf{b}_g + \mathbf{n}_5 \quad (3-15)$$

where $\tilde{\omega}_{ib}^b$ is the output vector of a quasi-static gyro triad, and \mathbf{n}_5 is the noise.

3.4 Tests and Results

3.4.1 Test description

To evaluate the proposed algorithm, different outdoor and indoor walking tests were conducted with three smartphones. At the end of each test, there was a quasi-static period to calculate the reference values of gyro biases. The tested motion conditions comprised typical phone locations and attitudes including handheld, phoning (i.e., close to the ear), dangling (walking with phone in hand), and in a pants pocket. The tested motion modes and the corresponding gyro and accelerometer readings are shown in Figure 3-3. We can see that dangling and pocket had stronger phone movement than other motion conditions. The maximum angular rate reached 200 deg/s when dangling or phoning.

The tests were performed with Samsung Galaxy S3 and S4 smartphones. To make the gyro errors more significant (i.e., to test the calibration algorithm), gyro biases of 3 deg/s, -3 deg/s and 3 deg/s were added into the raw gyro outputs before data processing. The rough reference values of the gyro biases are shown in Table 3-3.

Table 3-3. Rough reference values of gyro biases

	Phone #1	Phone #2	Phone #3
Gyro X (deg/s)	0.9	6.2	1.3
Gyro Y (deg/s)	-2.1	-2.1	-2.6
Gyro Z (deg/s)	2.8	4.0	2.0

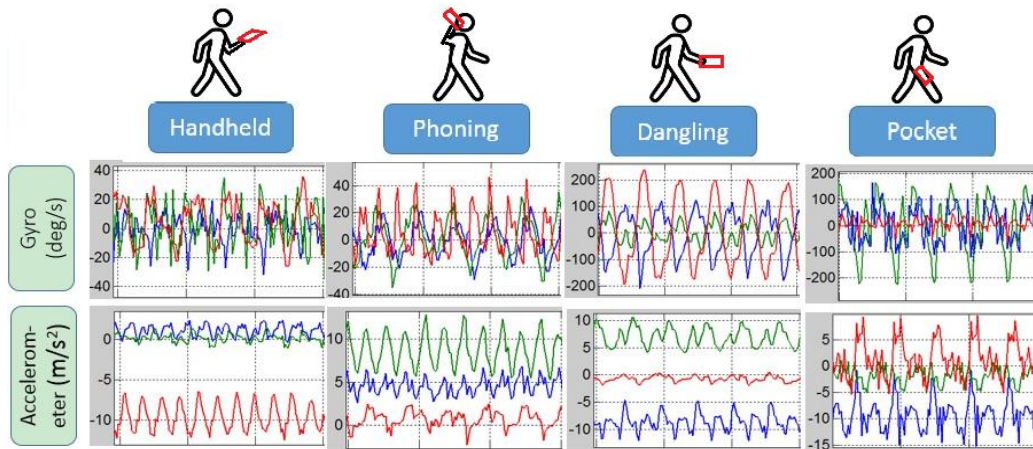


Figure 3-3. Tested motion conditions and corresponding gyro and accelerometer signals

The main difference between indoor and outdoor environments is the existence of magnetic perturbations. Figure 3-4 provides a sample of the outdoor and indoor magnetic environments. All figures are plotted using the magnetic information while walking (handheld) case. The figures in the first row of the table show the magnetometer readings and their magnitudes (cyan lines). The magenta dots indicate the QSMF periods. The figures in the second row show the calibrated LMF. The LMF kept stable during this outdoor test; on the other hand, it varied significantly during the indoor test. The outdoor and indoor tests will be given separately in the following two subsections.

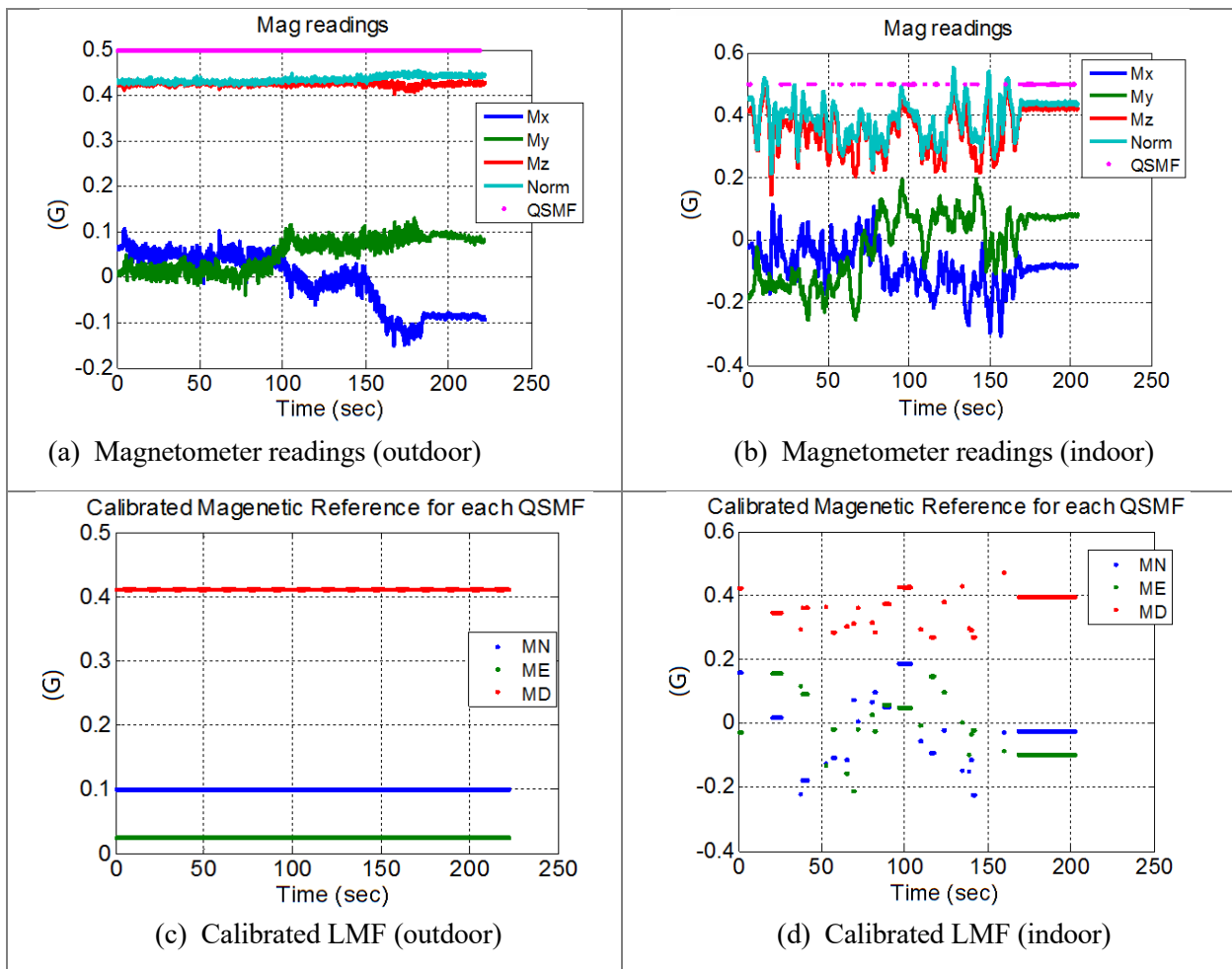


Figure 3-4. Magnetometer readings and calibrated LMF when walking (handheld) outdoors and indoors

3.4.2 Outdoor calibration tests

The outdoor test environment and trajectory are shown in Figure 3-5. It is a sidewalk crossing different parking lots. Thus, there is no building within 10 meters from the sidewalk.

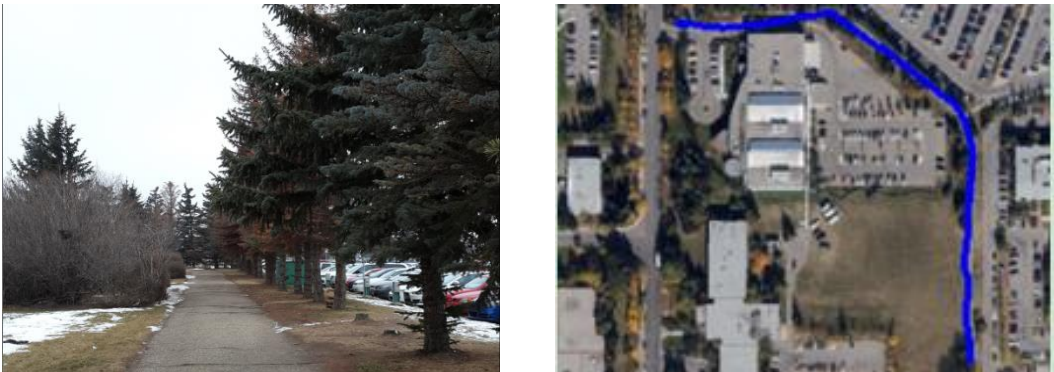


Figure 3-5. Outdoor test environment and trajectory

The figures of the calibration results are shown in Figure 3-6. The first column indicates the tested motion conditions, while the other three columns are the results of three phones. In each plot, the magenta dots indicate the availability of the magnetometer measurements. The pseudo-observation and accelerometer measurements were always available during these tests; therefore, the indicators for these constraints are not shown.

Most of the calibrated sensor errors have converged in the first 30 s, and all of them converged within 50 s. Table 3-4 shows the statistical results of the calibration errors under all scenarios with different phones. The mean and RMS errors were calculated using the differences between the calibration results at every epoch after convergence and the reference values obtained by averaging the gyro readings during the quasi-static periods at the end of each test.

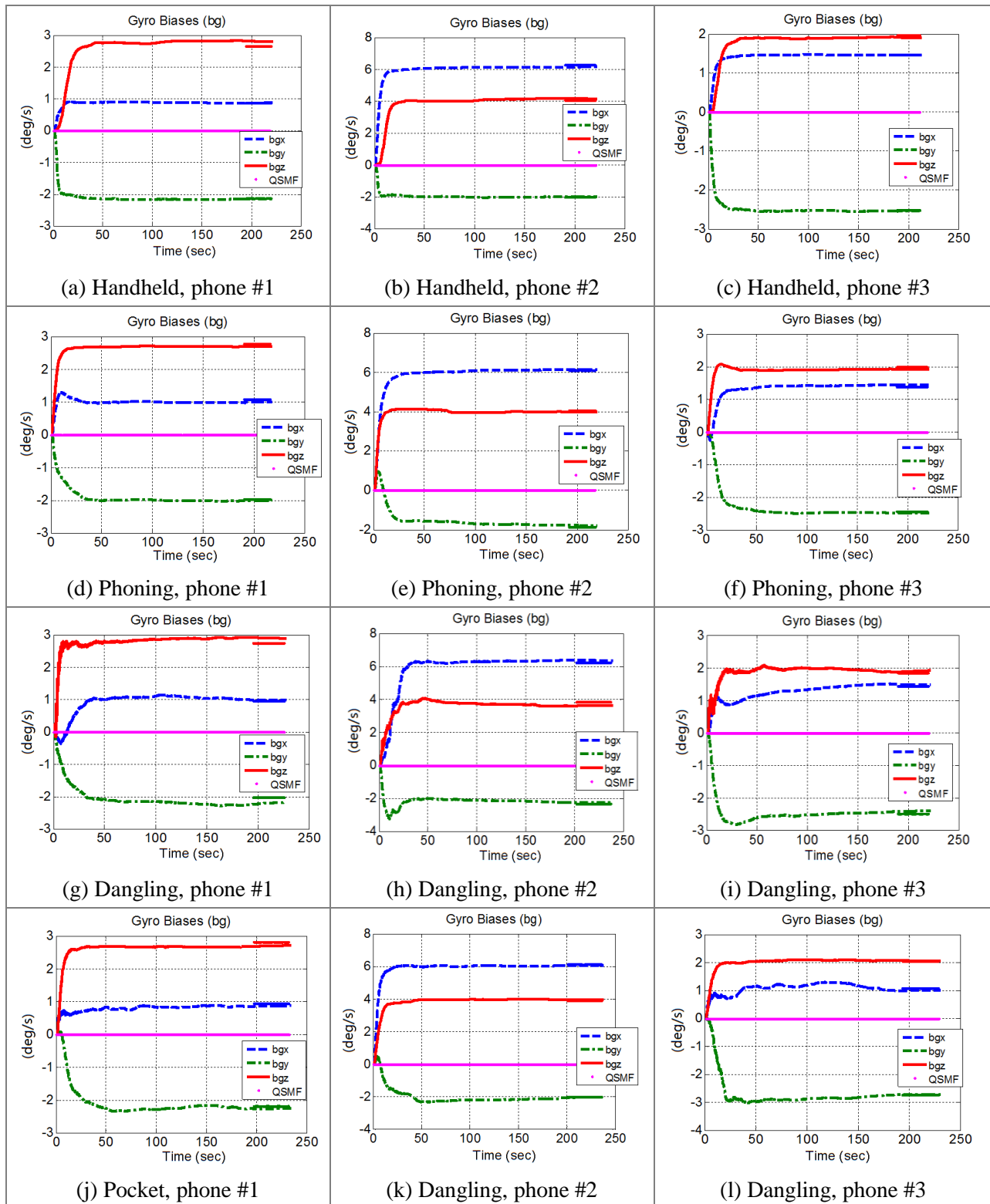


Figure 3-6. Figures of calibration results in outdoor tests (magenta dots indicate the availability of magnetometer measurements)

Table 3-4. Statistical results of the calibration errors under all scenarios

Phone	Values (deg/s)	X	Y	Z
#1	Reference	0.971	-2.099	2.776
	Mean	0.0588	0.0645	0.0845
	RMS	0.0682	0.0843	0.0986
#2	Reference	6.173	-2.017	3.981
	Mean	0.0737	0.0655	0.0743
	RMS	0.0787	0.0752	0.0883
#3	Reference	1.291	-2.587	1.973
	Mean	0.0603	0.0583	0.0503
	RMS	0.0707	0.0645	0.0605

The gyro biases reduced from several deg/s to under 0.1 deg/s. Although the gyros within different phones have different biases and some are more significant (e.g., 6 deg/s in phone #2), the results are all at the same level. This indicates the possible accuracy of the calibration method.

To investigate the effect of human motions on the calibration, we also calculated the statistical results under different motion modes. The results are shown in Table 3-5.

Table 3-5. Statistical results of the calibration errors under all scenarios

Motions	RMS error (deg/s)		
	X	Y	Z
Handheld	0.0633	0.0181	0.0589
Phoning	0.0610	0.0563	0.0643
Dangling	0.1157	0.1144	0.1230
Pocket	0.0882	0.0761	0.0815
General*	0.0855	0.0748	0.0857

* General - RMS of corresponding values under four motion conditions.

Dangling and pocket have larger calibration errors than the other motions modes. This meets our expectation, since both dangling and pocket provide stronger smartphone dynamics, as shown in Figure 3-3. Even under such challenging conditions, the gyro biases were reduced to under 0.13 deg/s and 0.1 deg/s, respectively.

3.4.3 Indoor calibration tests

The indoor tests were conducted at the main floor of the building E at the University of Calgary. There are metallic infrastructures inside Building E, which may bring in magnetic interferences. The test environment and trajectory are shown in Figure 3-7. This building has a main corridor which is 3 m wide, and a lobby which is about $30 \times 30 \text{ m}^2$. The test area at E was approximately $120 \times 40 \text{ m}^2$.



Figure 3-7. Indoor test environment trajectory

The result figures are shown in Figure 3-8. The solid line at the end of each curve indicates the reference value calculated from the quasi-static data.

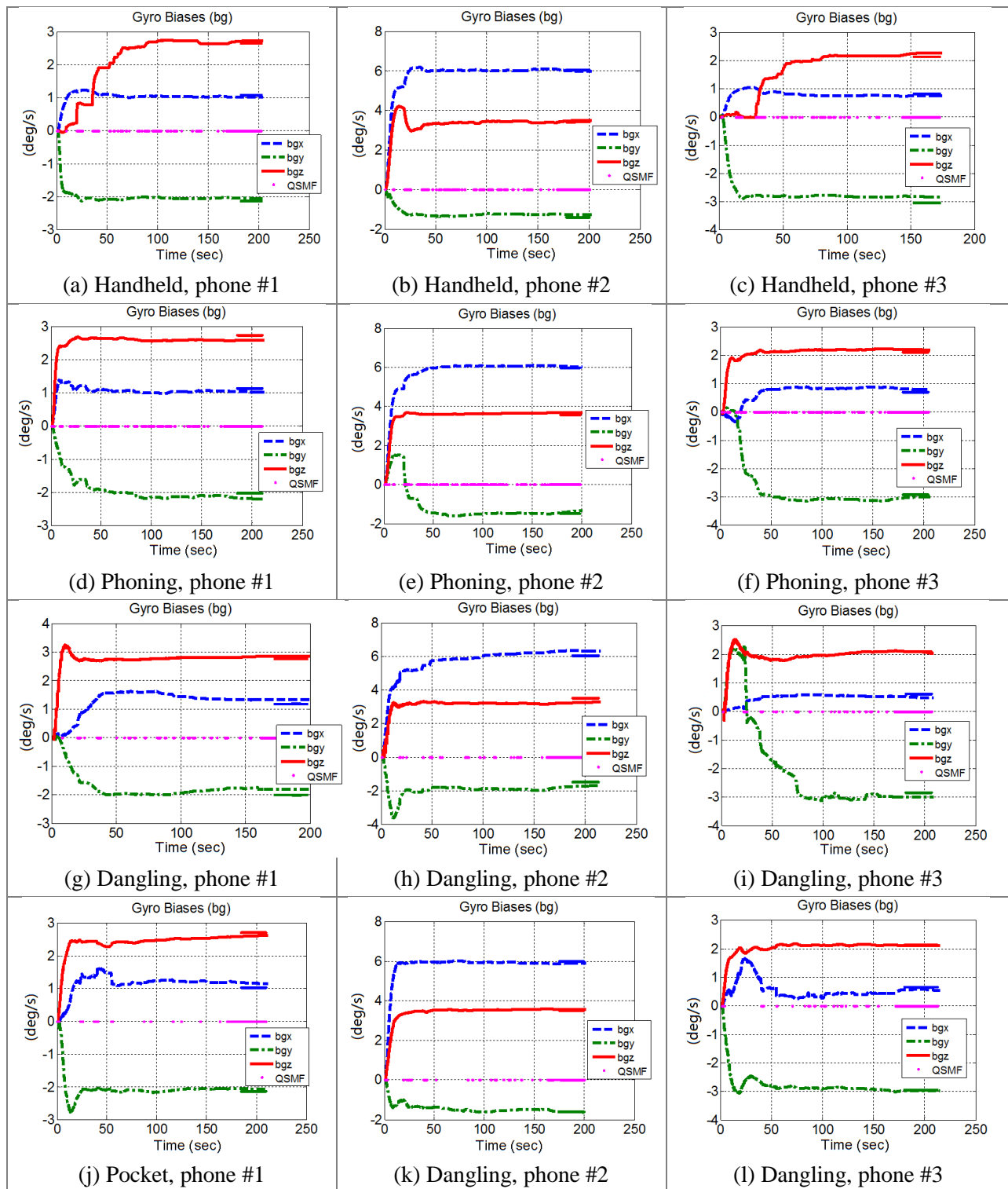


Figure 3-8. Figures of calibration results in indoor tests (magenta dots indicate the availability of magnetometer measurements)

The discontinuity of the periods with magnetometer updates indicates the frequent magnetic perturbations indoors. The convergence of gyro biases is not as smooth as those outdoors; however, even in such challenging environments, all the gyro biases have converged to the right values within 100 s under different human motions. This has verified the feasibility of the proposed method for pedestrian applications. Table 3-6 shows the statistical results of calibration errors under all scenarios with different phones, and Table 3-7 classifies the results by motion modes.

Table 3-6. Statistical results of the calibration errors under all scenarios

Phone	Values (deg/s)	X	Y	Z
#1	Reference	1.175	-2.226	2.648
	Mean	0.0825	0.0978	0.1032
	RMS	0.0886	0.1122	0.1049
#2	Reference	6.101	-1.356	3.562
	Mean	0.0637	0.1272	0.0550
	RMS	0.0772	0.1298	0.0666
#3	Reference	0.826	-3.043	2.129
	Mean	0.1183	0.1140	0.0847
	RMS	0.1270	0.1157	0.1063

Table 3-6 indicates that the proposed calibration method reduced the gyro biases from several deg/s to under 0.13 deg/s in the indoor tests, which is larger than the 0.1 deg/s outdoors. These results are promising for MEMS sensors, since the indoor environment is much harsher than the outdoor. In Table 3-7, the largest calibration errors under dangling and pocket are 0.17 and 0.14 deg/s, which are still larger than those under other motions. The calibration errors under handheld and phoning are less than 0.12 deg/s.

Table 3-7. Statistical results of the calibration errors under all scenarios

Motions	RMS error (deg/s)		
	X	Y	Z
Handheld	0.0534	0.1105	0.0786
Phoning	0.0930	0.1134	0.0920
Dangling	0.1376	0.1684	0.1462
Pocket	0.1364	0.1051	0.0789
General	0.1107	0.1270	0.1028

Comparing with previous methods such as the vertical gyro method or the methods that use accelerometers to estimate the horizontal gyro errors, an advantage of the proposed method is to use magnetometers during QSMF periods to calibrate the vertical component of gyro biases. Natural human motion signals are usually periodic, as indicated in Figure 3-3; therefore, not all the gyro axis has the chance to move to the horizontal direction. Thus, the magnetometers measurements during QSMF periods is important.

3.4.4 Indoor navigation tests

The indoor navigation tests were conducted at E. Figure 3-9 shows the test trajectory.



Figure 3-9. Indoor test environment trajectory

To illustrate the effect of magnetic perturbations at E, Figure 3-10 shows the magnetometer-derived heading solutions in a sample indoor test. The difference between the magnetometer-derived heading (the red dashed line) and the true value (the cyan solid line) reached over 100 degrees due to the existence of indoor magnetic interferences.

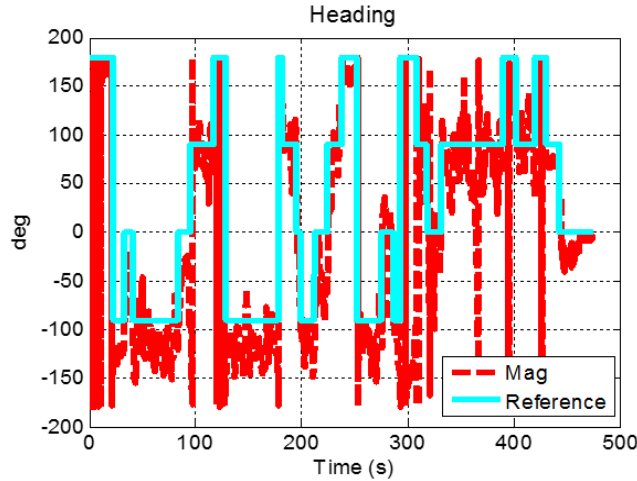


Figure 3-10. Heading provided by magnetometers indoors

Figure 3-11 illustrates the indoor pedestrian navigation results under different smartphone motion conditions. Since GNSS is available outdoors, we show only the indoor area (assuming the initialization was down by using GNSS results).

The heading errors were increasing because of the lack of external updates. Therefore, it was difficult to use sensors themselves to provide a long-term reliable navigation solution indoors without updates from external technologies such as GNSS or WiFi. However, even in such harsh indoor environments, the proposed algorithm provided accurate relative heading, that is, the shape of the navigation solutions is closed to that of the true trajectory. This outcome indicates that when external position updates are available, it is feasible to use them to correct the sensor-based solution and obtain a long-term accurate navigation solution. Therefore, the outcome from this research can

promote better utilizations of low-cost MEMS sensors in consumer portable devices. More detailed indoor navigation tests are provided in Chapters 4 and 5.

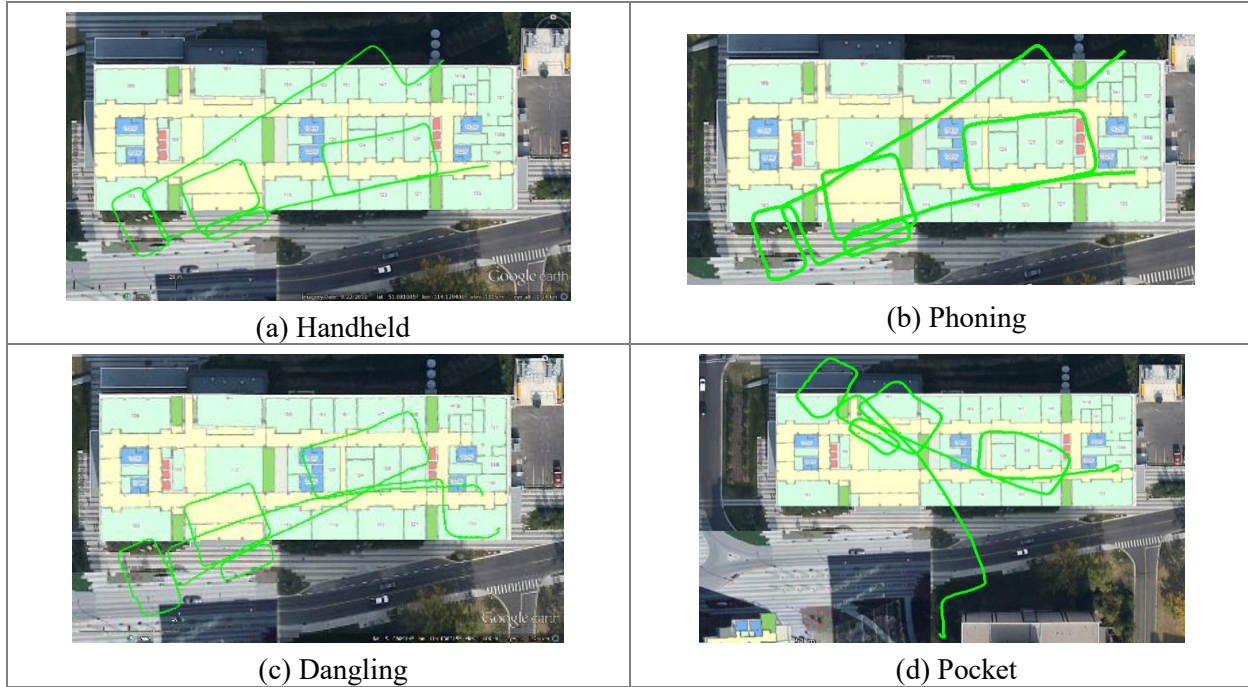


Figure 3-11. Indoor pedestrian navigation results

3.5 Summary

This chapter proposes a real-time calibration method without external equipment and without user intervention for gyro sensors in portable devices. The method was tested under walking tests with typical human motions, including handheld, phoning, dangling, pocket, belt, and backpack, both outdoors and indoors. The gyro biases of tested smartphones were reduced from several deg/s to under 0.15 deg/s indoors and 0.1 deg/s outdoors. Under the most challenging motion modes for sensors-based pedestrian navigation, i.e., dangling and pocket, the calibration errors were 0.17 and 0.14 deg/s indoors, and 0.13 and 0.09 deg/s outdoors. Under other motions, the calibration errors are less than 0.12 deg/s indoors and 0.07 outdoors. This calibration method can work in real-time and has a potential for calibration of the MEMS gyros within consumer electronics.

Figure 3-12 shows the gyro biases without and with the proposed real-time calibration. The gyro biases of tested phones were reduced from several deg/s to less than 0.15 deg/s even in indoor environments. Although the tested phones have different gyro bias values, the calibration errors are at the same level.

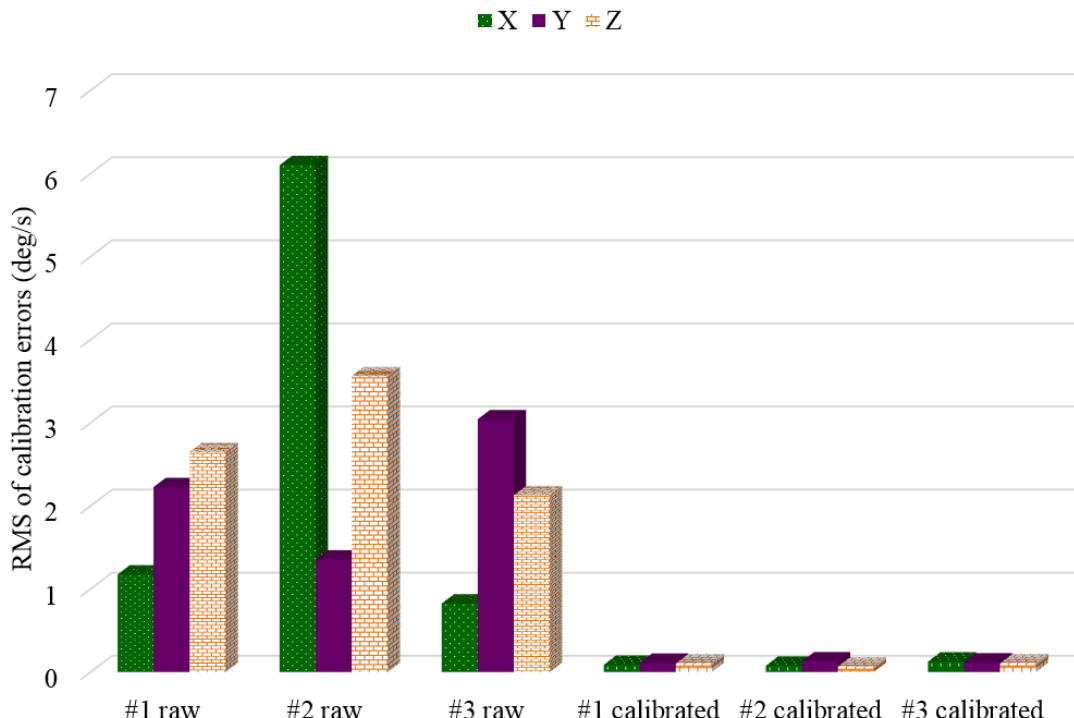


Figure 3-12. Gyro biases without and with the proposed real-time calibration

Figure 3-13 compares the calibration errors under different motion modes both indoors and outdoors. The results are better outdoors than indoors under all motion modes. This is most probably because of the harsh magnetic environment indoors. Dangling and pocket are two challenging motion modes for gyro calibration. Their calibration errors are 0.17 and 0.14 deg/s indoors, and 0.13 and 0.09 deg/s outdoors. Under other motions, i.e., handheld, phoning, belt, and backpack, the calibration errors are under 0.12 deg/s indoors and 0.07 outdoors. The calibration results are promising for low cost MEMS sensors in consumer portable devices, even when

considering that a part of the calibration errors may be caused by the temperature variations of the gyro errors themselves.

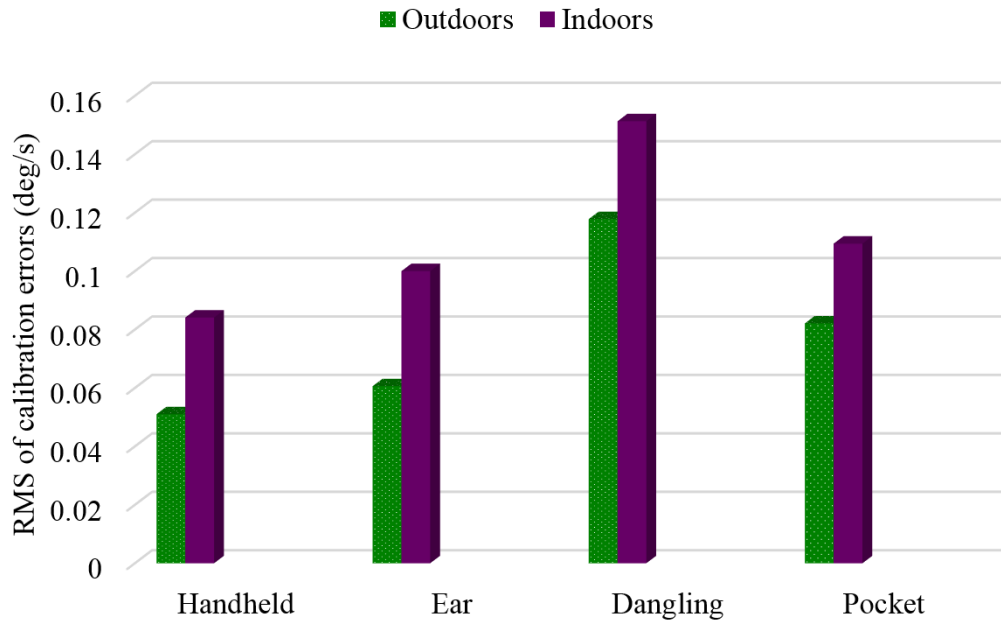


Figure 3-13. Calibration errors under typical motions both indoors and outdoors

CHAPTER 4: SELF-CONTAINED NAVIGATION WITH SENSORS AND MAGNETIC FEATURES

4.1 Introduction

The aim of this chapter is to provide a navigation solution that uses off-the-shelf sensors in consumer devices and is independent from any external infrastructure. Therefore, the algorithm should be able to provide continuous and reliable navigation results in indoor environments that does not have any WiFi signal or have WiFi signals with weak distribution. Considering the popularization of MEMS sensors and the omnipresence of magnetic field, this research combines sensor-based DR and MM to obtain the navigation solution.

Sensor-based DR algorithms are ideal for providing seamless indoor/outdoor navigation information, but suffer from accumulation of navigation errors due to the existence of sensor errors and the integration calculation in the DR mechanization. The research in Chapter 3 can significantly mitigate the drifts of navigation solutions, but cannot eliminate them because these drifts are the issue inherent to the DR mechanization. Therefore, to obtain navigation results with long-term accuracy, external positioning information is still needed to correct the DR solution.

To find a proper source to aid DR, environment features should be on the list because of their omnipresence. As reviewed in Chapter 1, indoor magnetic interferences have been exploited as fingerprints or landmarks to enhance navigation ([Xie et al., 2014](#), [Subbu et al., 2013](#)). A main challenge for MM is that the performance of MM is highly dependent on the LMF ([Pritt, 2014](#), [Li et al., 2015b](#)): MM solutions may be accurate in some areas but suffered from mismatches (e.g., matching to a point that is over 20 m away from the true value) in other areas. Therefore, when

integrating MM with other technologies, the key to enhance the navigation performance is to mitigate the impact of MM mismatches.

Furthermore, since indoor environments are commonly complex and unpredictable, it is preferred that the navigation algorithm is intelligent enough to set the weight of the MM positioning results and filter out MM mismatches automatically. For this purpose, this research uses a two-level mechanism mitigate the effect of MM mismatches. On the first level, the history of the LMF is investigated to remove the MM fingerprints that have indistinct features. On the second level, two strategies are introduced, including Strategy (a) that uses a threshold-based mechanism that sets the measurement noises of MM positions (i.e., the MM position uncertainties) based on their distances to the historical DR/MM position solutions, and Strategy (b) that uses an AKF that introduces the estimation of covariance of the innovation sequences into the calculation of the KF gain matrix directly instead of adjusting the KF measurement noises.

Also, to improve the performance of MM, several approaches are used. For example, (a) this research uses the profile-matching method in indoor pedestrian navigation. Specifically, it calculates the rough length of the measured profile using the steps detected by accelerometers, and utilizes the dynamic time warping (DTW) algorithm for matching with inaccurate profile length. (b) This research detects the roll and pitch angles using accelerometers in consumer devices and extract the vertical and horizontal magnetic intensities to increase the magnetic fingerprint dimension. (c) This research introduces the KNN algorithm, which is commonly used in WiFi fingerprinting, into MM to improve its robustness. Finally, (d) this research utilizes magnetic gradient fingerprints, instead of magnetic intensity fingerprints, to mitigate the effect of the hardware diversities and biases of magnetometers in mobile devices.

This chapter is organized as follows: Section 4.2 explains the magnetic matching algorithm; Section 4.3 describes details about the hybrid DR/MM algorithm; Section 4.4 shows the tests and results, and Section 4.5 provides the summary.

4.2 Magnetic Matching

MM is achieved in two steps: training and positioning. Training is conducted to build or update a <location, magnetic> DB that consists of a set of RPs with known coordinates and magnetic features, while the positioning step is implemented to find the closest match between the measured magnetic profile and those stored in the DB. These steps are described in this section.

4.2.1 Training step for magnetic matching

The key to generating a reliable DB is obtaining accurate RP coordinates. The choice of the DB training method is a trade-off between cost and accuracy. Different training approaches have been researched according to various requirements. Point-by-point methods can also improve the DB reliability by averaging the measurements at each RP ([Cheng et al., 2014](#)), but are time-consuming and labor-intensive ([Bolliger, 2008](#)). To reduce the cost, this research adopts the walk-survey method, which is based on floor plans (i.e., the true position of corners and intersections, and the true orientation of corridors), and constant-speed assumption. To use this method, a surveyor walks with a constant speed along each link between landmarks over the pre-designed path; therefore, the coordinates of RPs on the links are calculated by the arrival time and the geometrical relationship between landmarks. The walk-survey method is less accurate than the point-by-point method but significantly more time-effective. In this research, the steps detected by accelerometers are used to ease the constant-speed assumption to the constant-step-length assumption, and the short-term heading changes calculated from gyros are utilized to remove the requirement for straight walking.

Another reason for choosing the walk-survey method is that this research aim to obtain robust navigation solutions when MM results are not reliable, instead of obtaining the optimal MM results.

Magnetometers on smartphones have high sampling rates (commonly above 10 Hz). Therefore, all steps are stored as MM RPs. Additionally, it is assumed that the device moves with a constant speed between two adjacent steps; thus, the magnetic intensity at a set of points between these steps can be calculated through interpolation. The interpolated points are also stored as RPs. The fingerprint at the k-th RP is recorded as

$$\mathbf{FM}_k = \{\mathbf{pos}_k, \mathbf{m}_k\} \quad (4-1)$$

where \mathbf{pos}_k is the location of RP_k , and \mathbf{m}_k is the magnetic vector at RP_k .

With accelerometer-derived horizontal angles, the vertical and horizontal magnetic intensities can be extracted. The magnetometer measurement vector in the b-frame can be transferred to that in the n-frame by

$$\mathbf{B}^n = \mathbf{C}_b^n \mathbf{B}^b \quad (4-2)$$

where the DCM \mathbf{C}_b^n can be represented as ([Shin, 2005a](#))

$$\mathbf{C}_b^n = \begin{bmatrix} \cos \theta \cos \psi & -\cos \phi \sin \psi + \sin \phi \sin \theta \cos \psi & \sin \phi \sin \psi + \cos \phi \sin \theta \cos \psi \\ \cos \theta \sin \psi & \cos \phi \cos \psi + \sin \phi \sin \theta \sin \psi & -\sin \phi \cos \psi + \cos \phi \sin \theta \sin \psi \\ -\sin \theta & \sin \phi \cos \theta & \cos \phi \cos \theta \end{bmatrix} \quad (4-3)$$

where ϕ , θ , and ψ are the roll, pitch, and heading angles.

Denoting $\mathbf{B}^b = [B_x \ B_y \ B_z]^T$ and $\mathbf{B}^n = [B_N \ B_E \ B_D]^T$, the vertical magnetic intensity can be calculated by

$$B_D = -\sin \theta \cdot B_x + \sin \phi \cos \theta \cdot B_y + \cos \phi \cos \theta \cdot B_z \quad (4-4)$$

The magnetic intensity \mathbf{m} vector is $\mathbf{m} = [B \ B_D \ B_H]$, where $B = |\mathbf{B}^b|$ is the total magnetic intensity, and $B_H = \sqrt{B^2 - B_D^2}$ is the horizontal magnetic intensity.

Furthermore, this research applies magnetic gradient vectors, instead of magnetic intensity vectors, to mitigate the effect of the hardware diversities and biases of magnetometers. A magnetic gradient vector is generated by using every element in a magnetic intensity vector to subtract the first element in this vector, that is

$$\Delta\mathbf{m} = \mathbf{m} - m_0 \quad (4-5)$$

where $\Delta\mathbf{m}$ is the magnetic gradient vector, m_0 is the first element in the magnetic intensity vector \mathbf{m} .

4.2.2 Positioning step for magnetic matching

The basic idea of the profile-based MM is calculating the difference between the measured profile and the candidate profiles to find the optimal match. The “match” can be indicated by a certain formula, such as the two-dimensional Euclidean distance between two profiles:

$$D_i = |S - M_i| \quad (4-6)$$

where S and M_i are the measured profile and the i -th candidate profile, respectively, and D_i is the Euclidean distance between these profiles. Since it is difficult to estimate the accurate step length, this research utilizes the DTW algorithm ([Zhen et al., 2012](#)), which is originally used in the speech recognition field, for matching with inaccurate profile length.

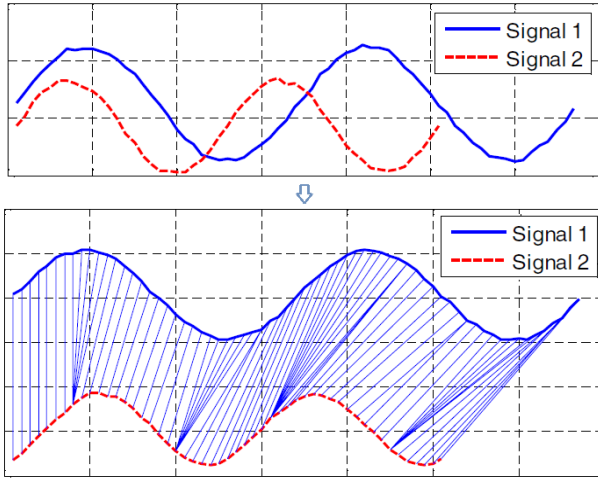


Figure 4-1. Aligning two sequences using DTW ([Zhen et al., 2012](#))

As shown in Figure 4-1, the technique in DTW is to compress or stretch the time axis of both (or one) sequences to achieve a better alignment. The goal is to find the best match between two sequences, $\mathbf{s}(i)$, $i = 1, 2, \dots, A$ and $\mathbf{m}(j)$, $j = 1, 2, \dots, B$, of different lengths ($A \neq B$). The best match is found by obtaining the optimal warping path w . The distance in DTW is defined as the minimum distance starting from the beginning of the DTW matrix to the current position (i, j) . The DTW matrix component $\mathbf{D}(i, j)$ can be computed by

$$\mathbf{D}(i, j) = \mathbf{d}(i, j) + \min(\mathbf{D}(i-1, j), \mathbf{D}(i, j-1), \mathbf{D}(i-1, j-1)) \quad (4-7)$$

where $\mathbf{D}(i, j)$ is the node cost associated with $\mathbf{s}(i)$ and $\mathbf{m}(j)$, $\mathbf{d}(i, j)$ can be represented as

$$\mathbf{d}(i, j) = (\mathbf{s}(i) - \mathbf{m}(j))^2 \quad (4-8)$$

To mitigate the impact of MM mismatches, this research also uses the KNN method, which is commonly used in WiFi fingerprinting ([Peng et al., 2011](#)), in MM. This method estimates the position by a weighted sum of the position of the k selected profiles that have the smallest Euclidean distances to the measured profile.

$$\hat{\mathbf{r}} = \sum_{i=1}^k \left(\frac{c_i}{C} \mathbf{r}_i \right) \quad (4-9)$$

where $c_i = 1/d_i$, $C = \sum_{i=1}^k c_i$, \mathbf{r}_i is the position of the i-th selected profile, and $\hat{\mathbf{r}}$ is the estimated position. The position of a profile denotes the position of the end point of this profile.

4.3 Hybrid DR/MM Navigation

In this research, the sensor-based DR algorithm is divided into two modules: attitude determination and position tracking, as shown in Figure 4-2. In the attitude-determination module, gyro-based attitude mechanization calculates continuous attitude predictions, while multi-level constraints update information through a KF. After obtaining the heading from the attitude-determination module, the position-tracking module utilizes PDR to provide position predictions and uses available MM positions as updates. The attitude-determination algorithm has been described in Chapter 3. Thus, this section only introduce the position-tracking KF algorithm, which is used to fuse predictions from PDR and updates from MM.

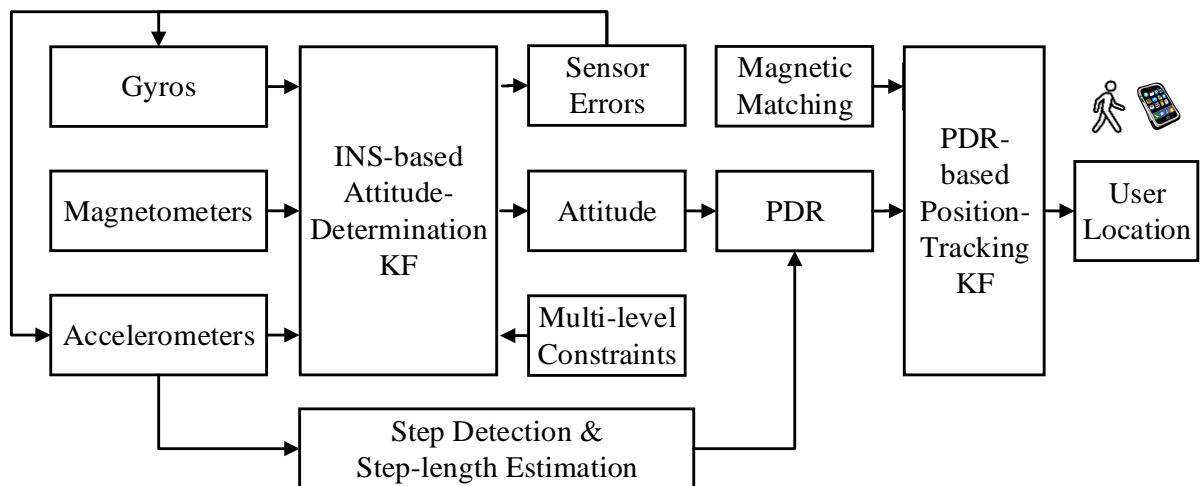


Figure 4-2. Two-filter based DR algorithm

4.3.1 Position-tracking KF system model

PDR is a relative means of determining of a new position from a previous known position using the latest heading and step length (or velocity). The system model is

$$\begin{bmatrix} \delta\dot{\varphi} \\ \delta\dot{\lambda} \\ \delta\dot{\psi} \\ \delta\dot{v} \end{bmatrix} = \begin{bmatrix} (-v \sin \psi \cdot \delta\psi + \cos \psi \cdot \delta v) / (R_m + h) \\ (v \cos \psi \cdot \delta\psi + \sin \psi \cdot \delta v) / [(R_n + h) \cos \varphi] \\ w_\psi \\ w_v \end{bmatrix} \quad (4-10)$$

where φ , λ , ψ , and v are latitude, longitude, heading and velocity, respectively; $\delta\varphi$, $\delta\lambda$, $\delta\psi$, and δv are the corresponding errors. w_ψ and w_v are the noises of heading and velocity; R_m and R_n are the radius of curvature of meridian and curvature in the prime vertical; and h is the altitude.

4.3.2 Position-tracking KF measurement model

MM positions are used to build the measurement model

$$\begin{bmatrix} \hat{\varphi}_{DR,k+1} - \tilde{\varphi}_{MM,k+1} \\ \hat{\lambda}_{DR,k+1} - \tilde{\lambda}_{MM,k+1} \end{bmatrix} = \begin{bmatrix} \delta\varphi + n_\varphi \\ \delta\lambda + n_\lambda \end{bmatrix} \quad (4-11)$$

where $\hat{\varphi}_{DR}$ and $\hat{\lambda}_{DR}$ are the latitude and longitude predicted by DR; $\tilde{\varphi}_{MM}$ and $\tilde{\lambda}_{MM}$ are the latitude and longitude from MM, and n_φ and n_λ are the measurement noises.

MM positioning results may suffer from mismatches ([Pritt, 2014](#), [Li et al., 2015b](#)), therefore, the integrated navigation algorithm should be able to set the weight of the MM positioning results and filter out MM mismatches automatically. For this purpose, this research introduces a two-level

mechanism to mitigate the effect of MM mismatches in indoor pedestrian applications. This mechanism is explained in the next subsection.

4.3.3 Mechanism for improving robustness of DR/MM solution

This research uses a two-level mechanism to mitigate the effect of MM mismatches on the DR/MM solution. On Level #1, the history of the LMF is investigated to remove the MM fingerprints with indistinct features. In Level #2, two strategies are used to set or tune the weight of MM position results in the DR/MM algorithm. Therefore, Level #1 is related with only the MM measurements, while Level #2 is on the DR/MM integration level. These strategies are explained separately.

(1) Level #1: mismatch detection on MM measurements

On this level, MM is conducted only when there is distinct magnetic feature in the MM fingerprint. The change range (i.e., the difference between the maximum and the minimum values) and the standard deviation value of the magnetometer measurement during a certain time period are calculated to detect the fingerprints with indistinct features. Specifically, the fingerprint T is detected to have magnetic gradients when $Diff_T > th_{m1}$ and $Std_T > th_{m2}$, where $Diff_T$ and Std_T are the range and standard deviation of the magnetic intensities at T respectively, th_{m1} and th_{m2} are the corresponding threshold values. If this is the case, the MM fingerprints pass the Level #1 mismatch-detection test, and are used for positioning.

(2) Level #2: threshold-based approach

For the threshold-based method, the MM position uncertainties at time k are set based on the distance d_k between the new MM position and the historical DR/MM position solutions: when $d_k \leq th_{mm1}$, the MM position uncertainties are set at σ_{mm} ; when $th_{mm1} < d_k \leq th_{mm2}$, the position

uncertainties are set as $s_{mm}\sigma_{mm}$, where s_{mm} is a scalar; when $d_k > th_{mm2}$, the position uncertainties are set as a large number σ_{mmMax} . In this situation, the new MM position will not contribute to the solution. th_{mm1} and th_{mm2} are empirical threshold values determined by preliminary tests in the same area. In this research, the values of th_{mm1} and th_{mm2} were set at the one time and three times of the expected accuracy of the DR/MM navigation solution σ_{mm} (e.g., 5 m); and the value of s_{mm} was set at d_k / σ_{mm} .

(3) Level #2: AKF based on innovation covariance estimation

Other than the threshold-based mechanism, an adaptive approach that uses an AKF is also utilized, which introduces the covariance estimation of the innovation sequence (i.e., the difference between the MM position updates and the position predicted by DR/MM) into the calculation of the KF gain matrix directly instead of adjusting the KF measurement covariance matrix (R). The AKF algorithm follows the research in ([Fang and Yang, 2011](#)). In this AKF, the innovation sequence is a directly observable parameter, which can be used as a reference for the filter performance by observing the covariance of the innovation sequence. In this case, when the value of the innovation sequence increases, the estimated innovation covariance will also increase. In turn, the filter gain will decrease, which indicates that the AKF depends less on the MM results. The AKF algorithm is shown as follows.

KF Prediction:

$$\hat{\mathbf{X}}_{k/k-1} = \Phi_{k/k-1} \hat{\mathbf{X}}_{k-1} \quad (4-12)$$

$$\mathbf{P}_{k/k-1} = \Phi_{k/k-1} \mathbf{P}_{k-1} \Phi_{k/k-1}^T + \mathbf{Q}_{k-1} \quad (4-13)$$

Innovation covariance estimation:

$$\tilde{\mathbf{Y}}_k = \mathbf{Z}_k - \mathbf{H}_k \hat{\mathbf{X}}_{k/k-1} \quad (4-14)$$

$$\hat{\mathbf{C}}_{\tilde{\mathbf{Y}}_k} = \frac{1}{N} \sum_{i=k-N+1}^k \tilde{\mathbf{Y}}_k \tilde{\mathbf{Y}}_k^T \quad (4-15)$$

KF update:

$$\mathbf{K}_k = \mathbf{P}_{k/k-1} \mathbf{H}_k^T \hat{\mathbf{C}}_{\tilde{\mathbf{Y}}_k}^{-1} \quad (4-16)$$

$$\hat{\mathbf{X}}_k = \hat{\mathbf{X}}_{k/k-1} + \mathbf{K}_k \tilde{\mathbf{Y}}_k \quad (4-17)$$

$$\mathbf{P}_k = [\mathbf{I} - \mathbf{K}_k \mathbf{H}_k] \mathbf{P}_{k/k-1} \quad (4-18)$$

where $\hat{\mathbf{X}}_{k/k-1}$ and $\mathbf{P}_{k/k-1}$ represent the *a priori* state estimation and covariance matrix at the epoch k ; $\hat{\mathbf{X}}_{k-1}$ and $\hat{\mathbf{X}}_k$ are *a posteriori* state estimation at the epochs $k-1$ and k , and \mathbf{P}_{k-1} and \mathbf{P}_k are *a posteriori* error covariance matrices; $\hat{\mathbf{C}}_{\tilde{\mathbf{Y}}_k}$ represents the innovation covariance estimation, $\tilde{\mathbf{Y}}_k$ is the innovation sequence, and \mathbf{K}_k is the filter gain; N is the window size over which the moving average $\tilde{\mathbf{Y}}_k \tilde{\mathbf{Y}}_k^T$ is taken as the estimation of the innovation sequence; \mathbf{H}_k is the design matrix, \mathbf{Q}_{k-1} is the system noise matrix, $\Phi_{k/k-1}$ is the system transformation matrix, and \mathbf{I} is the unit matrix.

4.4 Tests and Results

Walking tests with Samsung Galaxy S4 and Xiaomi 4 (S4 for training, and Xiaomi for positioning) smartphones were conducted in two indoor environments: building E that has frequent and severe magnetic interferences (the change of magnetic intensity reached 0.4 Gauss), and building B with less and weaker magnetic interferences (the change of magnetic intensity was below 0.25 Gauss). The sample rates for gyros, accelerometers, and magnetometers were set at 20

Hz. The interpolation distance for the magnetic DB was set at 0.1m. The tested motion conditions comprised typical phone motion conditions, including handheld, phoning, dangling, and in a pants pocket.

4.4.1 Tests at building E

The magnetic DB was generated by using four trajectories, as shown in Figure 4-3. Each trajectory lasted for 5-10 minutes. Coordinates of landmarks (i.e., corners, intersections, and start and end points) and orientations of corridors were obtained from the Google Earth.

The accuracy of RP positions in the walk-survey method was evaluated by using by walking on a straight path with known length for 50 times, and comparing the PDR-derived distance and the path length. The RMS value of the results of dividing the former with the latter was 1.12. Therefore, if there is not any averaging mechanism when determining the RP locations on one links, the maximum errors of RP positions may reach 10-20 percent of the length of the link, which is not acceptable. To assure the accuracy of the DB, dense landmarks were used to correct the PDR solution. The maximum distance between two adjacent landmarks was 10 m. This indicates that the maximum value of the RP location errors was approximate 1-2 m. Considering the averaging mechanism on each link, the actual position error of each RP should be much less than this value. Therefore, the RP locations obtained by the walk-survey method that used dense landmarks was accurate enough to build the DB and to generate reference trajectories for the positioning tests.



Figure 4-3. Trajectories used to generate magnetic DB

Figure 4-4 demonstrates the RPs in the DB, in which the colors indicate the magnetic intensity. The magnetic intensity was within 0.5 – 0.6 Gauss (the local geomagnetic intensity was 0.57 Gauss) at most of outdoor RPs, but varied from 0.3 Gauss to 0.8 Gauss indoors.

In the positioning process, the profile length for MM was set at 10 steps: MM started when the user had walked for 10 steps; after that, the magnetic fingerprints within the last 10 steps were used. The number k was set at 3 for the KNN approach. The threshold values for the mismatch detection Level #1 were set at $th_{m1} = 0.15$ Gauss and $th_{m2} = 0.1$ Gauss. The threshold value for detecting MM blunders using DR/MM solutions were set at $th_{mm1} = 10$ m, $th_{mm2} = 20$ m, and $\sigma_{mm} = 5$ m. The value N in the AKF was set at 3.

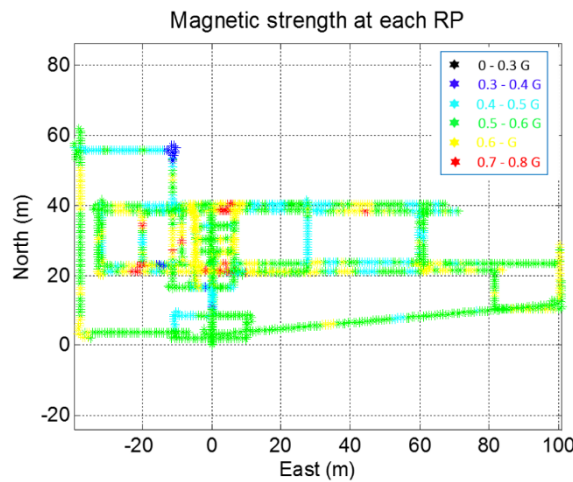


Figure 4-4. Distribution of magnetic intensities at E

Figure 4-5 illustrates the ranges of measured magnetic profiles in a test. The yellow and blue lines on the x-axis indicate indoors and outdoors. It was indicated that the magnetic features are more distinct indoors than outdoors.

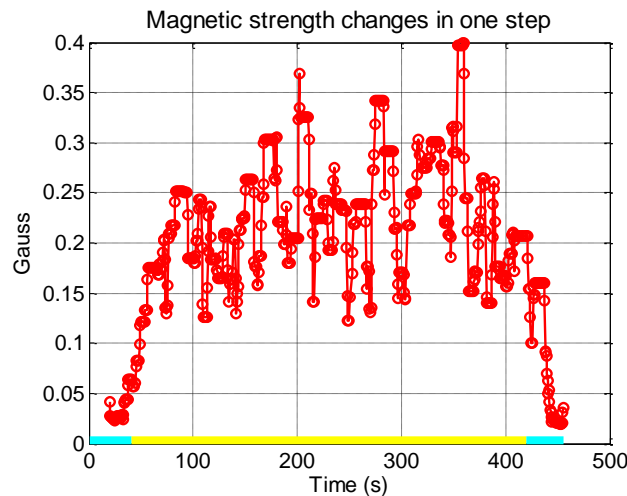


Figure 4-5. Magnetic ranges in magnetic profiles in one test

The test trajectory at E is illustrated in Figure 3-9, which is different from the training trajectories. Also, the walk direction on most of the main corridors were opposite from those on the training trajectories. Each test lasted for over 6 minutes.

This research compared the navigation solutions from six combinations of DR and MM:

- a) DR;
- b) MM1: MM results with Level #1 mismatch detection;
- c) MM2: MM results with Level #1 and #2 mismatch detection;
- d) DR/MM1: integrating DR and MM1 using KF;
- e) DR/MM2: integrating DR and MM2 using KF;
- f) DR/MM3: integrating DR and MM1 using AKF.

As illustrated in Figure 3-3, dangling and pocket provided stronger device dynamics than handheld and phoning motion conditions. Therefore, Figures 4-6 and 4-7 demonstrate the handheld and dangling results as examples. In each figure, (a) – (f) represent the results for DR, MM1, MM2, DR/MM1, DR/MM2, and DR/MM3, respectively.

Figures 4-6 and 4-7 indicate that DR solutions were continuous and had a similar shape as the true trajectories; however, the heading errors accumulated and led to position errors. Therefore, external positioning technologies were needed to correct for DR errors to provide long-term accuracy.

MM1 suffered from significant mismatches even when the MM measurements with indistinct features had been filtered out. Thus, it is necessary to further detect MM mismatches. The majority of these mismatches were eliminated through Level #2 mismatch detection by using the threshold-based method.

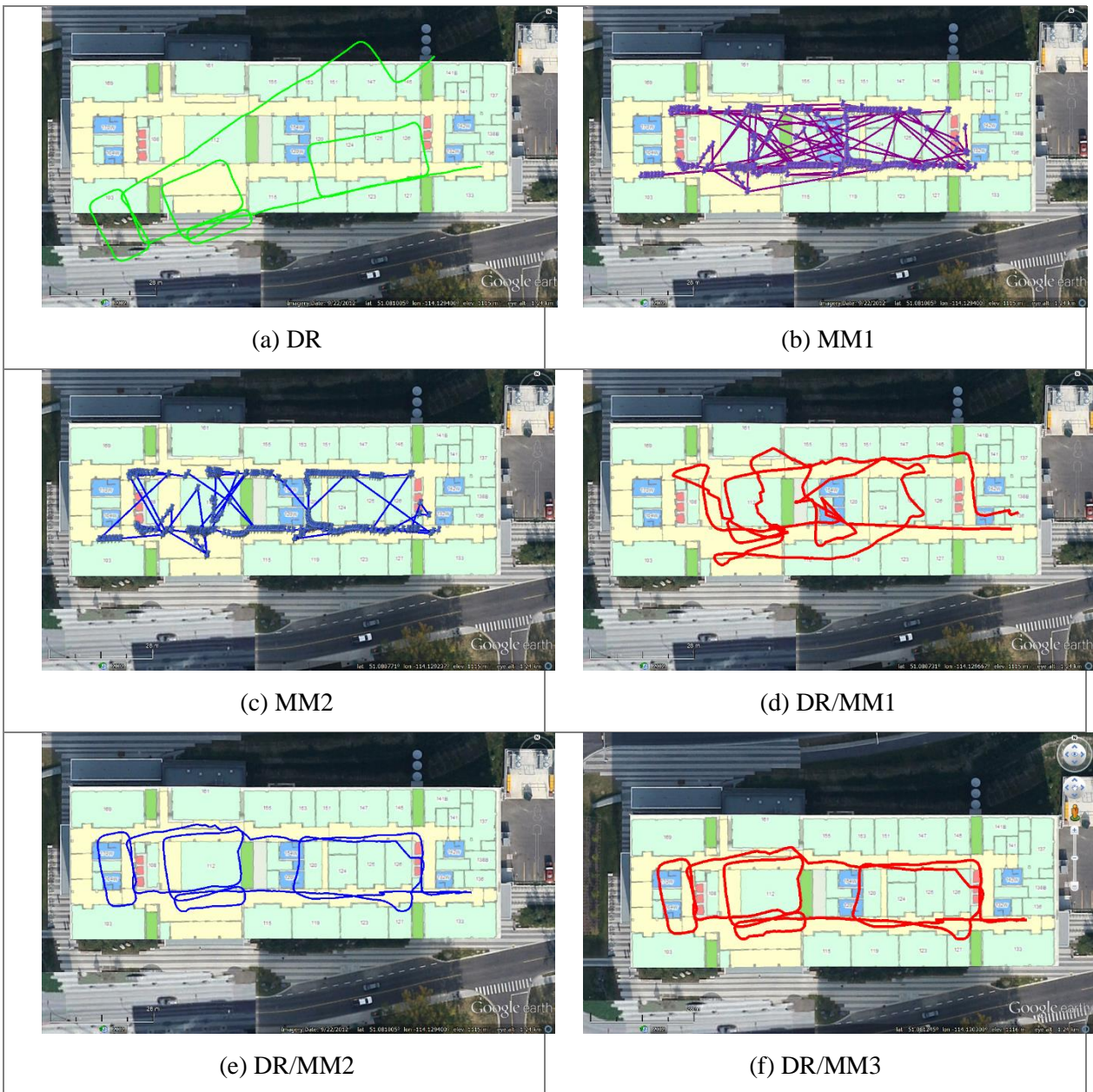


Figure 4-6. Positioning results at E (handheld)

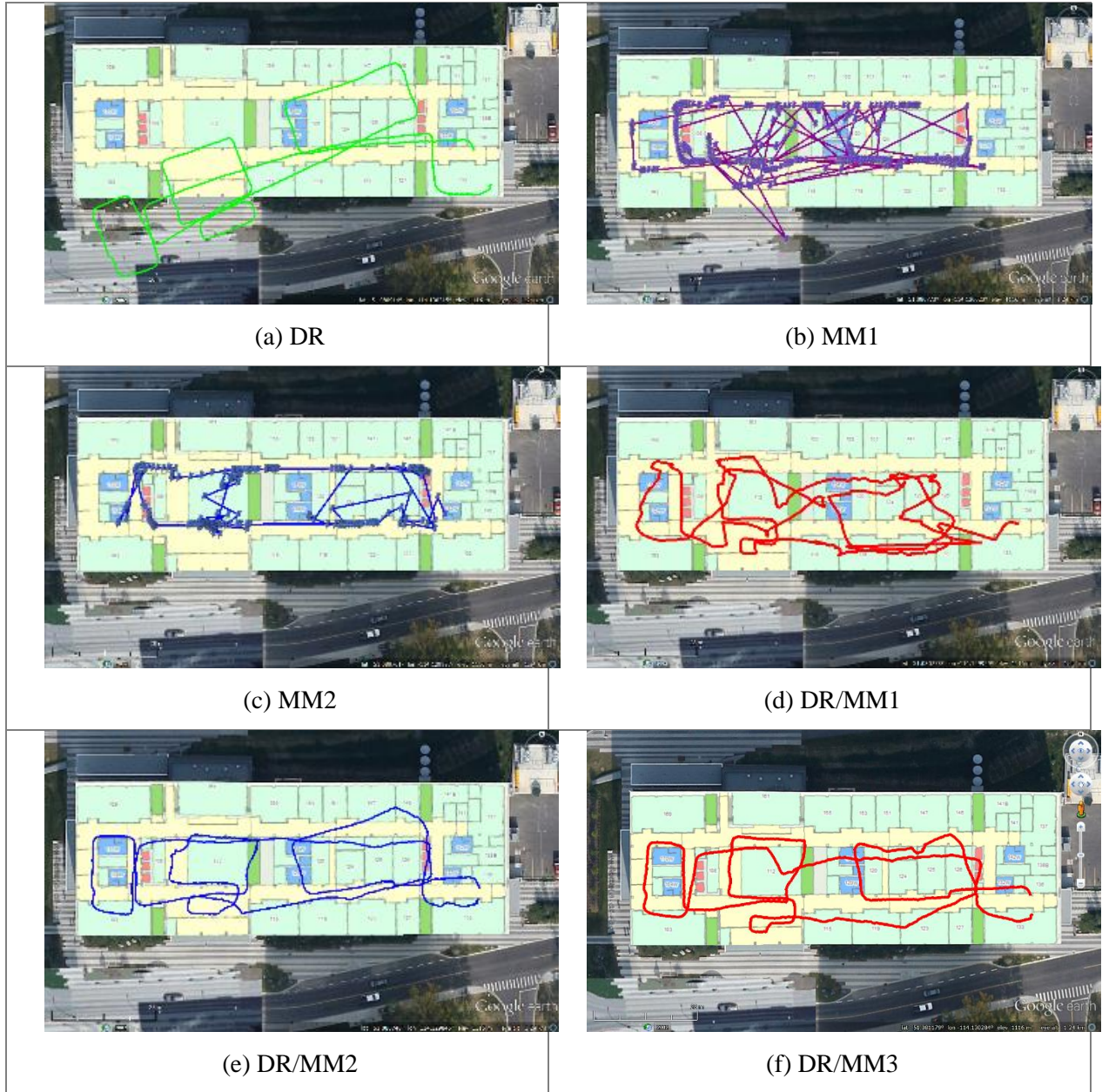
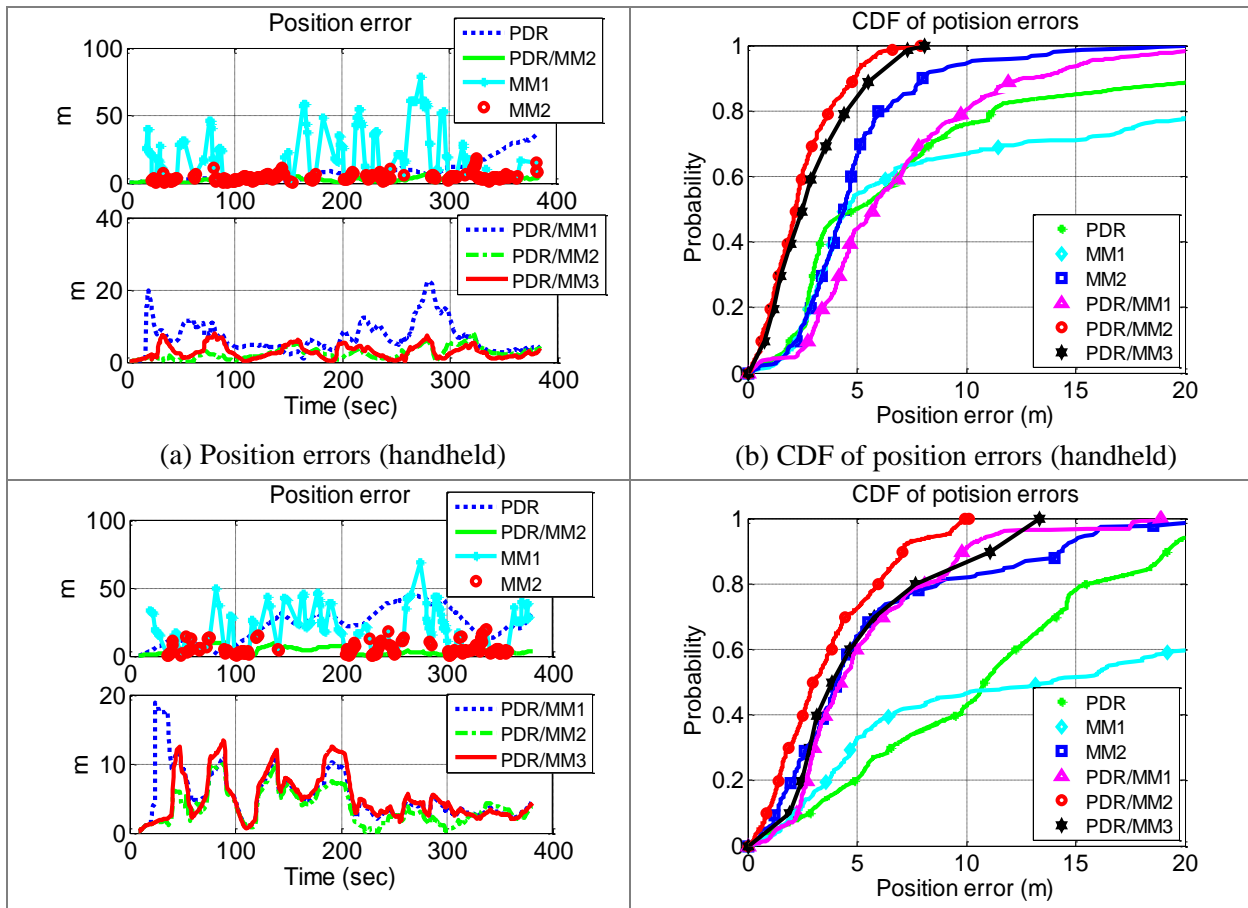


Figure 4-7. Positioning results at E (dangling)

Due to the existence of MM mismatches, the DR/MM1 results diverged from the true values on several occasions. However, in DR/MM2 and DR/MM3 results, these divergences were eliminated, and the shape of the results became closer to that of the reference trajectory. This outcome indicates the importance of mismatch detection in the DR/MM integration algorithm.

Figure 4-8 demonstrates the results when using different combinations of DR and MM under four motion conditions. The reference positions were obtained by using a floor plan to correct DR solutions. This process was similar to the work in the DB-training step. The left figures illustrate the error distances (i.e., the distance between position results and the corresponding reference values), while the right figures show the corresponding cumulative distribution function (CDF) curves.

The trends of MM solutions were correlated with time (or area): MM errors were below 10 m during some time periods but reached over 30 m during some other periods, for example, 50-100 s, 150-200 s, and 250-300 s. The largest MM error reached over 60 m. The largest error was reduced to nearly 20 m in MM2, which indicated that most of the mismatches were removed.



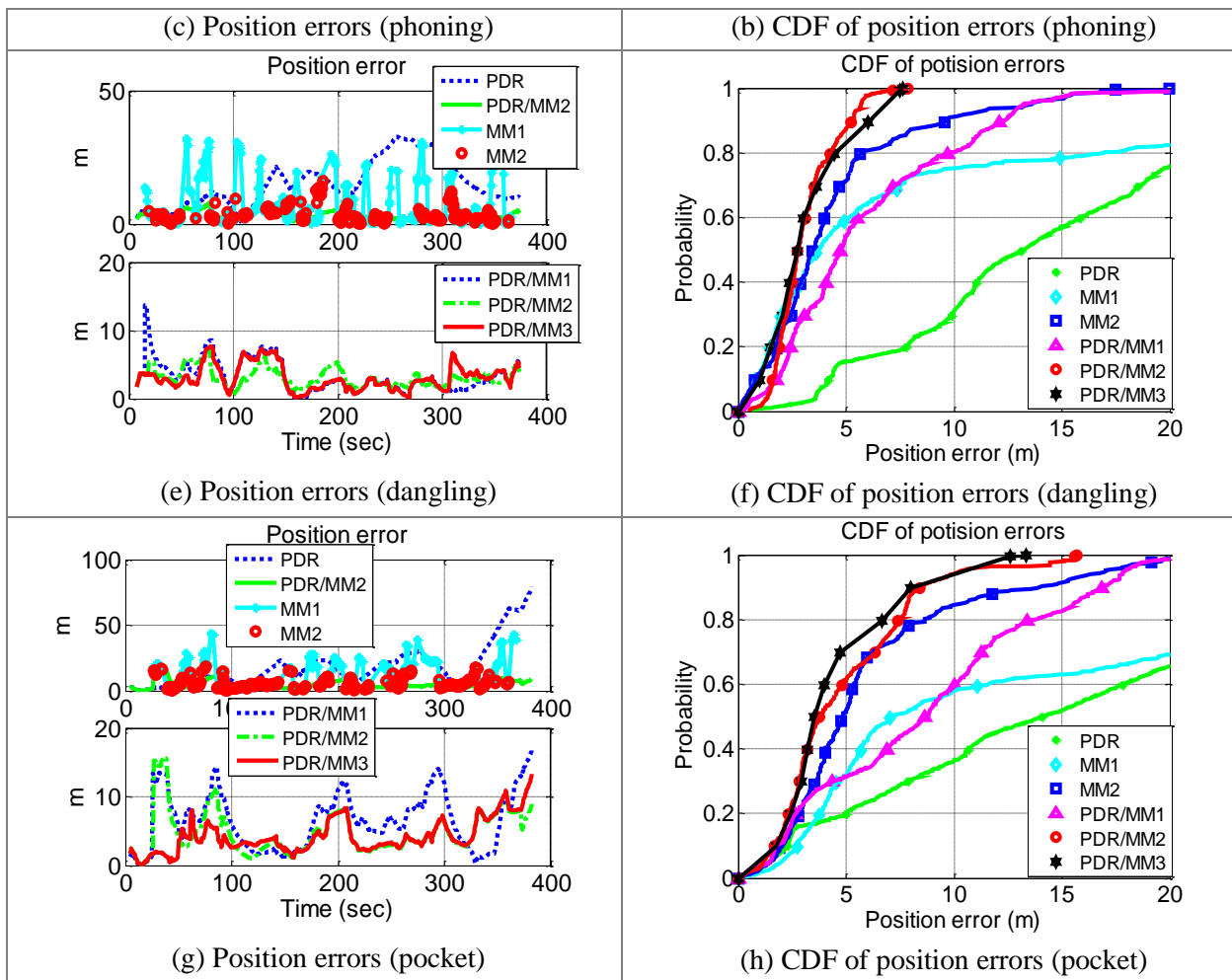


Figure 4-8. Position errors and corresponding CDF with different combinations of PDR and MM at E

When DR/MM2 or DR/MM3 was utilized, the position errors were at a same level under all tested motion conditions, which indicated that DR became less dependent on device movement when integrated with MM. Furthermore, the errors of both PDR/MM2 and PDR/MM3 results were significantly smaller than those of PDR/MM1. Taking the handheld result for example, the significant errors during 0-100 s and 250-300 s were mitigated.

The RMS values of position errors are shown in Table 4-1. Columns 2 - 6 illustrate the RMS values when using different combinations of DR and MM. The last row (i.e., general) provides the RMS of the values in the same column.

Table 4-1. RMS of position errors (unit: m) at E

Motion	DR	MM1	MM2	DR/MM1	DR/ MM2	DR/ MM3
Handheld	11.4	20.9	5.8	8.1	2.9	3.4
Phoning	12.2	25.4	7.5	6.5	4.4	6.0
Dangling	17.2	13.7	5.7	7.4	3.4	3.6
Pocket	24.4	18.2	7.7	10.2	5.8	4.9
General	17.1	20.0	6.7	8.2	4.3	4.6

Not only the the RMS values of DR errors, but also those of MM errors varied under different phone motions. The variety of DR errors was probably caused by the differences of sensor errors in n-frame when motion changed. The variety of MM errors indicated that motion conditions might also influent the performance of MM.

MM errors were reduced from 20.0 m to 6.7 m (improved by 66.5 %) by using the threshold-based method. When these MM results were used as position updates, the RMS value of the DR/MM position errors was reduced to 4.3 m in general. Meanwhile, when the AKF was used, the RMS value of position errors was 4.6 m in general. These outcomes show that both the threshold-based and AKF-based methods can significant mitigate the impact of MM mismatches. If external positioning technologies such as WiFi or bluetooth was applied, the performance may be further enhanced.

4.4.2 Tests at Building B

The test area at B is mainly used for walking. Therefore, there are less metallic infrastructures when compared with E. This area was approximately $140 \times 60 \text{ m}^2$. Figure 4-9 illustrates the indoor test environment, and Figure 4-10 shows the magnetic distributions on the test trajectory.

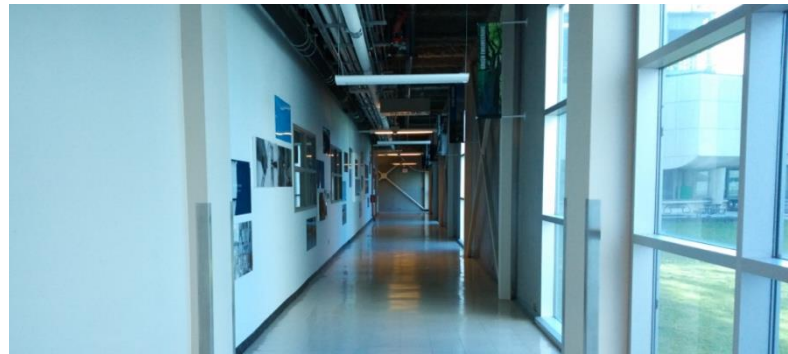


Figure 4-9. Indoor test environment at B

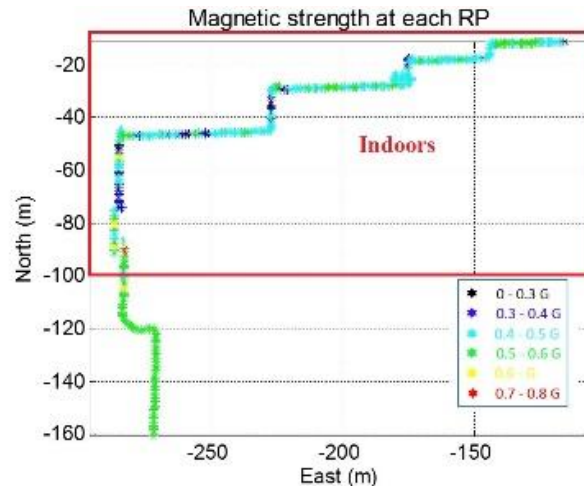


Figure 4-10. Magnetic intensities on test trajectory at B

Real-world indoor environments are commonly complex and unpredictable. Thus, although the environment at B was different from that at E, the same set of navigation parameters was used to evaluate the consistency of the proposed algorithm. Figure 4-11 illustrates the handheld results as

examples, in which (a) - (f) show the position results of DR, MM1, MM2, DR/MM1, DR/MM2, and DR/MM3, respectively.

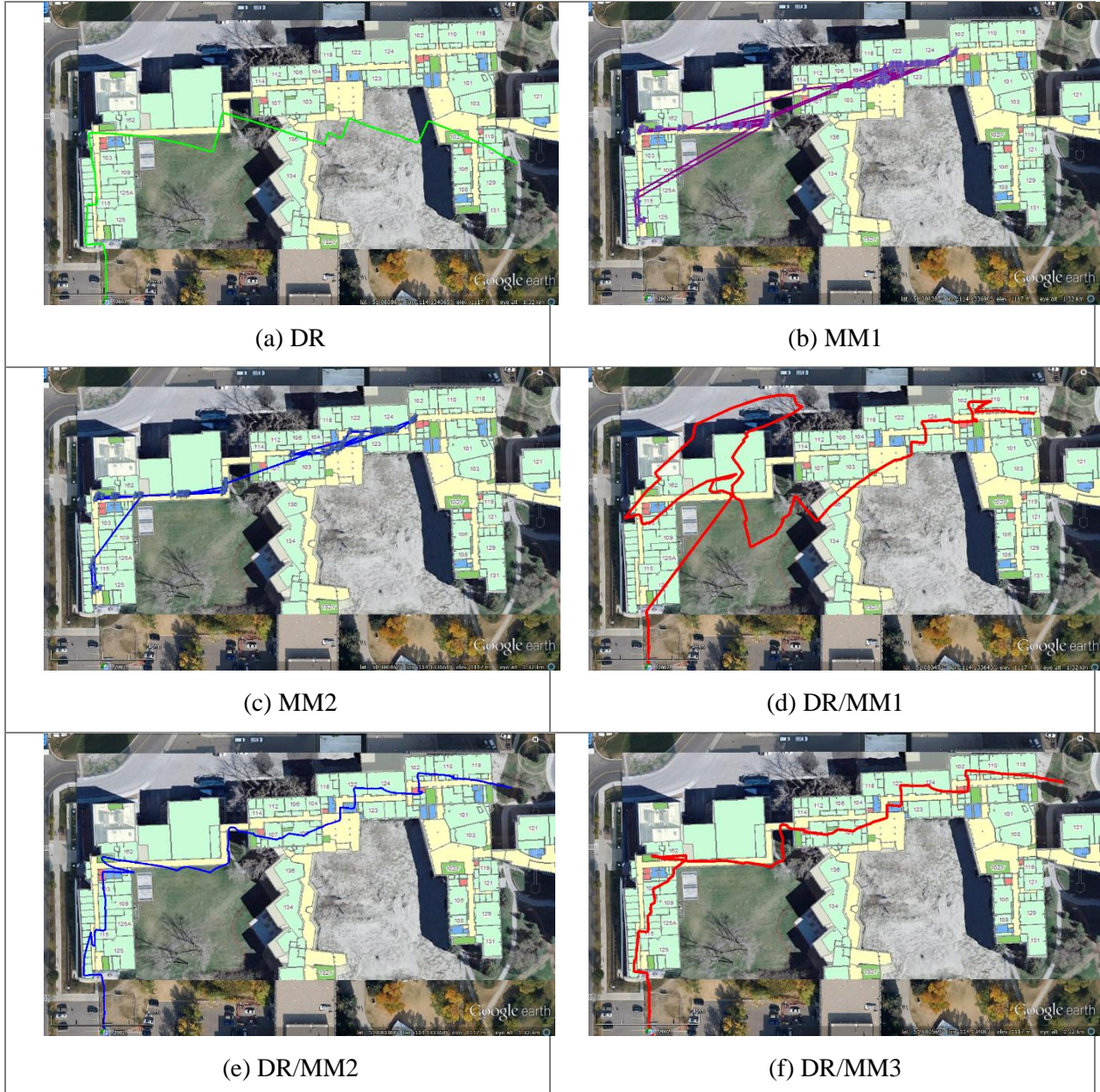


Figure 4-11. Positioning results at B (handheld)

Similar to the results at E, there were significant matches in the MM1 results. Accordingly, the PDR/MM1 result diverged in the middle area but went back to the right track in the end. However,

most of these mismatches were eliminated through mismatch detection on the DR/MM level by either using the threshold-based method or the AKF. The left figure in Figure 4-12 illustrates the error distances when using different strategies, while the right figure show the corresponding CDF.

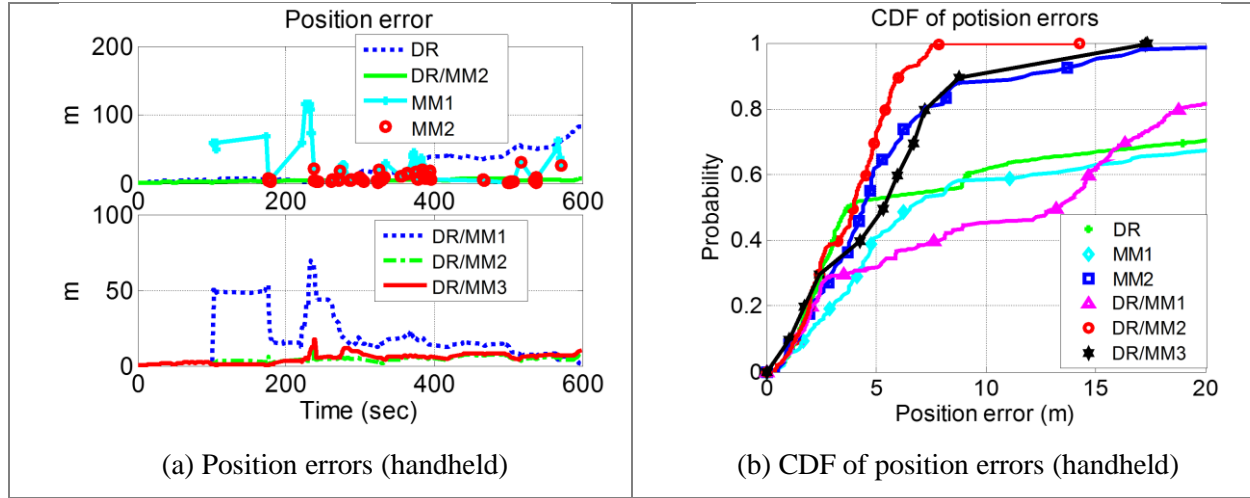


Figure 4-12. Position errors and corresponding CDF with different combinations of PDR and MM at B (handheld)

The MM results at B were sparser than those at E. The reason for this outcome was that more fingerprints were filtered out in Level #1 because the magnetic intensity changes were not significant at B. A sequence of DR/MM1 position errors reached over 40 m during 100 - 300 s. These errors were mitigated in the DR/MM2 and DR/MM3 results. At about 240 s, the significant MM errors were not totally eliminated in the DR/MM algorithm, which caused a jump in the DR/MM3 result. Even with such errors, the majority of the DR/MM2 and DR/MM3 errors were below 10 m. Table 4-2 demonstrates the RMS values of position errors at B.

The RMS value of MM1 errors at B (22.6 m) was 11.5 % larger than that at E (20.0 m). After mismatch detection on the DR/MM integration level, the difference was reduced to 2.9 % (the RMS value of MM2 errors was 6.9 m at B and 6.7 m at E).

Table 4-2. RMS of position errors (unit: m) at B

Motion	DR	MM1	MM2	DR/MM1	DR/ MM2	DR/ MM3
Handheld	30.2	26.0	7.1	20.9	5.1	5.7
Phoning	18.1	24.1	7.3	12.2	5.0	5.4
Dangling	20.4	17.1	7.4	14.1	5.4	5.7
Pocket	13.7	21.5	5.8	16.1	5.2	5.4
General	21.3	22.6	6.9	16.2	5.2	5.6

Both the threshold-based method and the AKF reduced the DR/MM position errors effectively in both environments. The RMS values of position errors with these two strategies were 4.3 m and 4.6 m at E, and 5.2 m and 5.6 m at B. These values were 47.6 % and 43.9 % less than those of the original DR/MM results at E, and 67.9 % and 65.4 % smaller than those at B.

The RMS values of the position errors when using the threshold-based method was 0.3 m and 0.4 m less than that when using the AKF at E and B, respectively, with a difference of 7.1 % and 6.5 %. Although the former method performed slightly better in our tests, the latter is totally adaptive and thus have more potentials.

4.5 Summary

The research in this chapter indicates the potential for continuous and reliable indoor navigation with off-the-shelf sensors in smartphones and magnetic features. However, the key is to mitigate the impact of frequent magnetic matching (MM) mismatches. The proposed algorithm and mismatch-detection strategies were tested by walking with two smartphones in two indoor environments that have different magnetic features, and under four device motion conditions. Both the threshold-based approach and the AKF were effective in our tests under two different indoor

environments. The RMS values of position errors when using these strategies under four different motion conditions (i.e., handheld, phoning, dangling, and pocket) were 4.3 m and 4.6 m in the area with frequent and severe magnetic interferences (the change of magnetic intensity reached 0.4 Gauss), and 5.2 m and 5.6 m in environment that had less and weaker magnetic interferences (the change of magnetic intensity was below 0.25 Gauss). The benefit of this algorithm is that it is totally self-contained, and the results were continuous and robust (i.e., no jump points).

This research can guide the improvement of the reliability of the navigation solution in challenging indoor environments that have frequent magnetic interferences. Furthermore, such a self-contained navigation algorithm can bridge short-term WiFi outages to provide continuous navigation results, and provide smoother and more reliable results when integrating with WiFi. Also, it can update WiFi DBs through a crowd-sourcing approach by using daily-life navigation solutions.

CHAPTER 5 HYBRID DR/WIFI/MM INDOOR NAVIGATION

5.1 Introduction

This chapter aims to further improve the performance of navigation, which uses consumer portable devices, when there are existing WiFi infrastructures. As reviewed in Subsection 1.2.1, WiFi receivers and transmitters are becoming ubiquitous, which has greatly promoted the development of WiFi positioning. On the other hand, there are challenges for reaching high WiFi accuracy, such as dependency on signal availability and geometry, RSS fluctuation due to NLoS conditions and multipath effects, and the time-variant nature of WiFi DBs. Although the effect of these issues can be mitigated by selecting important APs or adding APs at proper places, or conducting periodical DB training, it is not always affordable to modify the distribution of APs or to investigate the navigation environment in advance, or implement DB training periodically. When any of the above issues remain, the performance of WiFi positioning may be degraded.

Chapter 4 has indicated the potential of using MM to provide accurate position updates and utilize DR and MM to obtain a continuous and accurate navigation solution. From the perspective of estimation, it is expected that through fusing the information from DR, WiFi, and MM, one can obtain navigation results better than those from the integration of DR and MM. From the engineering perspective, different structures probably provide various results in practice. The main reason for this phenomenon is that each technology has its advantages and disadvantages, as illustrated in Chapters 1 and 2. Therefore, the performance of the integrated system is also largely dependent on the information fusion approach, i.e., how to maximize the advantages and minimize the disadvantages of each technology. This research compares various technologies or subsystems (e.g., DR, WiFi, MM, WiFi/MM, DR/WiFi, and DR/MM) and takes advantage of the merits of

each technology, and presents and evaluates two hybrid DR/WiFi/MM integration structures. This chapter describes the following aspects:

- The implementation of WiFi positioning. This research presents a profile-based WiFi fingerprinting algorithm by using the short-term trajectories from DR and geometrical relationships of various RPs in the space. The MD-DTW algorithm is introduced to match with inaccurate profile length for such a multi-dimensional system. Also, several important points – including AP localization and propagation-parameter determination, and utilization of differential RSS – are explained.
- The complementary characteristics of WiFi and MM. This research proposes a WiFi-aided MM algorithm, which uses the WiFi results to limit the MM search space to reduce both the mismatch rate and the computational load. The fusion of WiFi and MM are especially useful for improving the navigation applications that use medium or low-end consumer devices not equipped with gyros.
- The integration of DR, WiFi, and MM. This research provides designs for and evaluates two hybrid integration structures. Structure #1 utilizes the WiFi-aided MM algorithm, while Structure #2 uses both DR and WiFi results (i.e., the integrated DR/WiFi solutions) to limit the MM search space. Structure #2 is more effective than previous structures at detecting MM mismatches, even in areas with limited WiFi RSS or weak RSS distribution. Furthermore, a multi-level quality-control mechanism is designed, based on the interaction between different techniques, to improve the system's robustness. This mechanism has at least one more level than previous DR/WiFi/MM structures.

This chapter is organized as follows: Section 5.2 describes details about WiFi fingerprinting; Section 5.3 introduces the WiFi-aided MM algorithm; Section 5.4 explains the integration of DR, WiFi, and MM; Section 5.5 shows tests and results, and Section 5.6 provides the summary.

5.2 WiFi Fingerprinting

The $\langle \text{location}, \text{RSS} \rangle$ DB is generated simultaneous to the $\langle \text{location}, \text{magnetic} \rangle$ DB by using the floor-plan-aided walk-survey method described in Chapter 4. Compared with magnetometers, smartphones commonly have low WiFi update rates (e.g., 0.3 - 0.5 Hz for the tested Samsung Galaxy S3, S4 and Xiaomi 4 smartphones, and approximately 1 Hz for the tested Google Nexus 7 tablet, as recorded by the class “WifiManager” on the Android). Thus, new RSS values are combined with the coordinates of the latest step as a RSS fingerprint.

The flow chart and general description of the WiFi positioning algorithm is provided in Figure 5-1. The RSS values are first collected and pre-processed. The purpose of pre-processing is to improve the RSS reliability. Any RSS weaker than the threshold are filtered out. Moreover, the RSS at the latest two or three epochs are averaged to obtain a smoothed RSS. If there are enough (no less than four in this research) RSS values after pre-processing, the Euclidean distance between the smoothed RSS values and those in the DB are calculated to select the k RPs that have fingerprints closest to the measured fingerprint. The equation for this selection process is (2-2). To enhance the reliability, in this step, the selected k RPs should be close to one another; otherwise, an RP located far from others is regarded as a mismatch and removed. After this, the weighted average of the remaining selected RPs' positions is computed to obtain the positioning result. The equation for weighted averaging is (2-3). Finally, the current WiFi positioning result is compared with the latest historical positioning results. The current result may be treated as a mismatch if it locates far from the historical results.

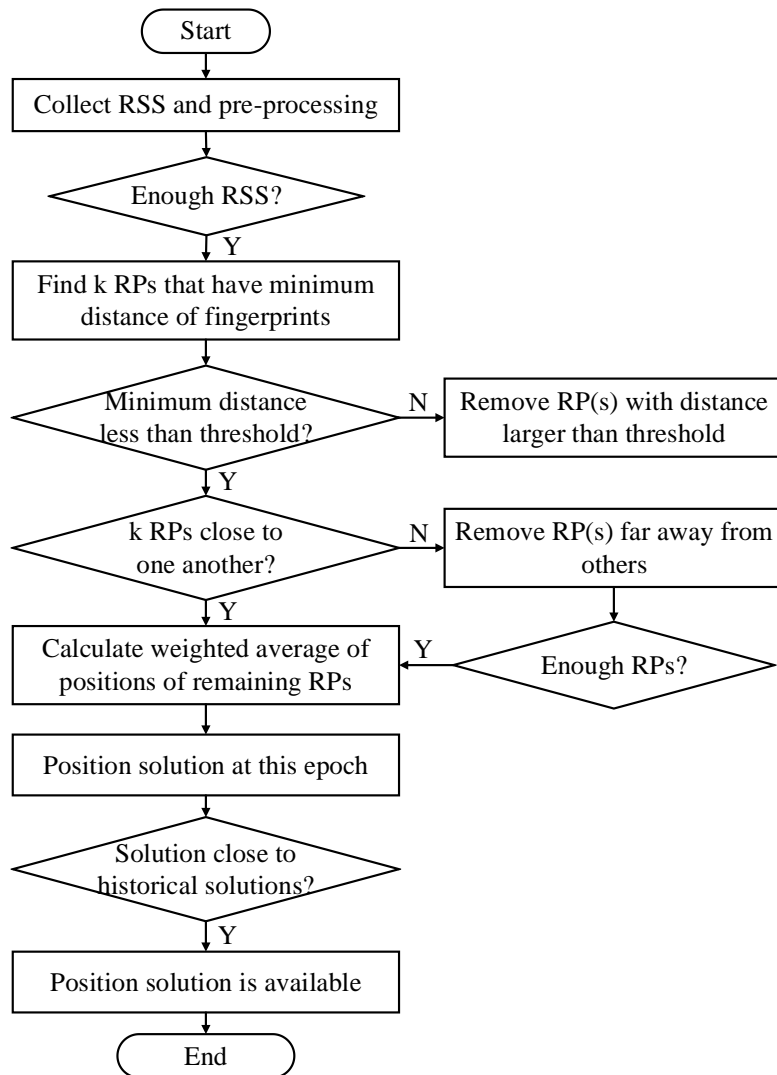


Figure 5-1. Flow chart of positioning phase of WiFi fingerprinting

This section first clarifies two fundamental but important aspects in WiFi positioning, including the implementation of AP localization and propagation-parameter determination, and the utilization of differential fingerprints. Then, this research proposes a profile-based WiFi fingerprinting approach that introduces both short-term trajectories from DR and geometrical relationships of various RPs in the space.

5.2.1 AP localization and propagation-parameter determination

Although fingerprinting-based approaches can provide position without knowledge of AP location or signal-propagation model, it is important to estimate the location and propagation parameters for the APs used for positioning. Through this process, one can obtain useful information, for example, (1) one can obtain the distribution of APs, and even weighted the importance of each AP. Based on the investigation of AP distribution, one can make use of APs selectively (or set more weights for the APs have more contributions to positioning), or add AP at places with weak RSS distribution if necessary, to assure a strong signal geometry; and (2) one can use the estimated AP locations and signal-propagation models to predict the RSS fingerprints at the areas that have not been pre-surveyed, as it is commonly difficult to cover a whole building in the pre-survey process.

As reviewed in Section 1.2.1, there are several research studies for AP localization. Compared with previous works, this research estimates the RSS propagation parameters together with AP locations by using multi-sensor based navigation solutions. This work illustrates the potential for a crowdsourcing system based on daily-life solutions from users ([Zhuang, 2015](#)).

A widely used simplified signal-propagation model can be expressed as ([Gang et al., 2012](#))

$$\text{RSS} = -10n\log_{10}(\sqrt{(x_0 - \mathbf{x}_u)^2 + (y_0 - \mathbf{y}_u)^2}) - A + X_\sigma \quad (5-1)$$

where A is a constant which has a typical range of $0 \sim 100$, n is the path-loss exponent with a typical range of $2 \sim 6$ indoors, and X_σ represents the parameter for the log-normal shadowing effect which is modeled as a Gaussian random variable with zero mean ([Atia et al., 2012](#)).

$\mathbf{RSS} = [RSS_1, RSS_2, \dots, RSS_k]^T$ is the RSS vector, (x_0, y_0) is the AP location, and

$\mathbf{x}_u = [x_1, x_2, \dots, x_k]^T$ and $\mathbf{y}_u = [y_1, y_2, \dots, y_k]^T$ are observed user's locations.

The observation model for the adjustment of AP locations and propagation parameters can be derived from (5-1). An implicit model is given by

$$f(\mathbf{x}, \mathbf{L}) = (x_0 - \mathbf{x}_u)^2 + (y_0 - \mathbf{y}_u)^2 - 10^{-\frac{\text{RSS}+A}{5n}} = 0 \quad (5-2)$$

where $\mathbf{x} = [x_0, y_0, n, A]^T$ and $\mathbf{L} = [\mathbf{x}_u^T, \mathbf{y}_u^T, \text{RSS}^T]^T$ represent the state vector and observed vector, respectively. The covariance matrix of \mathbf{L} can be provided by $\mathbf{C}_L = \text{diag}([\sigma_{x_1}^2 \ \sigma_{y_1}^2 \ \sigma_{RSS_1}^2 \ \dots \ \sigma_{x_k}^2 \ \sigma_{y_k}^2 \ \sigma_{RSS_k}^2])$, where $\sigma_{x_i}^2$, $\sigma_{y_i}^2$, and $\sigma_{RSS_i}^2$ are the variances of x_i , y_i , and RSS_i , respectively. The Taylor expansion is used to approximately linearize the propagation model. The expanded points are the initial approximation to the state vector ($\mathbf{x}^0 = [\text{mean}(\mathbf{x}_u), \text{mean}(\mathbf{y}_u), 3, 35]^T$) and the measured values of the observation vector (\mathbf{L}_{obs}). The covariance matrix of \mathbf{L}_{obs} is $\mathbf{C}_{L_{obs}}$. The linearized model is given in (5-3) ([El-Sheemy, 2000](#)), where $\mathbf{w} = f(\mathbf{x}^0, \mathbf{L}_{obs})$ is the misclosure vector, and \mathbf{A} and \mathbf{B} are design matrices.

$$\mathbf{w} + \mathbf{A}\delta + \mathbf{Bv} = 0 \quad (5-3)$$

$$\mathbf{A} = \frac{\partial f}{\partial \mathbf{x}} \Big|_{\mathbf{x}^0, \mathbf{L}_{obs}} = \begin{bmatrix} 2(x_0^0 - x_1) & 2(y_0^0 - y_1) & -10^{-\frac{RSS_1+A^0}{5n^0}} \cdot \frac{\ln(10)(RSS_1+A^0)}{5(n^0)^2} & 10^{-\frac{RSS_1+A^0}{5n^0}} \cdot \frac{\ln(10)}{5n^0} \\ \dots & \dots & \dots & \dots \\ 2(x_0^0 - x_k) & 2(y_0^0 - y_k) & -10^{-\frac{RSS_k+A^0}{5n^0}} \cdot \frac{\ln(10)(RSS_k+A^0)}{5(n^0)^2} & 10^{-\frac{RSS_k+A^0}{5n^0}} \cdot \frac{\ln(10)}{5n^0} \end{bmatrix}_{k \times 4} \quad (5-4)$$

$$\begin{aligned}
\mathbf{B} &= \frac{\partial f}{\partial \mathbf{L}} \Big|_{\mathbf{x}^0, \mathbf{L}_{obs}} \\
&= \left[\begin{array}{ccc}
2(x_1 - x_0^0) & 2(y_1 - y_0^0) & 10^{-\frac{RSS_1+A^0}{5n^0}} \cdot \frac{\ln(10)}{5n^0} \\
&&\ddots \\
2(x_k - x_0^0) & 2(y_k - y_0^0) & 10^{-\frac{RSS_k+A^0}{5n^0}} \cdot \frac{\ln(10)}{5n^0}
\end{array} \right]_{k \times 3k}
\end{aligned} \tag{5-5}$$

where x_0^0 , y_0^0 , n^0 , and A^0 represent elements of the expanded point of the state vector. k denotes the number of measured points. The Lagrange's method ([El-Sheemy, 2000](#)) can be used to solve (5-3). The adjusted result is obtained by

$$\begin{aligned}
\hat{\mathbf{d}} &= -(\mathbf{A}^T (\mathbf{B} \mathbf{P}^{-1} \mathbf{B}^T)^{-1} \mathbf{A})^{-1} \mathbf{A}^T (\mathbf{B} \mathbf{P}^{-1} \mathbf{B}^T)^{-1} \mathbf{w} \\
\hat{\mathbf{k}} &= (\mathbf{B} \mathbf{P}^{-1} \mathbf{B}^T)^{-1} (\mathbf{A} \hat{\mathbf{x}} + \mathbf{w}) \\
\hat{\mathbf{v}} &= -\mathbf{P}^{-1} \mathbf{B}^T \hat{\mathbf{k}} \\
\hat{\mathbf{x}} &= \mathbf{x}^0 + \hat{\mathbf{d}} \\
\hat{\mathbf{L}} &= \mathbf{L}_{obs} + \hat{\mathbf{v}}
\end{aligned} \tag{5-6}$$

where $\mathbf{P} = \mathbf{C}_{l_{obs}}^{-1}$, and $\hat{\mathbf{k}}$ is the Lagrange multiplier. This estimation is usually an iterative process. Equations (5-3) - (5-6) are repeated until $\hat{\mathbf{d}}_{(i+1)} - \hat{\mathbf{d}}_{(i)}$ approaches 0. The accuracy of AP localization can be obtained by evaluating the Dilution of Precision (DOP) matrix of the LS ([Petovello 2012](#)).

It has been demonstrated that some RSSs are strongly relevant in wireless positioning ([Kruskal and Liberman, 1983](#), [Fang and Lin, 2010](#)). Therefore, RSS from various APs may have different contributions to the location estimation. The research ([Fang and Lin, 2010](#)) has investigated the unequal contribution of different APs on location estimation, and provided a mechanism to measure the degrees of the AP importance. The importance of each AP is quantified by calculating the signal discrimination between different locations. Thus, an indicator, η_d , can be used to

represent the contained information of the d -th AP. A small η_d value indicates that an RSS is hardly used to extract the location information because the signal strength does not change with varying distances. Conversely, a large η_d value means changing at different locations is evident.

$$\eta_d = \frac{1}{R \cdot n_r} \sum_{r=1}^R \sum_{t=1}^{n_r} [x_{r,d}(t) - \bar{x}_d] \quad (5-7)$$

where $\bar{x}_d = \frac{1}{R \cdot n_r} \sum_{r=1}^R \sum_{t=1}^{n_r} x_{r,d}(t)$ is the global mean of the d -th AP; R is the number of RPs, and n_r is the number of RSS at the r -th location; $x_{r,d}(t)$ is the t -th RSS at the r -th RP and from the d -th AP.

5.2.2 Differential fingerprinting

Using differential RSS can mitigate the effect of device diversity, and may increase the dimensionality of RSS fingerprints. In order to introduce the differential fingerprinting algorithm, the principle of using differential RSS must be first demonstrated.

The relationship between the power at the transmitter and that at the receiver can be described by the path-loss model ([Bisio et al., 2013](#))

$$P(d) = P(d_0) + K - 10n \log_{10}\left(\frac{d}{d_0}\right) + w_d \quad (5-8)$$

where $P(d)$ is the RSS value at the WiFi receiver in dBm at a distance, d , from the transmitter, K is a unitless constant related with the antenna characteristics and the average channel attenuation, and w_d is the noise. $P(d_0)$ is the transmitted signal strength of an AP, which can be modelled as ([Zhuang et al., 2015b](#))

$$P(d_0) = 10 \log_{10} \left(\frac{P_{AP} G_{AP} G_{RC} \lambda_{AP}^2}{16\pi^2 d_0^2 L} \right) \quad (5-9)$$

where P_{AP} is the transmitter's transmitted power, G_{AP} and G_{RC} represent the antenna gains of the AP and the receiver, respectively, λ_{AP} is the transmitted carrier's wavelength, and L is the system loss factor.

Assuming a WiFi receiver measured the RSS values from two APs, AP₁ and AP₂, the path-loss model for the RSS from AP₁ and AP₂ can be written as

$$P(d_1) = 10 \log_{10} \left(\frac{P_{AP_1} G_{AP_1} G_{RC} \lambda_{AP_1}^2}{16\pi^2 d_1^2 L_1} \right) - 10n \log_{10} \left(\frac{d_1}{d_0} \right) + w_{d_1} \quad (5-10)$$

and

$$P(d_2) = 10 \log_{10} \left(\frac{P_{AP_2} G_{AP_2} G_{RC} \lambda_{AP_2}^2}{16\pi^2 d_2^2 L_2} \right) - 10n \log_{10} \left(\frac{d_2}{d_0} \right) + w_{d_2} \quad (5-11)$$

Subtract (5-11) from (5-10), one can obtain

$$\left[\frac{P(d_1)}{P(d_2)} \right] = 10 \log_{10} \left(\frac{\frac{P_{AP_1} G_{AP_1} \lambda_{AP_1}^2 L_2}{P_{AP_2} G_{AP_2} \lambda_{AP_2}^2 L_1}}{\frac{d_1}{d_2}} \right) - 10n \log_{10} \left(\frac{d_1}{d_0} \right) + 10n \log_{10} \left(\frac{d_2}{d_0} \right) + w_{d_1} - w_{d_2} \quad (5-12)$$

The differential RSS does not depend on G_{RC} . Therefore, although the differential calculation can increase the magnitude of noise, differential RSS will not be influenced by the receivers' hardware diversity.

There are several differential fingerprinting approaches, such as the differential (DIFF) approach ([Rashvand et al., 2014](#)), the mean differential fingerprinting (MDF) approach ([Zhang et al., 2015](#)), and the signal strength difference (SSD) approach ([Chen et al., 2014](#)). The DIFF approach takes the difference between all pairwise AP combinations; the MDF approach uses the mean fingerprint value to create the RSS differences; finally, the SSD method subtracts the RSS

of an anchor AP from the other RSS values to construct differential RSS. This research utilizes the DIFF method. Assuming that the RSS from n_r APs are received at the position to be determined, the differential fingerprint contains $n_r(n_r - 1)/2$ components. The differential fingerprint at RP_i is recorded as

$$\mathbf{DF}_i = \{\mathbf{pos}_i, (mac_{i,12}, RSS_{i,12}), \dots, (mac_{i,jk}, RSS_{i,jk}), \dots, (mac_{i,(n_r-1)n_r}, RSS_{i,(n_r-1)n_r})\} \quad (5-13)$$

where $RSS_{i,jk} = RSS_{i,j} - RSS_{i,k}$, $1 \leq j < k \leq n_r$; $RSS_{i,j}$ and $RSS_{i,k}$ are the RSS values of the j -th and k -th APs received at RP_i , respectively; $mac_{i,jk}$ is the indicator which is a combination of the MAC addresses of the j -th and k -th APs; \mathbf{pos}_i is the coordinate of RP_i . In the positioning phase, the optimal match of WiFi fingerprinting can be found through the minimum value of the two-dimensional Euclidean distance between the measured differential fingerprint and the candidate differential fingerprints in the DB by using equation (2-2).

Compared with traditional RSS, differential RSS increase fingerprint dimension from $O(n_r)$ to $O(n_r^2)$. Generally, increase of the fingerprint dimension is beneficial for enhancing the matching accuracy; however, a higher fingerprint dimension leads to a heavier computational load. Therefore, there is a trade-off between accuracy and computational load. It is preferred to use this method in areas that have sparse WiFi APs, or in other applications where it is worthwhile to sacrifice computational efficiency for accuracy.

4.2.3 Profile-based WiFi positioning using geometrical relationships in space

With DR-based continuous and reliable short-term (relative) navigation trajectories (i.e., profiles), this research proposes a profile-matching method, which simultaneously compares the

RSS fingerprints at a sequence of time epochs with the candidate profiles generated by the RPs in the DB. Before introducing the profile-matching method, one issue needs to be first addressed.

There are two types of ambiguity issues for wireless positioning: the RSS ambiguity issue and the position ambiguity issue. These ambiguity issues may be caused by the weak geometry of APs and the fluctuations of RSS values. The RSS ambiguity issue occurs when the locations of two RPs are geographically close to one another but the fingerprints at these RPs are distinct; the position ambiguity issue occurs when the fingerprints at two RPs are close to each other but the locations of these RPs are geographically far. The impact of the RSS ambiguity issue can be mitigated by combining the RSS measurements within a time period to obtain a smoothed measurement ([Zhuang, 2015](#)). Compared with the RSS ambiguity issue, the position ambiguity may cause more degradation of WiFi positioning: when this issue exists, the selected RPs, which have the fingerprints similar to the measured fingerprint, may locate far from the true position of the measured point. This mismatch problem may be eliminated through the KNN approach on some occasions, for example, the case demonstrated in Figure 5-2. In this figure, the blue-solid square represents the true position, and the red-dashed circles are the selected RPs in the KNN approach. The selected RPs that have a “✓” are used to calculate the final WiFi positioning result, while those have a “×” are not. The green-solid triangle component indicates the final WiFi positioning result, which is the weighted average of the RPs that have a “✓”.

Assuming $k = 4$ is used in the KNN algorithm. In this example, three selected RPs have fingerprints close to the measured one and locate geographically close to the true position, while the fourth selected RP has a fingerprint close to the measured one but locates far from the true position. If this is the case, the algorithm in Figure 5-2 can remove the fourth selected RP as a mismatch because it locates far from the other selected RPs.



Figure 5-2. Case 1 using single-point-based WiFi positioning

Thus, the position ambiguity issue will not degrade the WiFi positioning results in the above example because the majority of the selected RPs in the KNN method is close to the true position while the minority is not. However, it is also possible that half or more of the selected RPs locate far from the true position, as shown in Figure 5-3. In this situation, the algorithm may not detect or remove the mismatches correctly. Subsequently, the final KNN result may be degraded.

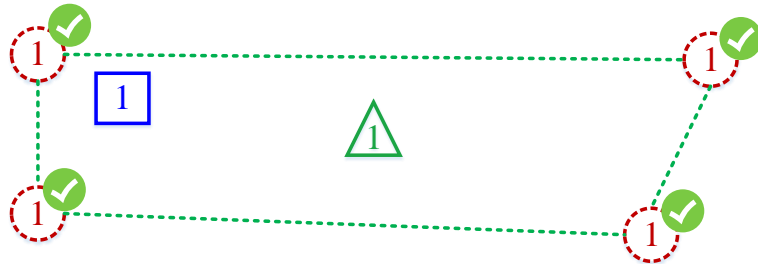


Figure 5-3. Case 2 using single-point-based WiFi positioning

With inertial sensors in consumer devices, this research proposes a profile-based WiFi fingerprinting approach. In this method, the short-term historical trajectory obtained from DR as well as the geometrical relationships between RPs are introduced to reduce the probability of mismatches. A sketch map of the above example when using the profile-matching method is shown in Figure 5-4. Compared with Figures 5-2 and 5-3, the difference in 5-4 is that the historical fingerprints are introduced. The squares and circles numbered “1” indicate for the true position of the current measured point and the corresponding selected RPs, while the squares and circles

numbered “2” and “3” represent the true position of the historical points and the corresponding selected RPs. Four red-dashed circles with number “1” are the selected RPs whose fingerprints are most similar to the measured fingerprint. If the single-point-based fingerprinting method is used, the coordinates of these selected RPs will be used to calculate the final WiFi positioning results, which leads to a significant position error. However, when the profile-based method is used, the two selected RPs numbered “1” on the right may be removed because their historical fingerprints are not close to the corresponding true values. Subsequently, the two remaining RPs on the left provide a WiFi positioning result that is close to the true position.

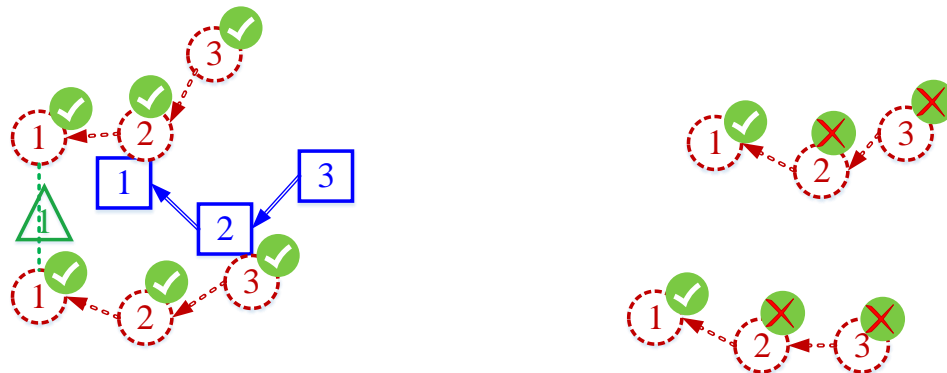


Figure 5-4. Case 2 using profile-based WiFi positioning

The flow chart and general description of the profile-based WiFi fingerprinting algorithm is provided in Figure 5-5. Compared with the traditional single-point-based method in Figure 5-1, the main advantage of the proposed profile-based method is that it introduced the short-term historical trajectory from DR and the geometrical relationships between RPs from the floor plan.

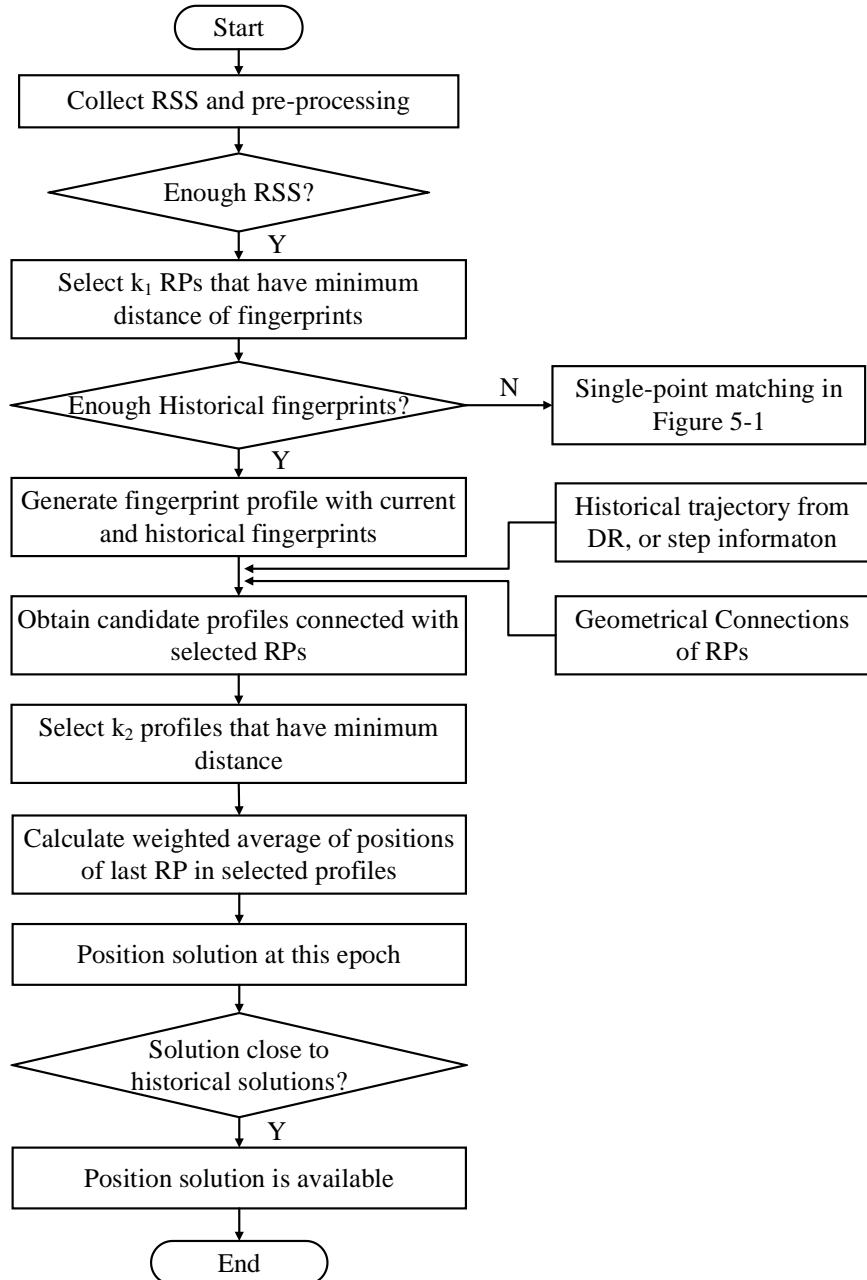


Figure 5-5. Flow chart of profile-based WiFi fingerprinting

The use of the profile-based approach can reduce the probability of mismatches. Specifically, assuming that the measured profile is comprised of points 1, 2, ..., and N , and the probabilities for a mismatch are $P(1)$, $P(2)$, ..., and $P(N)$ at these points, respectively. In a single-point-

matching method, the positioning for point 1, 2, ..., and N is independent from one another; thus, when profile-matching is used, the probability of mismatch is

$$P(\text{profile}) = P(1) \cdot P(2) \cdot \dots \cdot P(N) \quad (5-14)$$

In practical uses, the positioning results of point 1, 2, ..., and N may be correlated with each other because it is possible that a sequence of positioning results suffer from mismatches. If this is the case, the calculation of the probability of mismatch for the profile-based approach becomes a conditional probability problem, that is

$$P(\text{profile}) = P(1) \cdot P(2|1) \cdot P(3|21) \cdot \dots \cdot P(N|(N-1)(N-2)\dots21) \quad (5-15)$$

where $P(2|1)$ represents the probability of 2 (i.e., point 2 suffers from a mismatch), given 1 (i.e., point 1 suffers from a mismatch); $P(N|(N-1)(N-2)\dots21)$ denotes the probability of N, given $(N-1)(N-2)\dots21$ (i.e., points 1, 2, ..., and (N-1) suffer from mismatches). In (5-18), $P(\text{profile})$ is less than $P(1)$, as the values of $P(2|1)$, $P(3|21)$, ..., and $P(N|(N-1)(N-2)\dots21)$ are all less than 1. Therefore, the probability of mismatch is smaller in profile-matching than in single-point-matching.

Chapter 4 has described the profile-based MM algorithm, for which the basic idea is calculating the difference between the measured profile and the candidate profiles to find the optimal match. To obtain the optimal match, it is preferred that the length of the measured profile is same as that of the candidate profiles. However, it difficult to measure the accurate moving distance in indoor pedestrian applications because the sensor-based navigation errors will accumulate quickly, as sensors are low-end and there is no effective constraint when the device is not fixed on the body (e.g., on-foot or in-belt). Therefore, the algorithm in Chapter 4 calculates the rough length of the

measured profile by using the steps detected by accelerometers, and utilizes the DTW algorithm for matching with inaccurate profile length.

The principle of the profile-based WiFi fingerprinting is similar to that of MM but more complex. The main reason is that the profile-based WiFi fingerprinting is a multi-dimensional-matching topic. The profile-based WiFi fingerprinting is also more complex than the traditional single-point-based WiFi fingerprinting, which is a one-dimensional problem because only the RSS measurements at one time epoch are considered.

This research introduces the MD-DTW algorithm, which was previously used in gesture recognition ([Kang and Han, 2015](#)), to match with inaccurate profile length for such a multi-dimensional system. In this algorithm, the RSS values from each AP is regarded as a separate dimension, while the RSS values at different points on the profile constitute a time series. If one needs to apply the one-dimensional DTW algorithm to align the multi-dimensional time series, the most straightforward means is to implement DTW separately in each dimension. However, in this case, the calculation processes of different dimensions are uncorrelated, which is different from the actual condition. To solve this issue, the idea of the MD-DTW algorithm is to modify the distance matrix in (4-8) to (5-16).

$$\mathbf{d}(i, j) = \sum_{k=1}^K (\mathbf{s}(k, i) - \mathbf{m}(k, j))^2 \quad (5-16)$$

After this, the minimal path is obtained by the traditional method as in the original DTW. In this method, the feature values in all dimensions in each point of a pair of sequences will be synchronized at the same position. Figure 5-6 shows the algorithm for MD-DTW calculation.

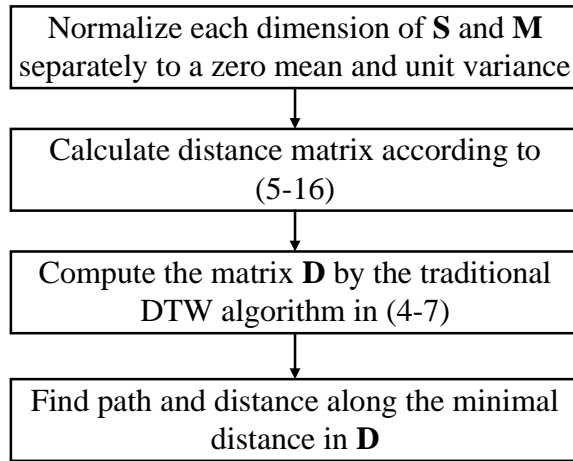


Figure 5-6. Flow chart of MD-DTW algorithm

5.3 Integration of WiFi and Magnetic Matching

WiFi fingerprinting and MM utilize similar ideas and both consist of the training phase and the positioning phase. Figure 5-7 shows the process of training and positioning phases of WiFi and MM. The training phase builds a <location, RSS> DB and a <location, magnetic> DB simultaneously, while the positioning phase determines the position through integration of WiFi fingerprinting and MM. WiFi and MM can be complementary: WiFi positioning is a single-point matching approach, while MM is based on profile-matching. Moreover, as illustrated in the tests and results subsection, MM results had small error fluctuations but had a significant mismatch rate. In contrast, WiFi fingerprinting can provided results with low mismatch rate; however, the WiFi fingerprinting accuracy strongly depended on the signal distributions. Therefore, there is a potential to use WiFi for a rough positioning, and then use MM for a more precise localization. For example, WiFi can be used to determine the region where the target device resides while MM narrows down further to determine the location of the device.

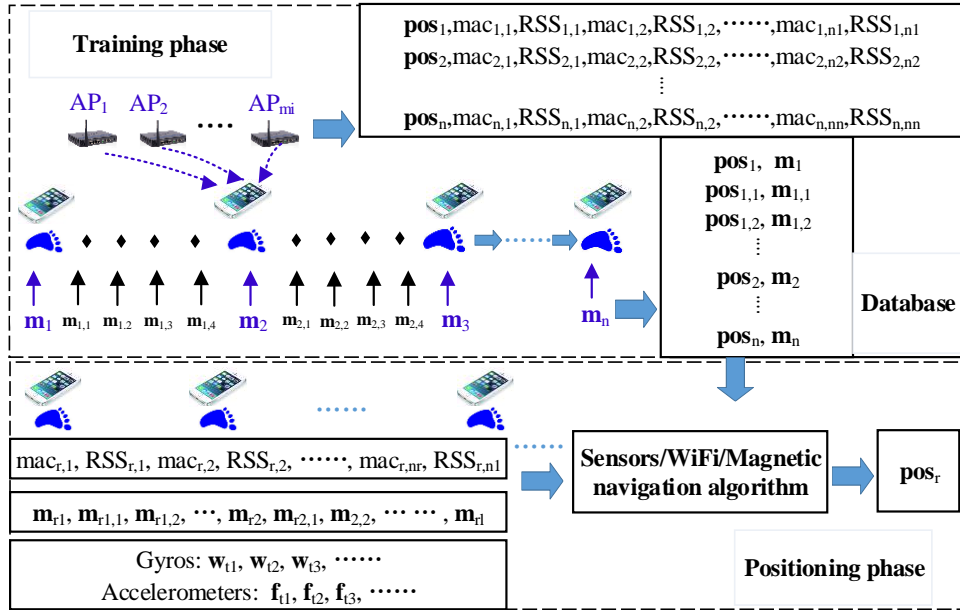


Figure 5-7. Process of training and positioning for WiFi and magnetic matching

Compared with previous research that uses region-point indoor localization approach via RSS-magnetic fingerprinting ([Ezani et al., 2014](#)) or regards the magnetic intensity and inclination as pseudo WiFi APs ([Pritt, 2014](#)), this research combines the information from WiFi and MM in a way that is easier to implement. Specifically, it utilizes WiFi results to limit the MM search space to reduce both the mismatch rate and computational load. The search space is limited to a circle around the WiFi results, as shown in Figure 5-8. The radius of the circle is set according to the WiFi accuracy.

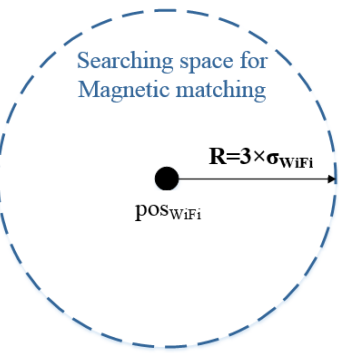


Figure 5-8. Using WiFi positioning results to limit search space for magnetic matching

The complementary characteristics between WiFi and MM are especially useful for navigation applications that use consumer devices not equipped with gyros. Results from this research supported that the WiFi-aided MM algorithm provided more reliable solutions than both WiFi and MM in the areas that have poor WiFi signal distribution or indistinctive magnetic-gradient features.

This methodology can also be extended to BLE or other wireless technologies. Since BLE can be used in a similar way as WiFi (either fingerprinting or trilateration), it is feasible to use BLE to determine a region first, then implement MM to determine the position. When both WiFi and BLE are available, both a WiFi result and a BLE result can determine a region. If this is the case, the position uncertainty of the integrated use of WiFi and BLE can be smaller than that of the independent use of WiFi or BLE. Accordingly, the position accuracy can be further improved.

5.4 Integration of Dead-reckoning, WiFi, and Magnetic Matching

Two hybrid DR/WiFi/MM navigation algorithm structures, Structure #1 and Structure #2, are designed and evaluated. In both structures, the initial position is provided by WiFi, while the initial heading is determined through integration of magnetometers and gyros. Then, after initialization, the software provides real-time indoor navigation and outputs the current user position. Also, both structures use the same DR algorithm, which consists of an attitude-determination module and a position-tracking module, described in Section 4.3. Figures 5-9 and 5-10 demonstrate the flow chart of Structures #1 and #2, respectively. In Structure #1, WiFi results are used to limit the MM search space. After this, both WiFi and MM (WiFi aided) results are utilized as updates to integrate with PDR. Structure #2 utilizes the DR algorithm to integrate with WiFi and use DR/WiFi results to limit the MM search space.

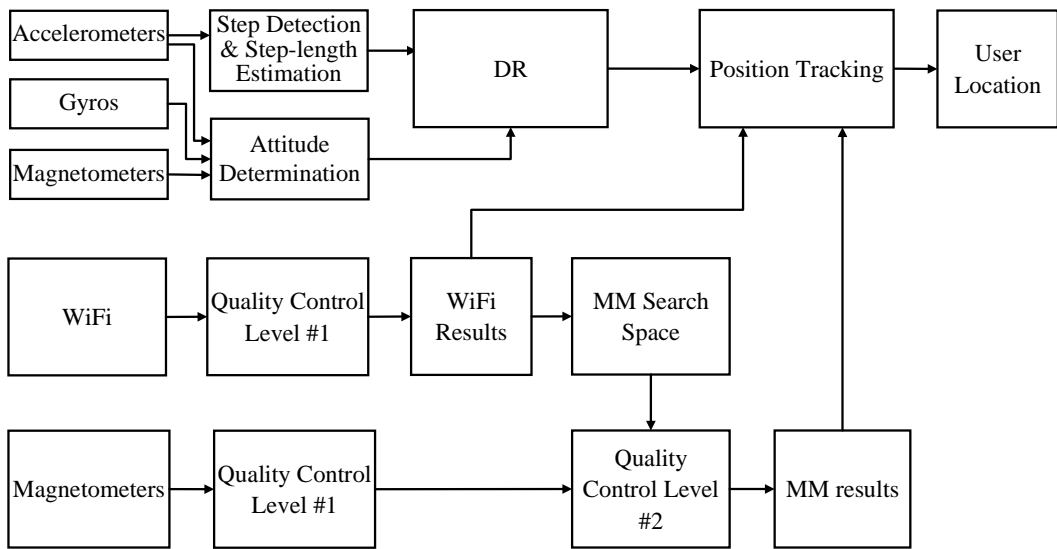


Figure 5-9. Structure #1 for DR/WiFi/MM integration

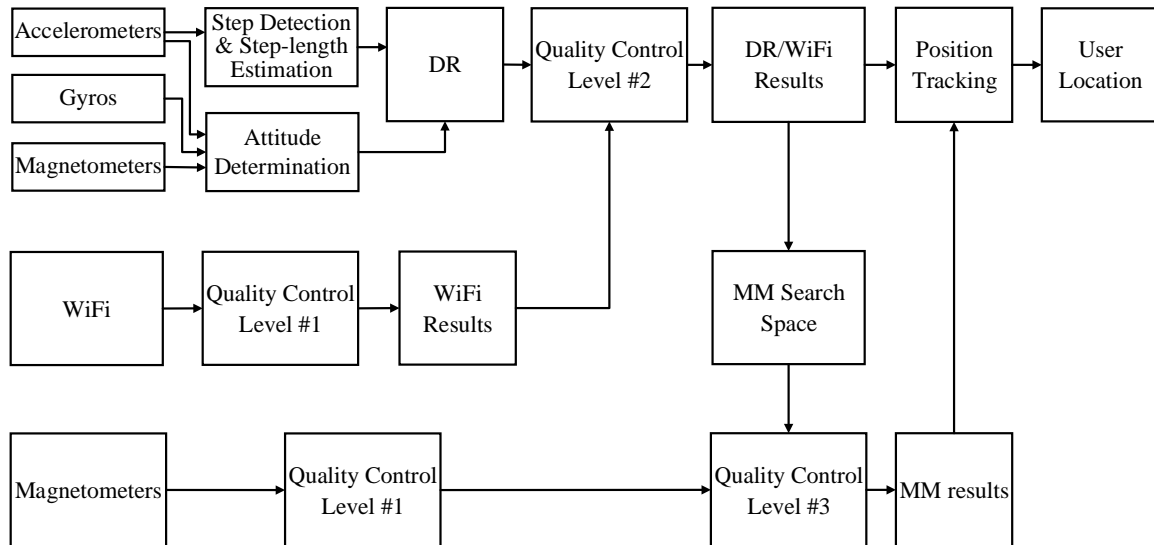


Figure 5-10. Structure #2 for DR/WiFi/MM integration

This research implements a multi-level quality-control mechanism based on the interaction between different techniques. This mechanism has three main levels, as illustrated in Figure 5-10. The explanations of these levels are provided below.

This research implements a multi-level quality-control mechanism based on the interaction between different techniques. This mechanism has three main levels, as illustrated in Figure 5-10. The explanations of these levels are provided below.

Level #1: Quality control on the WiFi and MM measurements. Several criterions are applied to detect WiFi blunders, such as 1) the number of observed APs must be over a minimum number; 2) the useful WiFi RSS should be strong enough; moreover, 3) the minimum Euclidean distance should be less than a threshold; 4) the selected k RPs should be close to one another; 5) the position result at the last epoch should be close to the historical position results, and finally, 6) if a WiFi trilateration approach is used, the DOP ([Drawil and Basir, 2014](#)) value should be less than a threshold. For MM, quality control can be applied based on the history of the local magnetic field, as described in Chapter 4. The MM results are used only when both the change range and the standard deviation value are larger than their corresponding threshold values.

Level #2: Quality control on the DR/WiFi fusion level. The KF innovation sequence (i.e., the difference between position predicted by DR and that measured by WiFi) are investigated to set the weight of the WiFi results. This process is similar to the threshold-based method introduced in Chapter 4. Extremely, if the innovation sequence is larger than the corresponding threshold values, the WiFi results will not be used as position updates.

Level #3: Using DR/WiFi positioning results to limit the MM search space and in turn reduce both mismatch rate and computational load. The search space is limited to a circle that lies around the DR/WiFi result. The radius of the circle can be determined by the position accuracy of DR/WiFi multiplied by a certain scale factor (e.g., two or three). The DR/WiFi position accuracy is obtained from the position-tracking KF covariance matrix. As shown in Figure 5-11, the position uncertainties can be reduced when a deeper level of information is used.

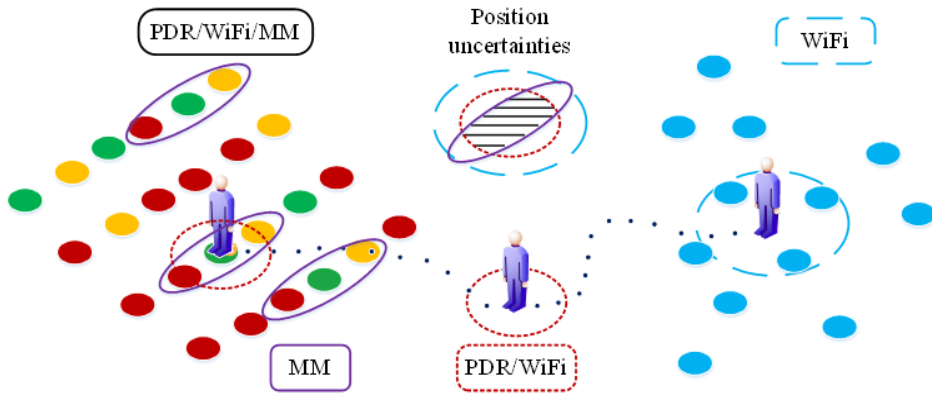


Figure 5-11. Position uncertainties when using different levels of quality controls

5.5 Tests and Results

Walking tests with Samsung Galaxy S4 and Xiaomi 4 smartphones were conducted in two indoor environments: building E with more WiFi APs (the average number of RSS was over 15 in this building) and severe magnetic interferences (the change of magnetic intensity reached 0.4 Gauss); and building B with less APs (the average number of RSS was nearly seven) and less magnetic interferences (the change of magnetic intensity was below 0.25 Gauss). The sample rates for gyros, accelerometers, and magnetometers were set at 20 Hz. Due to restriction by android operation system, the actual WiFi update rates for both phones were approximate 0.3 Hz. The length for profile-based WiFi fingerprinting was set at 10 steps. The other parameters related with DB training are same as those in Chapter 4. The tested motion conditions included handheld, phoning, dangling, and in a pants pocket.

5.5.1 Tests at building E

The WiFi and magnetic DBs were generated simultaneously by using the trajectories shown in Figure 4-3. Each trajectory lasted for 5-10 minutes. RPs in the WiFi and magnetic DBs are shown in Figures 5-12 and 4-4, respectively. The colors in Figure 5-12 indicate the weighted AP number,

which was over 15 in the middle indoor area, and over 10 were available in the marginal indoor areas. The weighted AP number at RP_i was calculated by $WAP_i = \sum_{j=1}^{n_i} a_{i,j}$, $i \in I_{RP}$, where n_i is the number of WiFi signals received at RP_i , I_{RP} is the location index set of RPs. The $a_{i,j}$ value is determined according to $RSS_{i,j}$ (i.e., the RSS of AP_j at RP_i) by the following rule: if $RSS_{i,j} > -60$ dBm, $a_{i,j} = 1$; if $-70 \text{ dBm} < RSS_{i,j} < -60 \text{ dBm}$, $a_{i,j} = 0.75$; if $-85 \text{ dBm} < RSS_{i,j} < -70 \text{ dBm}$, $a_{i,j} = 0.5$; if $RSS_{i,j} < -85 \text{ dBm}$, $a_{i,j} = 0$.

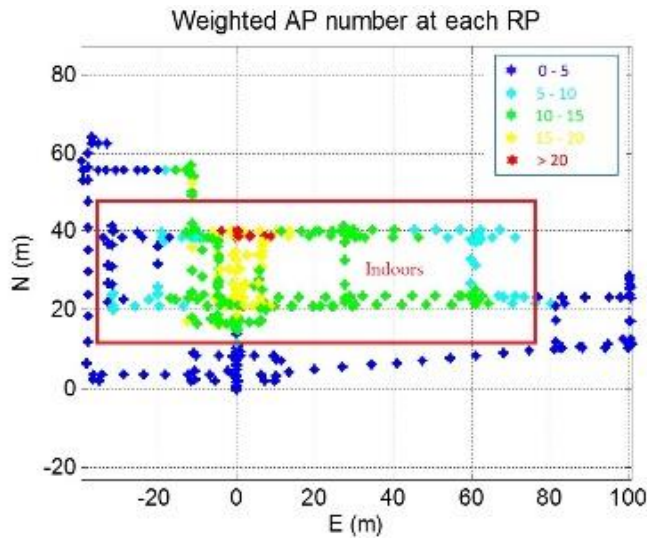


Figure 5-12. Distribution of WiFi signals at E

The estimates of the location and propagation parameters for some selected APs are illustrated in Figures 5-13 and 5-14, respectively. These APs are selected because their true positions are known. The blue eclipses in Figure 5-13 represent the standard confidence eclipses, which indicates a probability of 39.4% in 2D cases (Petovello 2012). Figure 5-13 clearly shows that the estimated AP locations are close to the true values, which illustrates the efficiency of the AP localization algorithm. In Figure 5-14, the true values of propagation parameters locate in typical ranges (2~6 for n indoors and 0~100 for A).

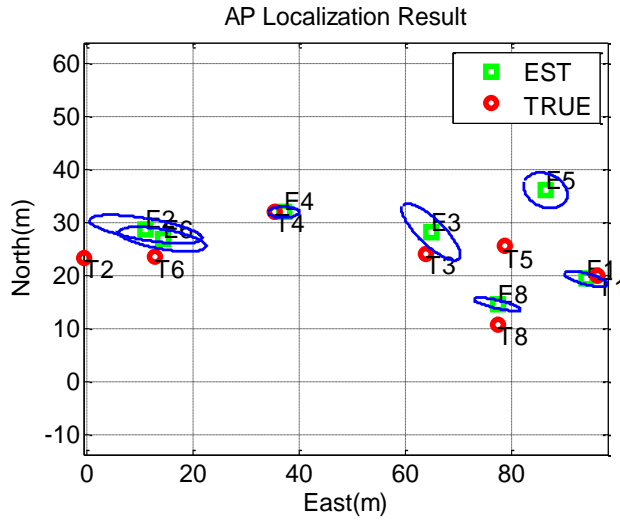


Figure 5-13. AP localization results

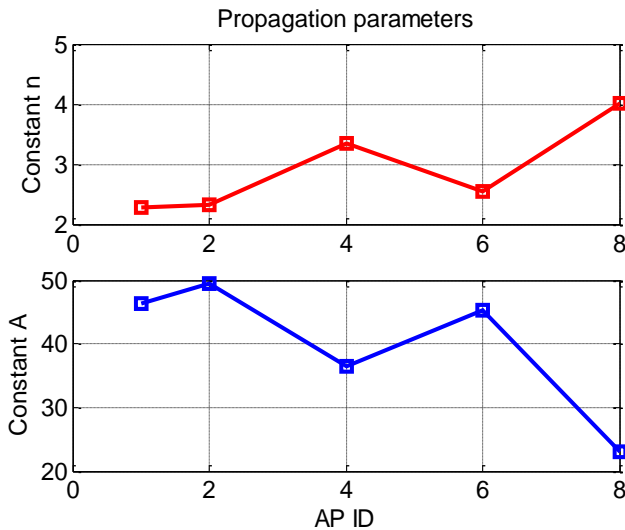


Figure 5-14. Propagation-parameter determination results

The test trajectory is shown in Figure 3-9. The threshold for available WiFi RSS was set at -85 dbm. The number k was set at 4 for the KNN approach. The threshold for the minimum magnetic intensity change range of available magnetic fingerprints was set at 0.1 Gauss. The profile length for MM was 10 steps. The radii of the MM search spaces determined by WiFi and DR/WiFi results was set at 15 m and 10 m, respectively. The threshold values for detecting WiFi and MM

mismatches using DR solutions were set at 15 m. The standard deviation values of both WiFi and MM measurement noises were set at 10 m.

A. Single-point and profile based WiFi results

As illustrated in Figure 3-3, dangling and pocket provided stronger device dynamics than handheld and phoning motion conditions. Therefore, Figures 5-15 and 5-16 demonstrate the phoning and pocket results as examples. In each figure, (a) - (e) represent the navigation results of WiFi (point), WiFi (profile), DR/WiFi (point), DR/WiFi (profile) and DR, and (f) illustrates the true trajectory.

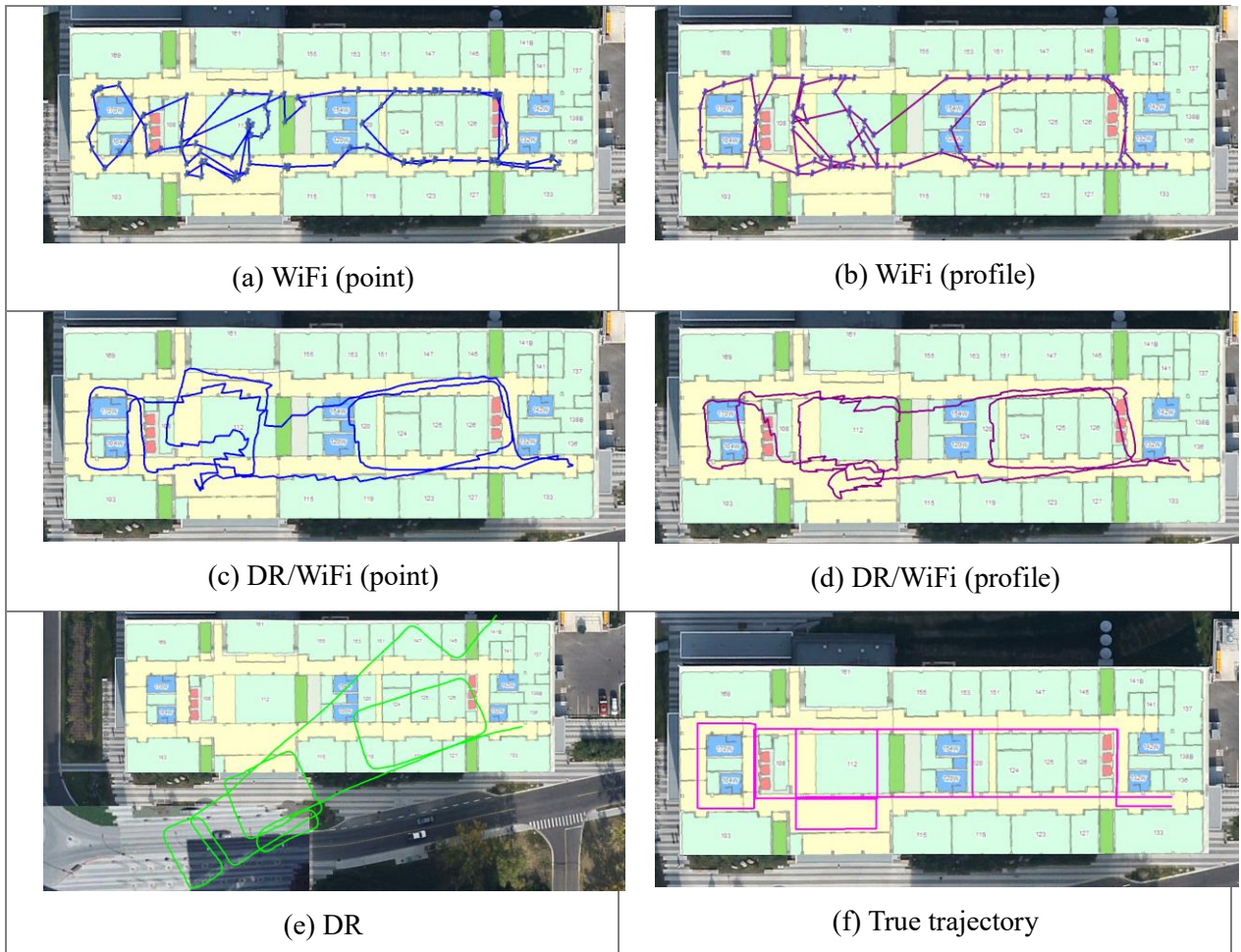


Figure 5-15. Results of WiFi (point), WiFi (profile), and their fusion with DR, phoning

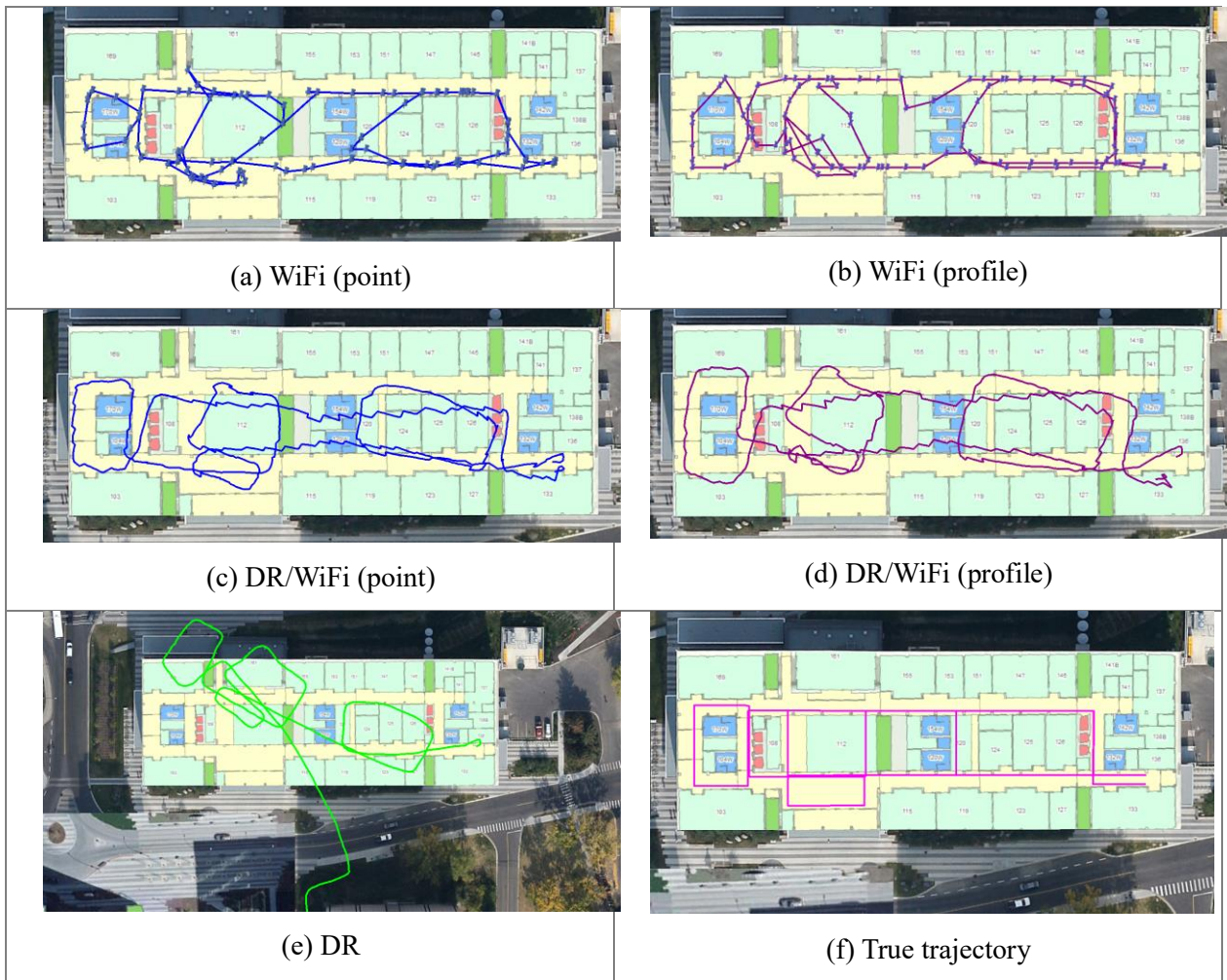


Figure 5-16. Results of WiFi (point), WiFi (profile), and their fusion with DR, pocket

DR solutions were continuous and had a similar shape as the true trajectories; however, the heading errors accumulated and led to position errors. Therefore, external positioning technologies were needed to correct for DR errors and provide long-term accurate solutions. On the other hand, WiFi provided results with long-term accuracy. However, WiFi results had low sampling rates and had fluctuations, especially in the lobby area. When integrated with DR, the results became continuous and had smaller fluctuations.

Figure 5-17 compares the position errors in the WiFi (point) and WiFi (profile) results, and Figure 5-18 illustrates the position errors in the DR/WiFi (point) and DR/WiFi (profile) results. In each figure, (a) - (d) illustrate the errors under four motion conditions, respectively.

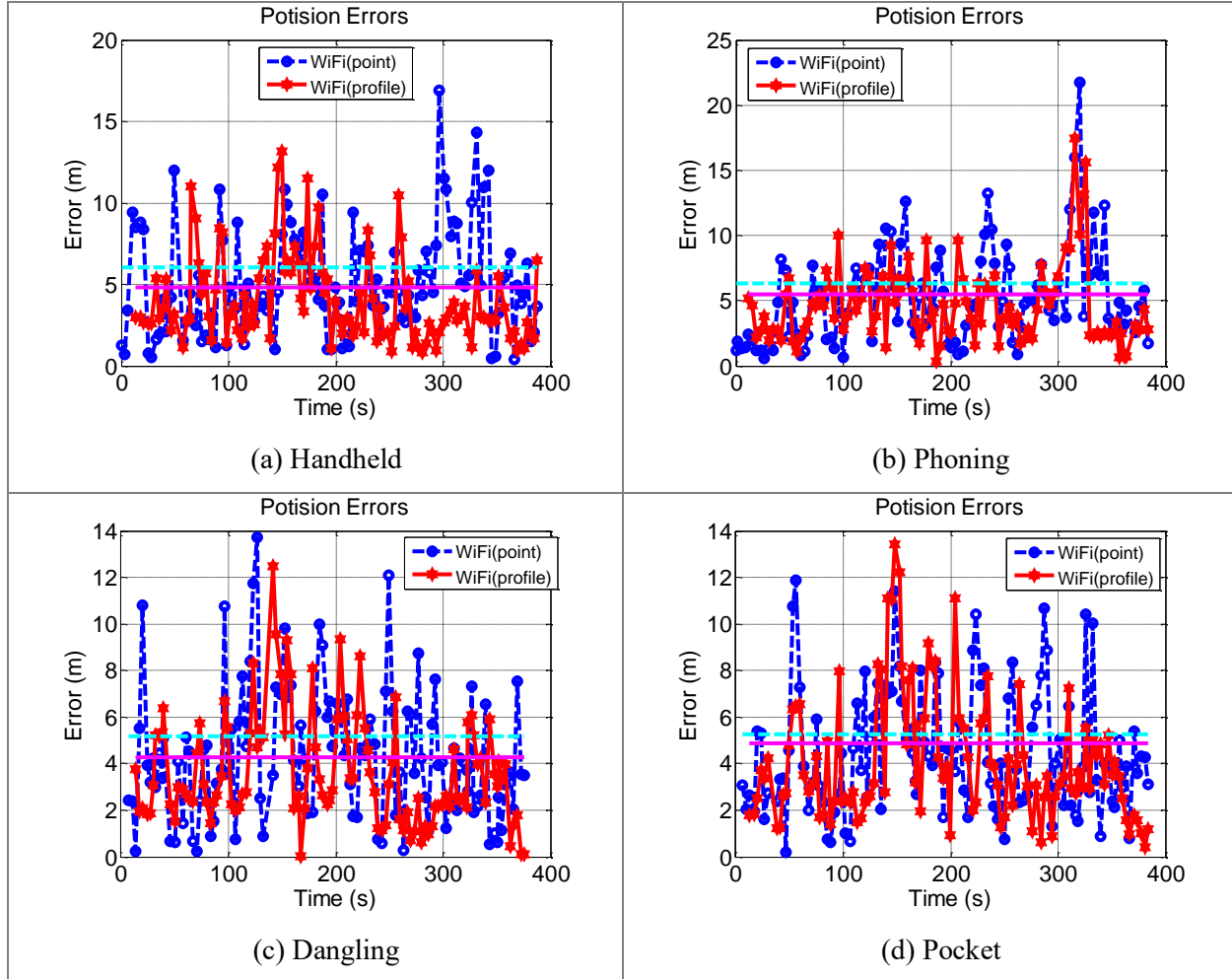


Figure 5-17. Errors in WiFi (point) and WiFi (profile) results

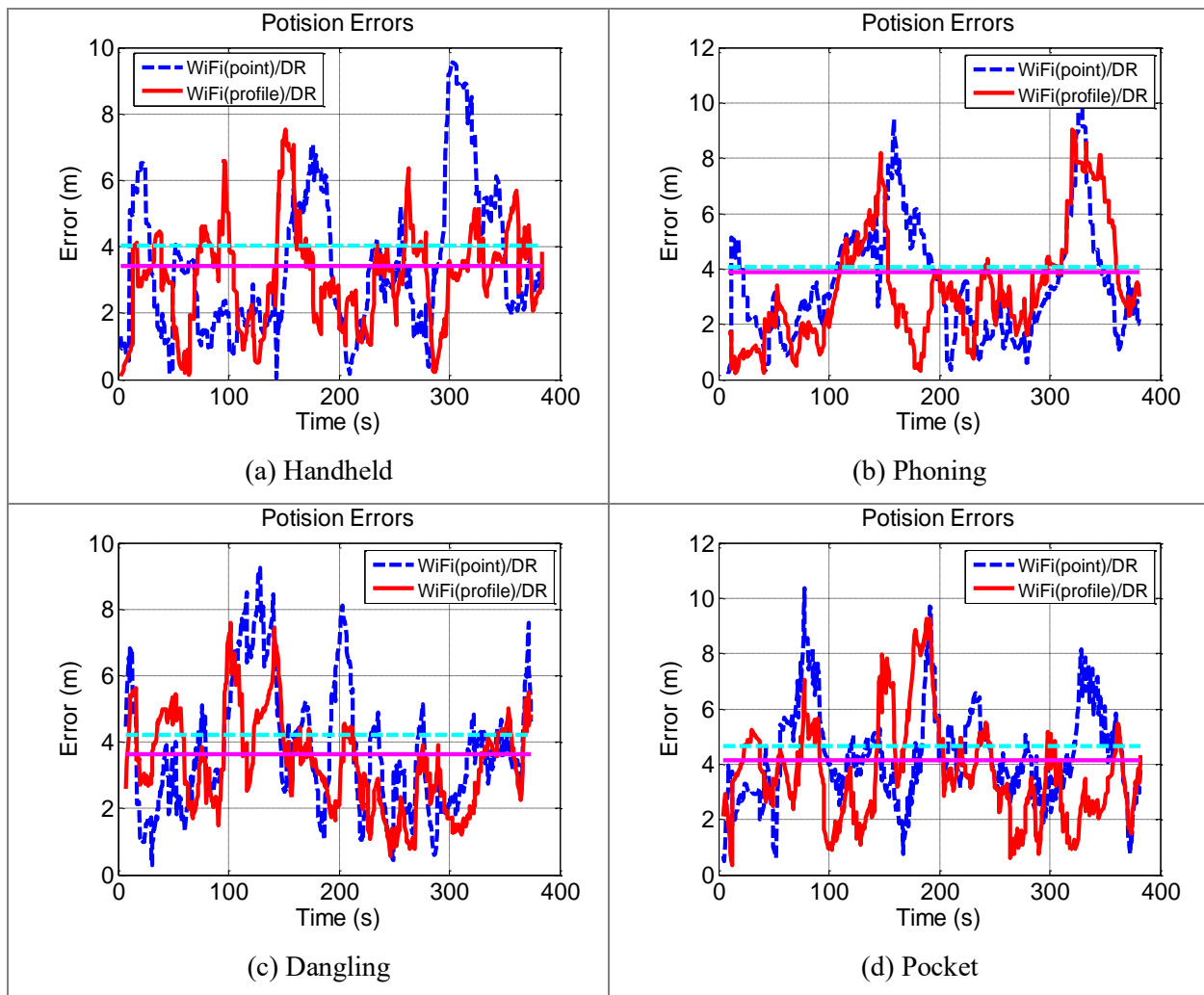


Figure 5-18. Errors in DR/WiFi (point) and DR/WiFi (profile) results

According to Figures 5-17, several mismatches in the single-point-matching results, such as the errors during 300 -350 s in the phoning result and those during 250-300 s in the pocket result, were removed when using the profile-matching method. Although there was a minority of time periods during which the position errors in the profile-matching results were larger, the RMS values of position errors in the profile-matching results were generally less.

WiFi errors jumped to over 10 m on several occasions. When integrated with DR, the solutions became smooth because some blunders were removed. Most of the DR/WiFi position errors were below 10 m. Besides, because the WiFi results became more accurate when the profile-based

approach was implemented, the DR/WiFi results also became more accurate. All DR/WiFi (profile) position errors were less than 10 m.

Table 5-1 compares the statistical values of position errors when using WiFi (point), WiFi (profile), and their integration with DR.

Table 5-1. Statistical values of position errors (unit: m) of WiFi (point), WiFi (profile), and their integration with DR at E

		DR	WiFi (point)	WiFi (profile)	DR/WiFi (point)	DR/WiFi (profile)
Handheld	Mean	10.1	5.1	4.0	3.4	3.1
	RMS	11.4	6.1	4.8	4.0	3.4
	80 %	14.8	7.8	5.8	5.2	4.2
Phoning	Mean	10.6	5.2	4.6	3.5	3.5
	RMS	12.2	6.3	5.5	4.1	3.9
	80 %	16.3	7.6	6.6	5.0	5.3
Dangling	Mean	15.0	4.3	3.6	3.8	3.3
	RMS	17.2	5.2	4.3	4.2	3.6
	80 %	22.9	6.5	5.4	5.2	4.6
Pocket	Mean	18.0	4.5	4.1	4.3	3.7
	RMS	24.4	5.3	4.9	4.6	4.1
	80 %	24.1	7.1	6.0	5.6	4.9
General	Mean	13.8	4.8	4.1	3.8	3.4
	RMS	17.1	5.7	4.9	4.2	3.8
	80 %	19.9	7.3	6.0	5.3	4.8

The RMS value of single-point WiFi positioning errors was 5.7 m under all tested motion conditions. This was a medium accuracy for WiFi positioning with consumer portable devices. When the profile-matching method was used, this RMS value was reduced to 4.9 m, with an improvement of 14.0 %. When integrated with DR, the RMS of position errors in the single-point- and profile-based WiFi position results were reduced to 4.2 m and 3.8 m, respectively. Such

significant decreases illustrate the effectiveness of integrating DR with WiFi. The RMS value of the DR/WiFi (profile) errors was 9.5 % less than that of the DR/WiFi (point).

B. WiFi-aided and DR/WiFi-aided MM results

Figure 5-19 demonstrates the navigation results of MM, MM (WiFi aided), and MM (DR/WiFi aided) under the phoning motion condition, while Figure 5-20 illustrates those under the pocket motion. Figures 5-21 (a) - (d) compare the corresponding position errors. Because the purpose of this subsection is mainly focus on improving the navigation through interaction between different technologies, instead of optimizing the performance of one single technology, the single-point-based WiFi fingerprinting was used.

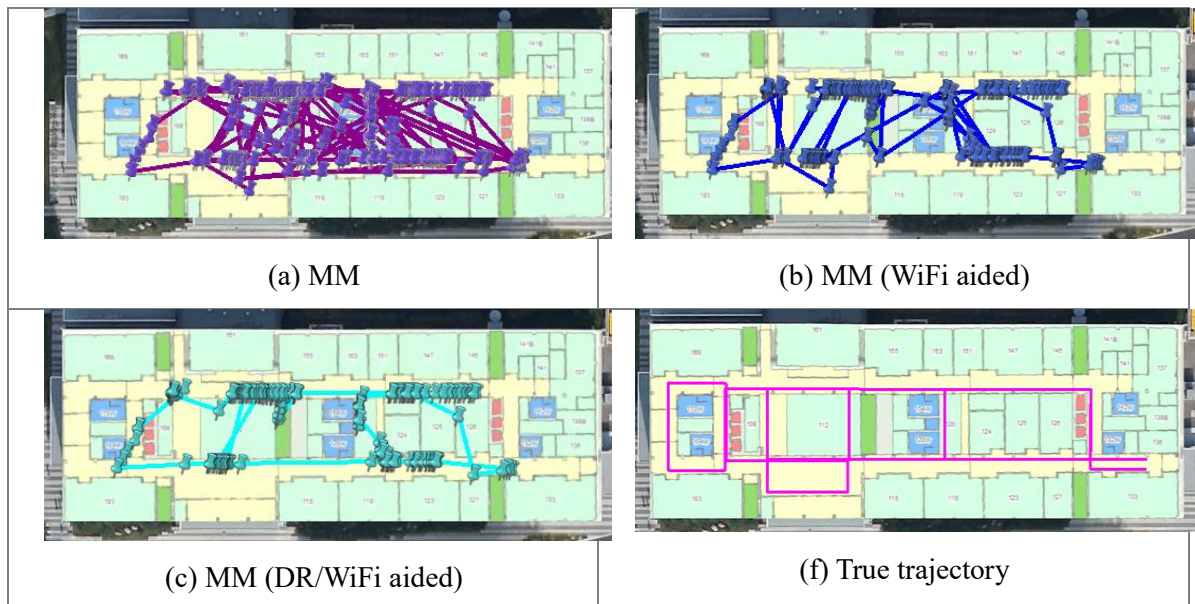


Figure 5-19. Results of MM, MM (WiFi aided), and MM (DR/WiFi aided), phoning

Figures 5-19, 5-20, and 5-21 demonstrate that MM errors were below 10 m in some areas but reached over 40 m on some occasions. However, the largest MM error dropped from over 80 m to approximate 20 m when aided by WiFi. Therefore, the WiFi aided MM algorithm can reduce dependency on single technology, either WiFi or MM, as its RMS values were less than those of

WiFi or MM. Besides, when aided by DR/WiFi, the majority of MM errors were reduced to below 10 m. The largest MM error occurred during 150 - 200 s in the dangling test. The reason for this fact was that there were a series of MM mismatches; some mismatches were detected by DR/WiFi while others were not.

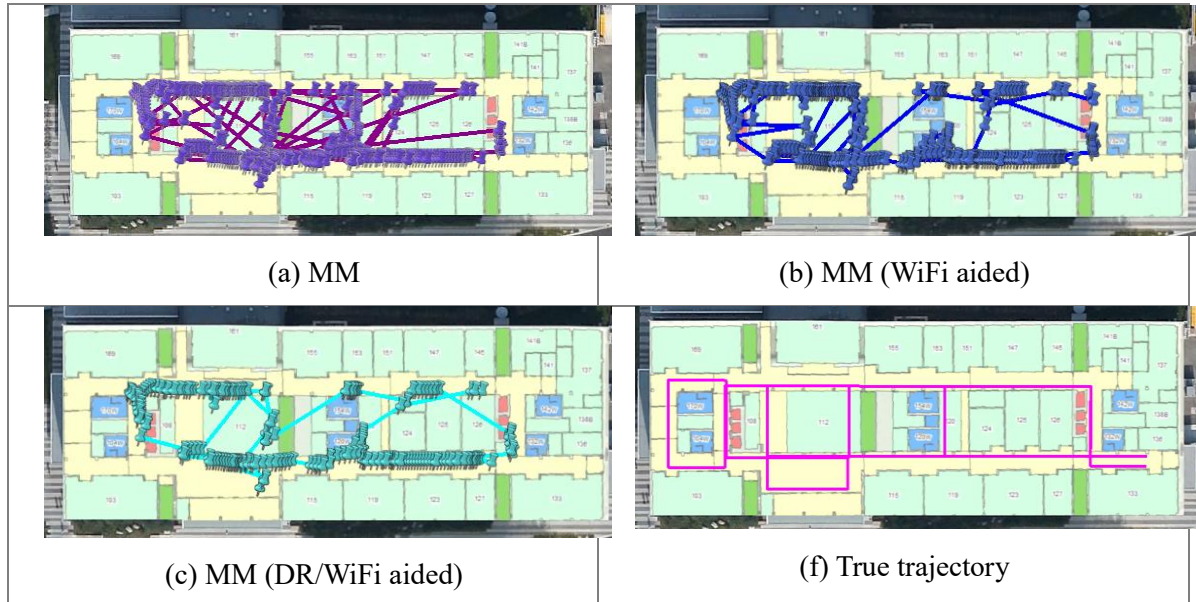


Figure 5-20. Results of MM, MM (WiFi aided), and MM (DR/WiFi aided), pocket

MM (DR/WiFi aided) results were not continuous but accurate. Thus, these results can be used as reliable updates in the position-tracking KF. The statistical values for the position errors in MM, MM (WiFi-aided), and MM (WiFi/DR-aided) results are illustrated in the next subsection, together with the DR/WiFi/MM results.

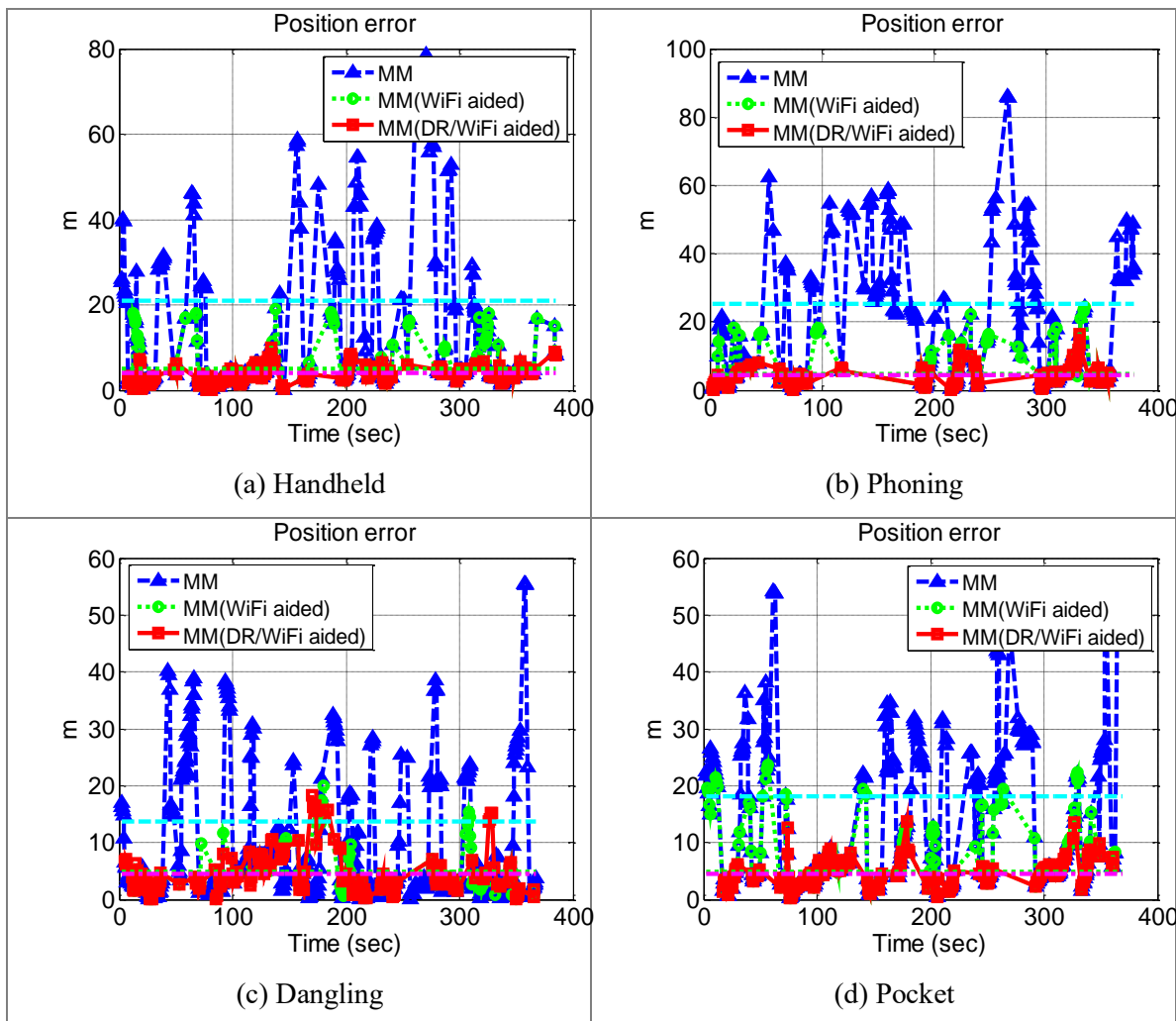


Figure 5-21. Errors in MM, MM (WiFi aided), and MM (DR/WiFi aided) results

Figures 5-22 and 5-23 demonstrate the navigation results of DR/WiFi/MM (WiFi aided) and DR/WiFi/MM (DR/WiFi aided) under the phoning and pocket motion conditions, respectively. Figure 5-24 compares the navigation error in these results under different motion conditions. DR/WiFi/MM (WiFi-aided) results were already continuous and accurate; all position errors were below 10 m under all tested motion conditions. Furthermore, an additional improvement was identified when replacing MM (WiFi-aided) with MM (DR/WiFi-aided), for example, during the time period 0-100 s in the handheld test, and 50-150 s in the phoning test. In most of the time, the

DR/WiFi/MM (DR/WiFi aided) results were more or equally accurate when compared with the DR/WiFi/MM (WiFi aided) results.

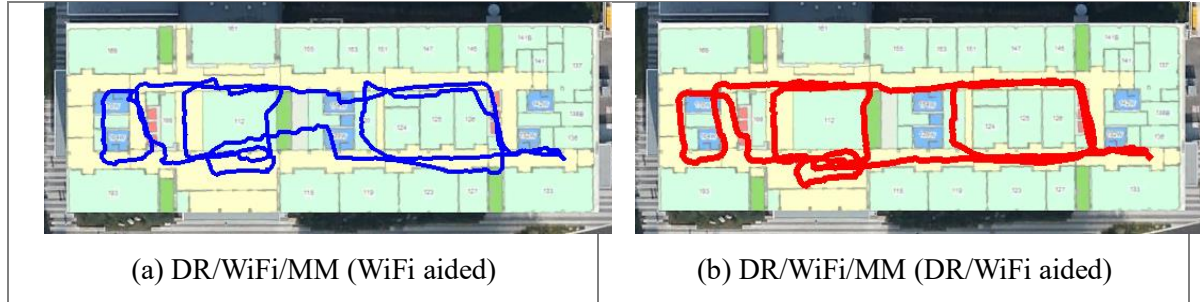


Figure 5-22. Results of DR/WiFi/MM (WiFi aided) and DR/WiFi/MM (DR/WiFi aided), phoning

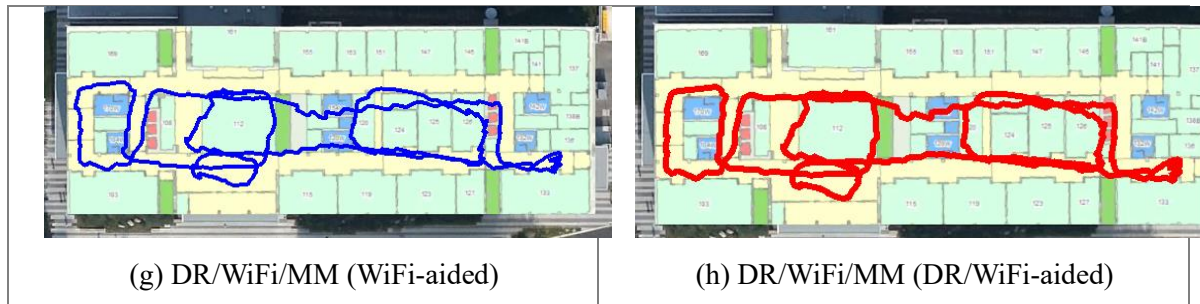


Figure 5-23. Results of DR/WiFi/MM (WiFi aided) and DR/WiFi/MM (DR/WiFi aided), pocket

According to Figure 5-24, when integrating MM (WiFi aided) with DR and WiFi, navigation solutions could be improved. On the other hand, the introduction of MM (WiFi aided) increased the position errors during some time periods, for example, 0 - 100 s in the handheld test. The reason was that the errors of MM (WiFi aided) were significant (nearly 20 m) during this time period, as shown in Figure 5-21. The DR/WiFi/MM (DR/WiFi aided) algorithm provided the most accurate results at most of the time.

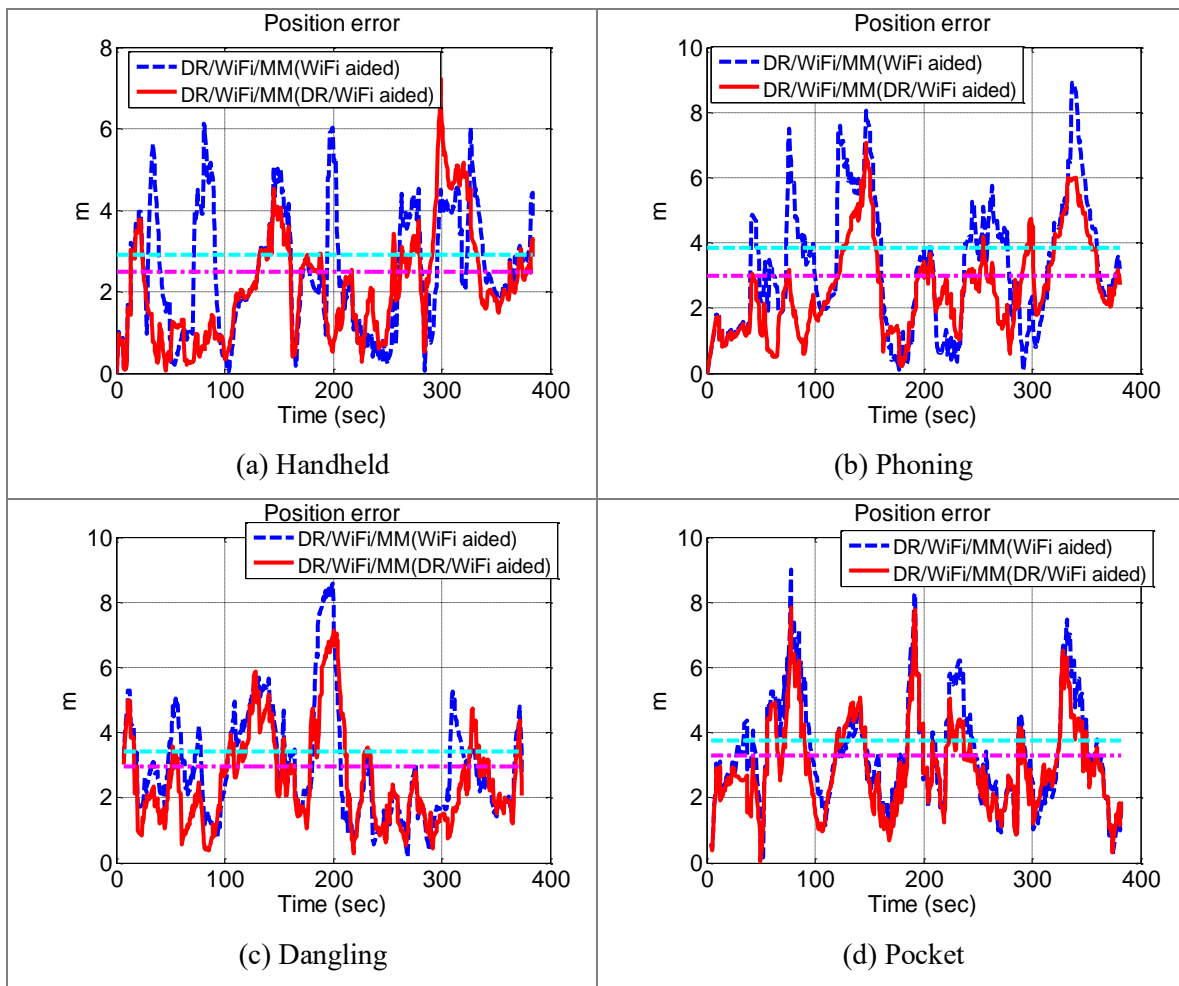


Figure 5-24. Errors in DR/WiFi/MM (WiFi aided) and DR/WiFi/MM (DR/WiFi aided) results

C. Summary of results

To summarize, Figures 5-25 (a) - (d) provide the CDF curves of the position errors from all used strategies, and Table 5-2 illustrates the statistical values of the errors, including the mean value, RMS, and the error within which the probability is 80 %. Moreover, Figure 5-26 compares the statistical values of errors under different motions conditions.

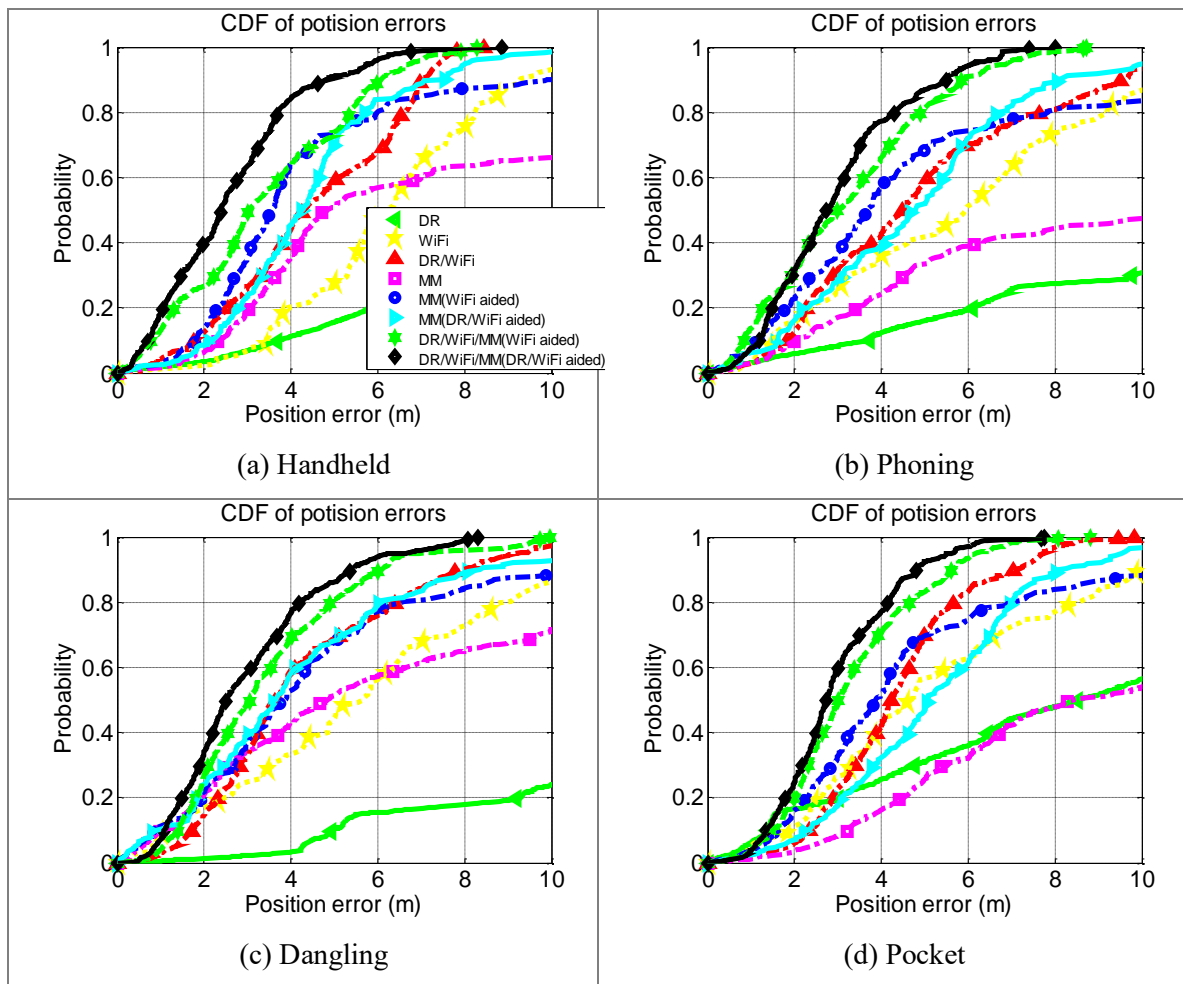


Figure 5-25. CDF of position errors when using different strategies

Figures 5-25, 5-26 and Table 5-2 illustrate that the independent use of WiFi fingerprinting provided a better performance (RMS 5.7 m) than DR (RMS 17.1 m) and MM (RMS 20.0 m).

When integrated with DR, the RMS of WiFi errors were reduced to 4.0 m. Also, when aided by WiFi, the RMS of MM errors decreased to 5.1 m.

When integrated with external techniques such as WiFi and MM, DR became less dependent on device movement. Especially, when DR/WiFi/MM was utilized, the navigation performance was similar under all tested motion conditions.

Structure #2 performed better than Structure #1. The RMS of MM errors were further reduced from 5.1 m (WiFi aided) m to 4.6 m (DR/WiFi aided). The RMS of DR/WiFi/MM (DR/WiFi aided) errors was 3.0 m, which was 0.5 m smaller than that of DR/WiFi/MM (WiFi aided).

Table 5-2. Statistical values of position errors (unit: m) at E

Motion	Error	A*	B	C	D	E	F	G	H
Handheld	Mean	10.1	5.6	3.4	13.0	4.0	3.7	2.5	2.1
	RMS	11.4	5.9	3.7	20.9	5.1	4.1	2.9	2.5
	80 %	14.8	7.3	5.1	21.9	5.2	4.8	4.0	3.0
Phoning	Mean	10.6	5.1	3.4	18.6	4.4	4.2	3.3	2.6
	RMS	12.2	6.2	3.9	25.4	5.8	5.0	3.8	3.0
	80 %	16.3	7.5	5.3	32.2	6.7	5.8	5.0	3.8
Dangling	Mean	15.0	4.6	3.6	8.6	3.6	3.5	3.0	2.6
	RMS	17.2	5.2	4.2	13.7	4.7	4.5	3.4	3.0
	80 %	22.9	6.5	5.3	17.0	4.8	4.8	4.2	3.6
Pocket	Mean	18.0	4.8	4.3	13.5	3.8	4.2	3.4	3.0
	RMS	24.4	5.6	4.6	18.2	4.8	4.6	3.7	3.3
	80 %	24.1	7.5	5.5	24.6	5.4	5.4	4.8	4.2
General	Mean	13.8	5.0	3.7	13.9	4.0	3.9	3.1	2.6
	RMS	17.1	5.7	4.0	20.0	5.1	4.6	3.5	3.0
	80 %	19.9	7.2	5.0	24.6	5.6	5.2	4.5	3.7

* A- DR; B- WiFi; C- DR/WiFi; D- MM; E- MM(WiFi aided); F- MM(DR/WiFi aided); G-DR/WiFi/MM(WiFi aided); H- DR/WiFi/MM(DR/WiFi aided)

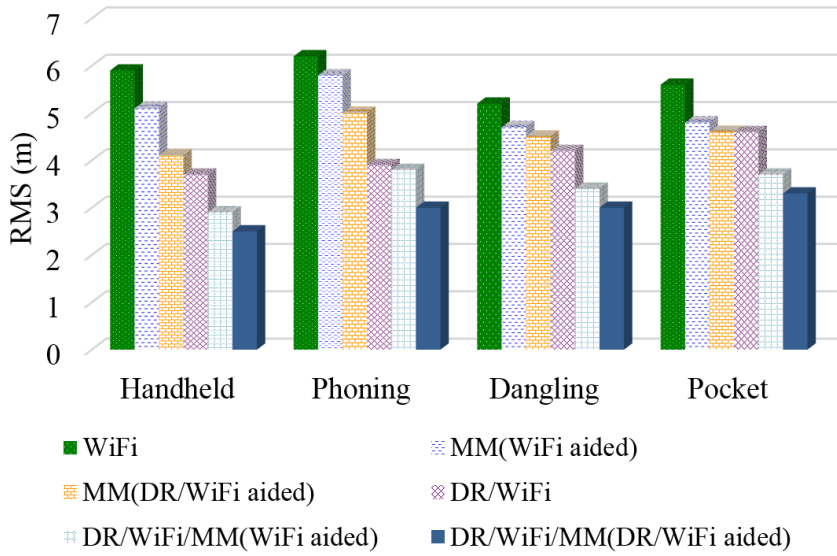


Figure 5-26. RMS values of position errors under different motions

5.5.2 Tests at Building B

Building B is mainly used for walking. Therefore, the environment at B is different from that at E. Compared with E, there are less WiFi APs and less metallic infrastructures at B. Figures 5-27 and 4-10 show the RSS and magnetic distributions on the test trajectory, respectively.

Although the environment at B was different than that at E, the same set of parameters was used for navigation to evaluate the consistency and robustness of the algorithm. Figure 5-28 illustrates the handheld results as examples, in which (a) - (h) show the position results when using eight strategies: DR, WiFi, DR/WiFi, MM, MM (WiFi aided), MM (DR/WiFi aided), DR/WiFi/MM (WiFi aided), and DR/WiFi/MM (DR/WiFi aided).

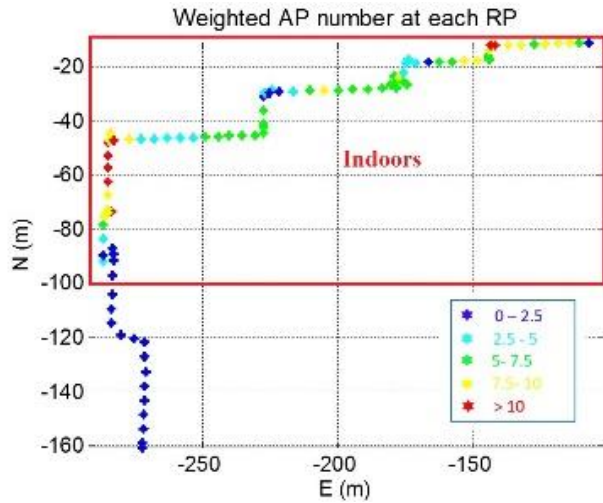


Figure 5-27. RSS distribution on test trajectory at B

Compared with the MM results at E, the MM results at B were sparse. The reason for this outcome was that the magnetic intensity changes were not significant; thus, more MM results were removed as blunders.

Figure 5-29 (a) compares the position errors in WiFi (point) and WiFi (profile) results under the handheld motion condition, while (b) illustrates the position errors in DR/WiFi (point) and DR/WiFi (profile) results. A significant mismatch at the beginning of the WiFi (point) result was removed when the profile-based WiFi fingerprinting was utilized. This outcome indicates the feasibility of using the profile-based method to obtain a more accurate initialization for position as soon as a user starts navigating. However, during 80-100 s, the errors in the WiFi (profile) result were significantly larger than those in the WiFi (point) result. This phenomenon indicates that there is still a risk of mismatch when a profile is used for matching. When integrated with DR, the navigation solution became smooth, and the maximum position error dropped to approximate 8 m in both DR/WiFi (point) and DR/WiFi (profile) solutions.

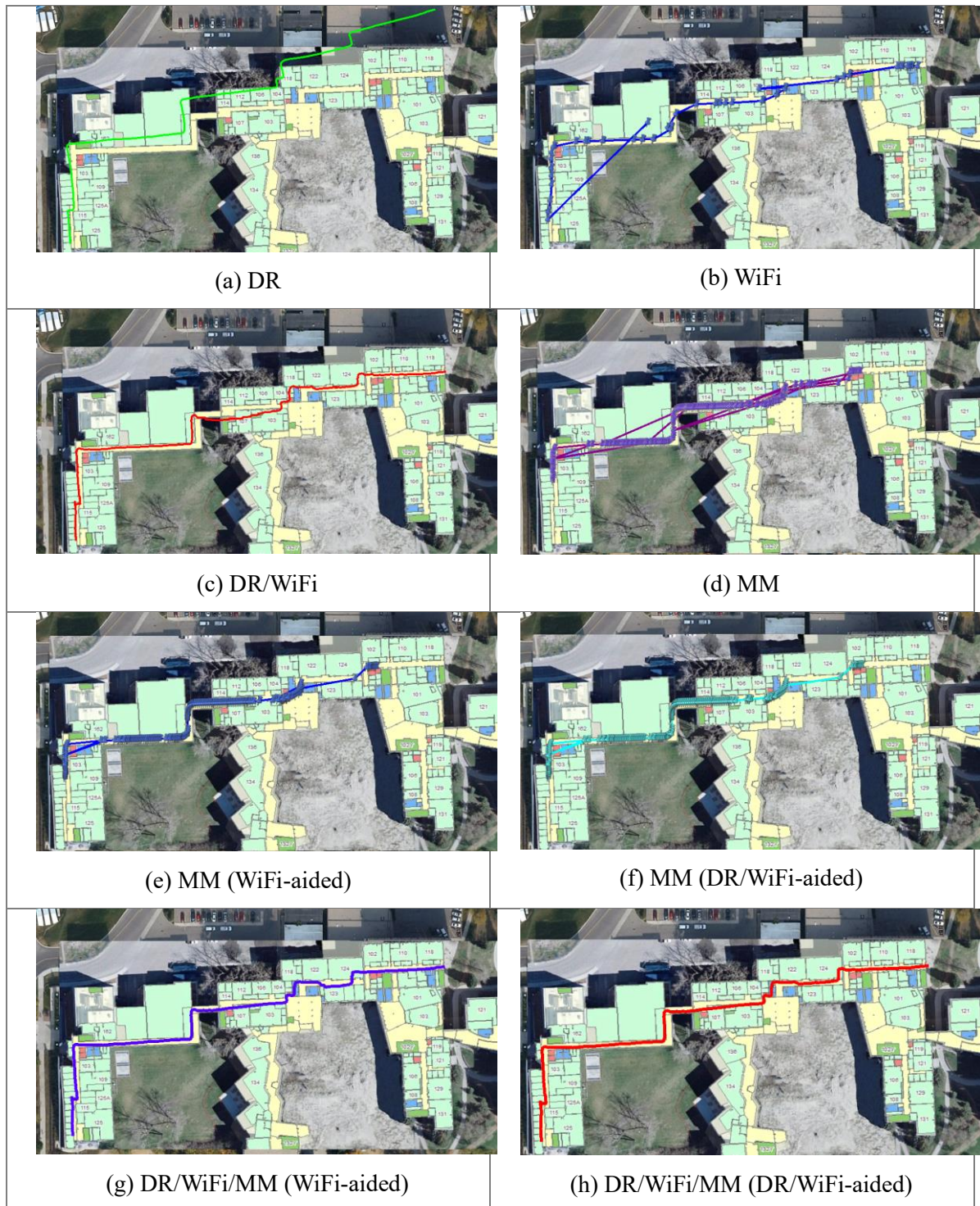


Figure 5-28. Position results when using different strategies (handheld)

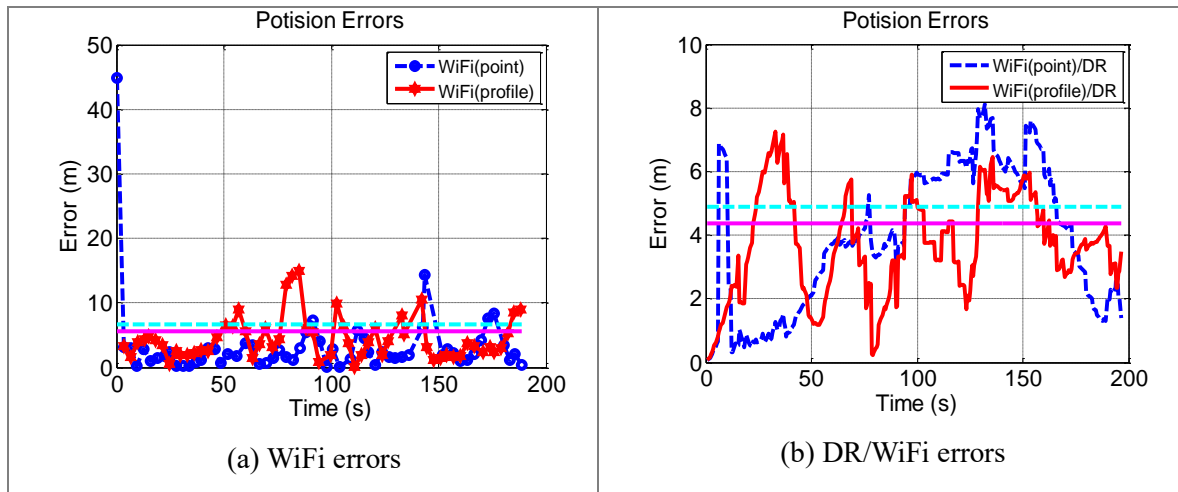


Figure 5-29. Errors in results of WiFi (point) and WiFi (profile), and their integration with DR, handheld

Figure 5-30 (a) illustrates the position errors in MM, MM (WiFi aided), and MM (DR/WiFi aided) results, while (b) compares the errors of DR/WiFi/MM (WiFi aided) and DR/WiFi/MM (DR/WiFi aided). Figure 5-30 (a) shows that the largest MM error dropped from over 100 m to approximate 20 m when aided by WiFi or DR/WiFi. Moreover, DR/WiFi detected more MM mismatches than WiFi. Figure 5-18 (b) demonstrates that the introduction of MM results (either WiFi aided or DR/WiFi aided) made DR/WiFi results more accurate. The DR/WiFi/MM (DR/WiFi aided) results were similar to DR/WiFi/MM (WiFi aided) before 80 s and were significantly better after 80 s. This reason for this outcome was that the large position errors in the MM (WiFi aided) result after 140 s was removed in the MM (DR/WiFi aided) result.

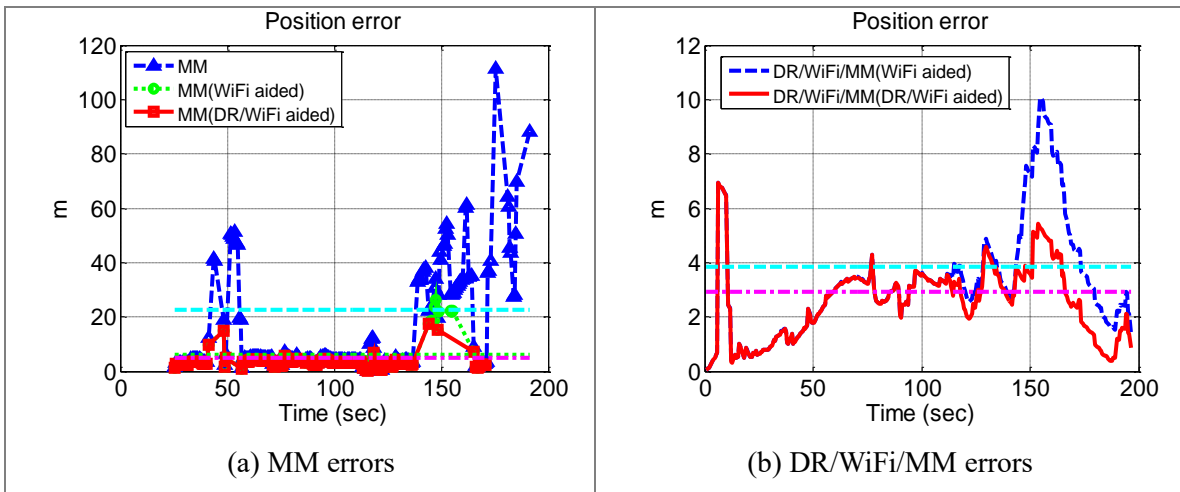


Figure 5-30. Errors in results of MM, MM (WiFi aided), and MM (DR/WiFi aided), handheld

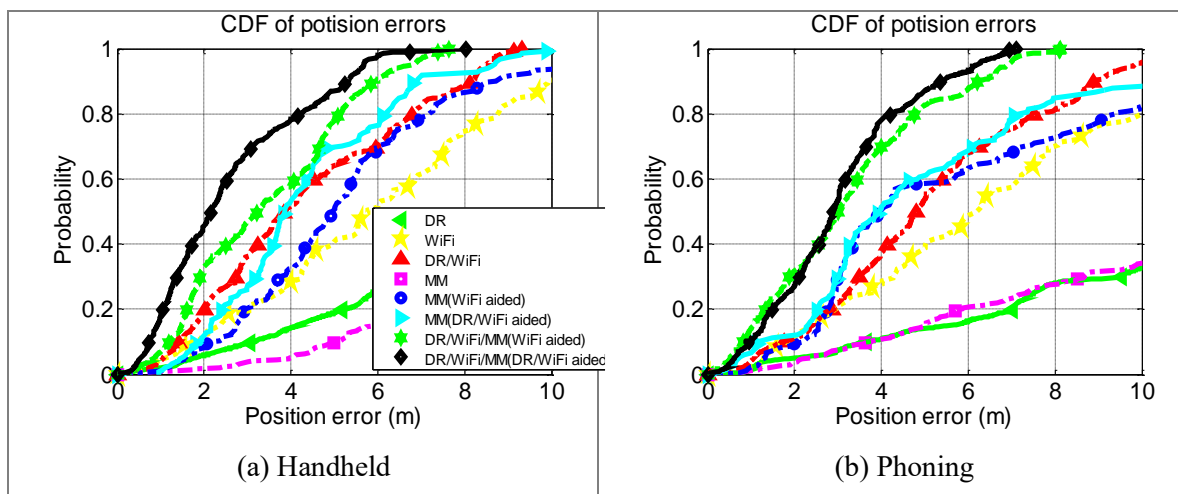
To summarize, Figures 5-31 (a) - (d) provide the CDF curves of the position errors from different strategies, and Table 5-3 illustrates the statistical values of the errors. Figure 5-31 and Table 5-3 illustrate that the RMS of MM errors at B (RMS 21.6 m) was similar to that at E (RMS 20.0 m); however, MM results in B were sparser than those at E because more MM results that had indistinct magnetic intensity changes were removed as blunders. Meanwhile, WiFi errors (RMS 7.0 m) at B were more significant than those at E (RMS 5.7 m). Accordingly, the errors of the WiFi-aided MM results at B (RMS 6.3 m) were larger than those at E (RMS 5.1 m).

The proposed DR/WiFi/MM (DR/WiFi aided) Structure #2 mitigated the effect of poor RSS distribution or indistinctive magnetic features. The RMS value of position errors was 3.0 m at E and 3.4 m at B, with a difference of only 0.4 m. The RMS values when using Structure #2 were 0.5 m less than those when using Structure #1 at both E and B. When comparing the results in two environments under each motion mode, the RMS values of position errors when using Structure #2 were 0.4 to 0.8 m smaller than those using Structure #1. The improvement was 10.8 % to 23.1 %.

Table 5-3. Statistical values of position errors (unit: m) at B

Motion	Error	A*	B	C	D	E	F	G	H
Handheld	Mean	11.9	6.0	4.3	17.6	5.3	4.3	3.4	2.6
	RMS	13.5	6.7	5.0	22.5	6.0	4.8	3.9	3.1
	80 %	18.7	8.8	6.8	24.2	7.2	6.2	5.1	4.2
Phoning	Mean	15.5	6.6	5.1	19.2	5.6	5.0	3.2	3.0
	RMS	18.1	7.6	5.7	24.1	6.7	5.9	3.8	3.4
	80 %	23.7	10.1	7.6	29.0	9.4	7.4	4.8	4.2
Dangling	Mean	15.0	6.0	4.6	14.7	5.2	4.9	3.4	3.0
	RMS	20.4	7.2	5.1	17.7	6.4	5.8	4.0	3.6
	80 %	23.4	9.1	6.6	22.9	9.6	6.8	5.3	4.8
Pocket	Mean	10.3	5.5	4.3	16.7	4.8	4.9	3.3	3.0
	RMS	14.7	6.5	4.7	21.5	6.2	5.9	3.7	3.3
	80 %	15.6	8.2	6.1	27.7	7.9	8.0	4.7	4.1
General ^{**}	Mean	13.4	6.1	4.6	17.1	5.2	4.8	3.3	2.9
	RMS	16.9	7.0	5.1	21.6	6.3	5.6	3.9	3.4
	80 %	20.6	9.1	6.8	26.1	8.6	7.1	5.0	4.3

* A- DR; B- WiFi; C- DR/WiFi; D- MM; E- MM(WiFi aided); F- MM(DR/WiFi aided); G-DR/WiFi/MM(WiFi aided); H- DR/WiFi/MM(DR/WiFi aided)



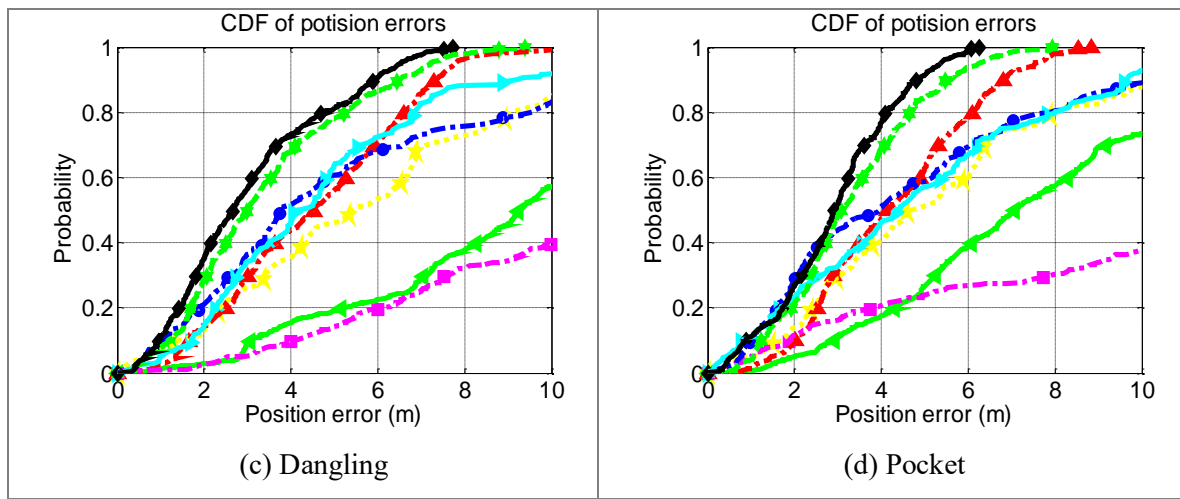


Figure 5-31. CDF of position errors when using different strategies

Figure 5-32 illustrates the RMS values of position errors when using different technologies or combinations in two environments. The effect of environment was mitigated when more technologies were used. Moreover, DR/WiFi/MM (DR/WiFi aided) provided more accurate results (RMS 3.0 m at E and 3.4 m at B) than other combinations or structures with off-the-shelf sensors available in consumer portable devices and existing WiFi infrastructures.

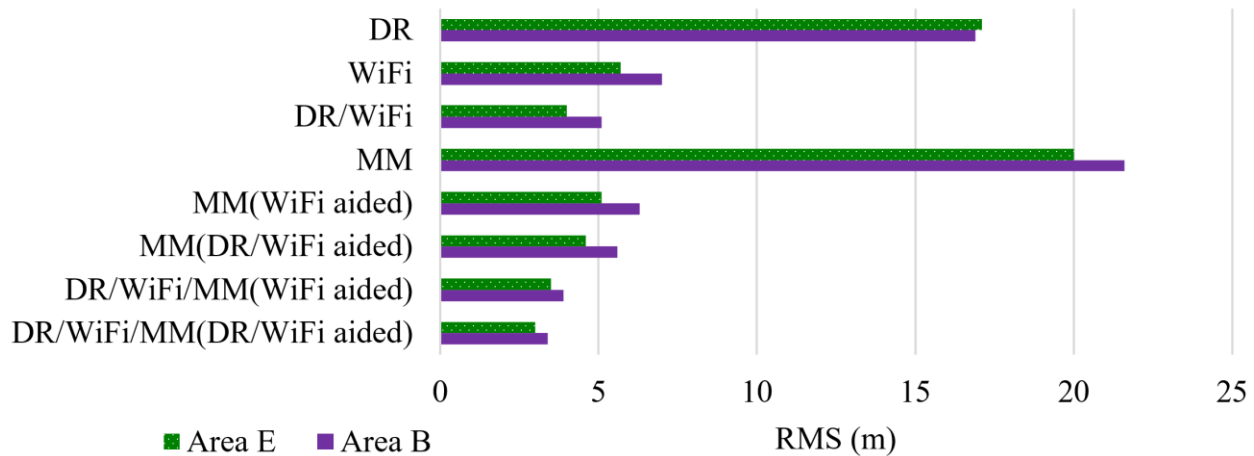


Figure 5-32. RMS values of position errors when using different technologies or combinations in two different environments

5.6 Summary

This chapter describes the following aspects:

- 1) This chapter presents a profile-based WiFi fingerprinting algorithm by using the short-term trajectories from DR and geometrical relationships of RPs in the space. The MD-DTW algorithm is introduced. The algorithms were tested with different smartphones, under various motion conditions, and in different indoor environments (i.e., E with more WiFi APs, and B with less WiFi). It was found that:
 - The proposed profile-based fingerprinting method reduced the RMS values of WiFi positioning errors from 5.7 m to 4.9 m, with an improvement of 14.0 %. Especially, a significant position error (over 40 m) in the single-point-based WiFi result was eliminated in the profile-based WiFi result. This outcome indicates the feasibility of using the profile-based method to obtain a more accurate initialization for position as soon as a user starts navigating.
 - When integrated with DR, the RMS values of position errors were 4.2 m and 3.8 m respectively when the single-point and profile-based methods were utilized. The RMS value of the DR/WiFi (profile) errors was 9.5 % less than that of the DR/WiFi (point) errors.
- 2) This research proposes a WiFi-aided MM algorithm, which uses the WiFi results to limit the MM search space to reduce both the mismatch rate and computational load, especially in environments with poor WiFi signal distributions. The complementary characteristics of WiFi and MM are especially useful for improving the navigation applications that use consumer devices not equipped with gyros. Moreover, when aided by either WiFi or

DR/WiFi to remove mismatches, MM results can be used as reliable updates in the position-tracking KF. Tests in two environments illustrated that:

- MM had significant mismatch rates. The RMS values of MM errors reached 20.0 m (E) and 21.6 m (B). However, when we used WiFi to limit the MM search space, the RMS reduced to 6.3 m and 5.1 m, respectively. Therefore, the key to obtaining accurate MM solutions is to remove the mismatches using information from other technologies.
- MM (WiFi aided) provided more reliable results than either WiFi or MM. Compared with WiFi-only results, the RMS values of the MM (WiFi aided) errors was 10.5 % and 10.0 % less at E and B, respectively.
- MM (DR/WiFi aided) removed more mismatches than MM (WiFi aided). The RMS values of position errors for MM (WiFi aided) and MM (DR/WiFi aided) were respectively 5.1m and 4.6 m at E, and respectively 6.3 m and 5.6 m at B. The decreases were 9.8 % at E and 11.1 % at B.

3) This chapter provides designs for and evaluates two hybrid integration structures. Structure #1 utilizes the WiFi-aided MM algorithm, while Structure #2 uses both DR and WiFi results (i.e., the integrated DR/WiFi solutions) to limit the MM search space. Structure #2 is more effective than previous structures at detecting MM mismatches, even in areas with limited WiFi RSS or weak RSS distribution. Furthermore, a multi-level quality-control mechanism is designed, based on the interaction between different techniques, to improve the system's robustness. It was found that:

- Fusion of DR, WiFi, and MM mitigated the effect of poor RSS distribution or indistinctive magnetic features. When DR, WiFi, and MM were employed, the difference between the RMS values of position errors at E and B was 0.4 m, which was

less than the differences when WiFi (1.3 m), MM (1.6 m), WiFi-aided MM (1.2 m), or DR/WiFi (1.1 m) was used.

- Fusion of DR, WiFi, and MM reduced dependency on device movement. Especially, when the proposed DR/WiFi/MM (DR/WiFi aided) structure was used, the difference between the RMS values of position errors under different motion conditions were 0.8 m at E and 0.5 m at B.
- The proposed structure performed better than the previous DR/WiFi/MM (WiFi aided) structure when replacing WiFi with DR/WiFi. The RMS values of the DR/WiFi/MM (DR/WiFi aided) errors were 3.0 m at E and 3.4 m at B, which were 0.5 m less than those of DR/WiFi/MM (WiFi aided) at both E and B.

CHAPTER 6 CONCLUSIONS AND FUTURE WORKS

This chapter summarizes the conclusions and contributions of the research and provides recommendations and possible future work.

6.1 Conclusions

This thesis provides a reliable indoor pedestrian navigation solution by using off-the-self sensors in consumer portable devices, local magnetic features, and existing WiFi infrastructures. By taking better advantage of the merits of DR, WiFi, and MM, the proposed algorithm can provide a navigation solution that has accuracy of 3-5 m (RMS), and do not suffer from failures or jumps. Furthermore, this algorithm can run in real time on portable devices, and can be easily combined with other techniques such as GNSS and BLE.

Also, by taking better advantage of the merits of DR, WiFi, and MM, the proposed algorithm has the following advantages:

- 1) The algorithm can significantly improve the attitude-determination and DR results with commercial-grade MEMS gyros (typically have biases of up to several deg/s) without the need for any external calibration equipment or user intervention.
- 2) The algorithm can provide reliable and continuous indoor navigation results when external positioning technologies (e.g., WiFi and BLE) are not available; also, it can achieve optimal system performance when an external technology is available.
- 3) The algorithm can reduce dependency on navigation environments. For example, the algorithm works in indoor environments that have weak WiFi signal distribution, or in environments with frequent magnetic interferences.

- 4) The algorithm can reduce dependency on device motion conditions. Specifically, the algorithm can work under natural motion conditions such as handheld, phoning (i.e., close to the ear), dangling (i.e., walking with phone in hand), and in pants pockets.

To be specific, compared with previous hybrid navigation algorithms or structures, the main innovation points of this research are:

- 1) Chapter 3 presents a real-time calibration method for gyro sensors in consumer portable devices. The calibration happens automatically without the need for external equipment or user intervention. Multi-level constraints – including the pseudo-observations, the accelerometer and magnetometer measurements, the norm vector of the accelerometer and magnetometer measurements, and the quasi-static attitude updates – are used to make the method reliable and accurate under natural user motions. This method provided promising calibration results even under challenging motion modes such as dangling and pocket, and in challenging indoor environments with frequent magnetic interferences.

The method was tested under walking tests with typical human motions, including handheld, phoning, dangling, pocket, belt, and backpack, both outdoors and indoors. The gyro biases of tested smartphones were reduced from several deg/s to under 0.15 deg/s indoors and 0.1 deg/s outdoors. Under the most challenging motion modes for sensors-based pedestrian navigation, i.e., dangling and pocket, the calibration errors were 0.17 and 0.14 deg/s indoors, and 0.13 and 0.09 deg/s outdoors. Under other motions, the calibration errors are less than 0.12 deg/s indoors and 0.07 outdoors. This calibration method can work in real-time and has a potential for calibration of the MEMS gyros within consumer electronics.

- 2) Chapter 4 proposes an autonomous navigation algorithm for challenging indoor environments that do not have any WiFi signal or have WiFi signals with a weak

distribution by integrating DR and MM. Several approaches are used to improve the DR and MM performance. Furthermore, realized that the key to enhance the DR/MM performance is to mitigate the impact of MM mismatches, this research introduces and evaluated two mismatch-detection approaches, including a threshold-based method that sets the measurement noises of MM positions based on their distances to the historical DR/MM position solutions, and an AKF based method that introduces the estimation of the innovation sequence covariance into the calculation of the KF gain matrix.

- 3) This research indicates the potential for continuous and reliable indoor navigation with off-the-shelf sensors in smartphones and magnetic features. However, the key is to mitigate the impact of frequent magnetic matching (MM) mismatches. Both the threshold-based approach and the AKF were effective in our tests under two different indoor environments. The RMS values of position errors when using these strategies under four different motion conditions (i.e., handheld, phoning, dangling, and pocket) were 4.3 m and 4.6 m in Environment #1 (i.e., the area with frequent and severe magnetic interferences, where the change of magnetic intensity reached 0.4 Gauss), and 5.2 m and 5.6 m in Environment #2 (i.e., the environment that had less and weaker magnetic interferences, where the change of magnetic intensity was below 0.25 Gauss). This accuracy is acceptable for many indoor location-based services because it is already within a user's sensing range. The benefit of this algorithm is that it is totally self-contained, and the results were continuous and robust (i.e., no jump points).
- 4) Chapter 5 presents a profile-based WiFi fingerprinting algorithm by using the short-term trajectories from DR and geometrical relationships of RPs in the space. The MD-DTW algorithm in introduced. The use of the profile-based approach can reduce the probability

of mismatches. Furthermore, the profile-based approach is especially useful to provide a more accurate initialization for position as soon as a user starts navigating.

The proposed profile-based fingerprinting method reduced the RMS values of WiFi positioning errors from 5.7 m to 4.9 m, with an improvement of 14.0 %. Especially, a significant position error (over 40 m) in the single-point-based WiFi result was eliminated in the profile-based WiFi result, which supported the advantage of the profile-based method for initialization of position. When integrated with DR, the RMS values of position errors were 4.2 m and 3.8 m respectively when the single-point and profile-based methods were utilized. The RMS value of the DR/WiFi (profile) errors was 9.5 % less than that of the DR/WiFi (point) errors.

- 5) This research proposes a WiFi-aided MM algorithm, which uses the WiFi results to limit the MM search space to reduce both the mismatch rate and computational load. The complementary characteristics of WiFi and MM are especially useful for improving the navigation applications that use consumer devices not equipped with gyros (e.g., many medium- and low-end smartphones contain accelerometers and magnetometers but do not have gyros). Furthermore, when aided by either WiFi or DR/WiFi to remove mismatches, MM results can be used as reliable updates in the position-tracking KF.

The RMS values of MM errors were reduced from 20.0 m at E and 21.6 m at B to 6.3 m at E and 5.1 m at B respectively when the WiFi positioning results were used to limit the MM search space. This outcome indicated that the key to obtaining accurate MM solutions is to remove the mismatches using information from other technologies. MM (WiFi aided) provided more reliable results than either WiFi or MM. Compared with WiFi-only results, the RMS values of the MM (WiFi aided) errors was 10.5 % and 10.0 % less at E and B,

respectively. Furthermore, MM (DR/WiFi aided) removed more mismatches than MM (WiFi aided). The RMS values of position errors for MM (WiFi aided) and MM (DR/WiFi aided) were respectively 5.1m and 4.6 m at E, and respectively 6.3 m and 5.6 m at B. The decreases were 9.8 % at E and 11.1 % at B.

- 6) Chapter 5 provides designs for and evaluates two hybrid integration structures that uses off-the-shelf sensors in consumer portable devices and existing WiFi infrastructures. Structure #1 utilizes the WiFi-aided MM algorithm, while Structure #2 uses both DR and WiFi results (i.e., the integrated DR/WiFi solutions) to limit the MM search space. Furthermore, a multi-level quality control mechanism is designed based on the interaction between different techniques and utilized in Structure #2. This mechanism has at least one more level than those in previous DR/WiFi/MM structures. Therefore, Structure #2 is more effective than previous structures at detecting MM mismatches, even in areas with limited WiFi RSS or weak RSS distribution. This structure reduced dependency on both navigation environments and motion condition. It provided consistent positioning accuracy in indoor environments with frequent magnetic interferences, and under different motion conditions.

The algorithms were evaluated by walking in two types of indoor environments, with two smartphones, and under four motion conditions. It was found that:

Fusion of DR, WiFi, and MM mitigated the effect of poor RSS distribution or indistinctive magnetic features. When DR, WiFi, and MM were employed, the difference between the RMS values of position errors at E and B was 0.4 m, which was less than the differences when WiFi (1.3 m), MM (1.6 m), WiFi-aided MM (1.2 m), or DR/WiFi (1.1 m) was used.

Fusion of DR, WiFi, and MM reduced dependency on device movement. Especially, when the proposed DR/WiFi/MM (DR/WiFi aided) structure was used, the difference between the RMS values of position errors under different motion conditions were 0.8 m at E and 0.5 m at B.

The accuracy and reliability of the navigation solutions from this thesis can meet the requirement for many mobile LBS applications. Furthermore, the proposed algorithms in this thesis use off-the-shelf sensors available in consumer portable devices and existing WiFi infrastructures, which need no additional BOM cost or extra manpower cost. Therefore, this thesis can guide the improvement of the reliability of the navigation solution with in challenging indoor environments.

6.2 Recommendations for Future works

Based on the achieved results and conclusions about the implementation of an autonomous multi-sensor navigation algorithm, it is recommended to optimize it and extend this research for future developments. The future works include

- Having deeper investigations on the requirements for different application scenarios (e.g., hospitals, malls, underground, etc.), and optimizing the algorithm according to the specific requirements. If necessary, introducing other techniques such as BLE and RFID to further enhance the navigation performance.
- Further reducing the time- and manpower- cost of building and updating the WiFi and magnetic database. For example, updating these databases through a crowdsourcing approach by using daily-life data from users
- Expanding the proposed algorithm from walking to other moving cases such as running and jogging.

- It is also worthwhile to connect the proposed pedestrian navigation algorithm with existing INS-based navigation for vehicles, as it is common that the motion of a user changes from a vehicle mode to a pedestrian mode.
- As the most economical system is desired, a simplified version of the multi-sensor navigation algorithm needs to be developed for the portable devices.

Last but not least, the real-time algorithm needs to be tested thoroughly for a variety of scenarios such as buildings with multiple floors and with more complex internal structures.

LIST OF PUBLICATIONS DURING PHD PERIOD

Published or Accepted Journal Articles

- [J1] **You Li**, Yuan Zhuang, Haiyu Lan, Peng Zhang, Xiaoji Niu, and Naser El-Sheimy. (2015) "WiFi-Aided Magnetic Matching for Indoor Navigation with Consumer Portable Devices", *Micromachines* 2015, no. 6, pp. 747-764, doi: 10.3390/mi6060747.
- [J2] **You Li**, Jacques Georgy, Xiaoji Niu, Qingli Li, and Naser El-Sheimy. (2015) "Autonomous Calibration of MEMS Gyros in Consumer Portable Devices," *IEEE Sensors Journal*, vol. 15, no.7, pp. 4062-72.
- [J3] **You Li**, Xiaoji Niu, Quan Zhang, Hongping Zhang and Chuang Shi. (2012). An in situ Hand Calibration Method Using a Pseudo-observation Scheme for Low-end Inertial Navigation Units, *Measurement Science and Technology*, vol.23, No.10, 2012.
- [J4] Xiaoji Niu, **You Li**, Hongping Zhang, Qingjiang Wang and Yalong Ban. (2013). Fast Thermal Calibration of Low-Grade Inertial Sensors and Inertial Measurement Units, *Sensors*, 2013 (9): 12192-12217.
- [J5] **You Li**, Xiaoji Niu, Yahao Cheng, Chuang Shi, and Naser El-Sheimy (2015), “The Impact of Vehicle Maneuvers on the Attitude Estimation of GNSS/INS for Mobile Mapping”, *Journal of Applied Geodesy*, accepted.
- [J6] Qingjiang Wang, **You Li**, and Xiaoji Niu (2015), “Thermal Calibration Procedure and Thermal Characterization of Low Grade Inertial Measurement Units”, *Journal of Navigation*, accepted.
- [J7] Yuan Zhuang, Haiyu Lan, **You Li**, and Naser El-Sheimy (2015), “PDR/INS/WiFi integration based on handheld devices for indoor pedestrian navigation”, *Micromachines*, vol. 6, no. 6, pp. 793-812.
- [J8] Yuan Zhuang, **You Li**, Haiyu Lan, Zanaib Syed, and Naser El-Sheimy, (2015), Smartphone-based WiFi access point localization and propagation parameter estimation using crowdsourcing, *IET Electronics Letters*, accepted.
- [J9] Peng Zhang, Qile Zhao, **You Li**, Xiaoji Niu, Yuan Zhuang, Jingnan Liu. (2015) “Collaborative WiFi Fingerprinting using Sensor-based Navigation on Smartphones”, *Sensors* 2015(15):17534-17557.
- [J10] Yuan Zhuang, Zainab Syed, **You Li**, and Naser El-Sheimy, “Evaluation of Two WiFi Positioning Systems Based on Autonomous Crowdsourcing of Handheld Devices for Indoor Navigation”, *IEEE Transactions on Mobile Computing*, accepted.
- [J11] Haiyu Lan, Chunyang Yu, Yuan Zhuang, **You Li**, and Naser El-Sheimy, “A Novel Kalman Filter with State Constraint Approach for the Integration of Multiple Pedestrian Navigation Systems”, *Micromachines* 2015 (6), pp. 926-952.
- [J12] Xiaoji Niu, Qingjiang Wang, **You Li***, Qingli Li, and Jingnan Liu (2015). "Using Inertial Sensors in Smartphones for Curriculum Experiments of Inertial Navigation Technology." *Educ. Sci.* 5, no. 1: 26-46.

- [J13] Xiaoji Niu, **You Li**, Quan Zhang, Yahao Cheng and Chuang Shi, (2012), Observability Analysis of Non-Holonomic Constraints for Land-Vehicle Navigation Systems, *Journal of Global Positioning Systems 2012*, vol. 11, no. 1, pp. 80-88.
- [J14] Xiang Min, Xiaoji Niu, **You Li** and Chuang Shi, (2013), Algorithm Development and Simulation Verification of GNSS/INS Integration for Earthquake Monitoring, *Journal of Navigation and Positioning*, 2013,1(2), pp.60-65.

Under Reviewing Journal Articles

- [J15] **You Li**, Peng Zhang, Yuan Zhuang, Xiaoji Niu, and Naser El-Sheimy (2015), “A Hybrid WiFi/Magnetic Matching/PDR Approach for Indoor Navigation with Consumer Portable Devices”, under review (2nd round), *IEEE Communications Letters*.
- [J16] **You Li**, Yuan Zhuang, Peng Zhang, Haiyu Lan, Xiaoji Niu, and Naser El-Sheimy (2015), “An Improved Dead-Reckoning/WiFi/Magnetic Matching Integration Structure for Indoor Navigation”, *Information Fusion*, under review.
- [J17] **You Li**, Haiyu Lan, Yuan Zhuang, Xiaoji Niu, and Naser El-Sheimy, “Autonomous Indoor Pedestrian Navigation using MEMS Sensors in Consumer Portable Devices and Magnetic Features” under review, *IEEE Transaction on Instrument and Measurement*.
- [J18] Xiaoji Niu, **You Li***, and Naser El-Shemiy (2015). “Study the Relation between Attitude Estimation and Inertial Sensor Error Estimation in GNSS/INS Integration through an Observability Analysis Method”, under review (1st round), *International Journal of Navigation and Observation*.
- [J19] Yuan Zhuang, Zainab Syed, **You Li**, and Naser El-Sheimy, “Wireless Access Point Localization and Propagation Parameter Determination Using Nonlinear Least Squares and Multi-Level Quality Control”, *IEEE Wireless Communications Letters*, minor revision.

Conference papers

- [C1] **You Li**, Yuan Zhuang, Haiyu Lan, Xiaoji Niu, Peng Zhang, and Naser El-Sheimy, “Smartphone-based Indoor Navigation using PDR and Magnetic Matching”, submitted to ION GNSS+ 2015.
- [C2] **You Li**, Haiyu Lan, Yuan Zhuang, Xiaoji Niu, and Naser El-Sheimy, “Real-time attitude tracking of mobile devices”, submitted to IPIN 2015.
- [C3] **You Li**, Yuan Zhuang, Haiyu Lan, Xiaoji Niu, and Naser El-Sheimy, “A modularized real-time indoor navigation algorithm on smartphones”, submitted to IPIN 2015.
- [C4] **You Li**, Jacques Georgy, Xiaoji Niu, Chris Goodall and Naser El-Sheimy, 2014, An Automatic Multi-level Gyro Calibration Architecture for Consumer Portable Devices, International Conference on Indoor Positioning and Indoor Navigation (IPIN) 2014, October 27-30, Busan, Korea.

- [C5] **You Li**, Xiaoji Niu, Qingjiang Wang and Chuang Shi. (2013) Robustness Evaluation and Improvements of an In-situ Hand Calibration Method for Low-end IMUs in Pedestrian Navigation Applications, *Proc. ION GNSS plus 2013*, Sept. 17-21, Nashville, Tennessee.
- [C6] **You Li**, Qijin Chen, Xiaoji Niu, Chuang Shi (2012) Simulation Analysis for the Influences of Vehicle Maneuvers to the Attitude Estimations of GNSS/INS Navigation Systems. *Lecture Notes in Electronic Engineering –CSNC 2012*, pp. 679-94.
- [C7] **You Li**, Yalong Ban, Qingjiang Wang and Xiaoji Niu, 2013, Fast Thermal Calibration of Low-Grade Inertial Sensors and Inertial Measurement Units, *MMT 2013*, May 1-3, 2013, Taiwan.
- [C8] **You Li**, Xiaoji Niu, Quan Zhang, Yahao Cheng and Chuang Shi. (2012) Observability Analysis of Non-Holonomic Constraints for Land-Vehicle Navigation Systems, *Proc. ION GNSS 2012*, Sept. 17-21, Nashville, Tennessee.
- [C9] **You Li**, Xiaoji Niu and Hongping Zhang. (2011). An IMU Calibration Method Using Simple Machinary and the Comprehensive Error Analysis (in Chinese), *China Satellite Navigation Conf. 2010*, May 18-20, Shanghai, China, pp. 1426-33.
- [C10] Xiaoji Niu, Quan Zhang, **You Li**, Yahao Cheng and Chuang Shi, 2012, Using Inertial Sensors of iPhone 4 for Car Navigation, *Proceedings of IEEE/ION PLANS 2012*, Myrtle Beach, South Carolina, April 2012, pp. 555-561.

Patents

- [P1] Chinese patent: A Fast Calibration Method for Inertial Measurement Units, Chinese patent, Authorization date: Nov 15, 2014, Patent No.: 201210056759.2, Applicant: Wuhan University, Completer: Xiaoji Niu, **You Li**, Quan Zhang, Chuanchuan Liu, Hongping Zhang and Chuang Shi.
- [P2] Chinese patent: A fast thermal calibration method for Inertial Measurement Units, Chinese patent, Authorization date: June 18, 2014, Patent No.: 201310270889.0, Applicant: Wuhan University, Completer: Xiaoji Niu, **You Li** and Qingjiang Wang.
- [P3] US patent: A Fast Calibration Method for Inertial Measurement Units. International patent application No.: PCT/CN201/072202, Applicant: Wuhan University, Completer: Xiaoji Niu, **You Li**, Quan Zhang, Chuanchuan Liu, Hongping Zhang, Chuang Shi and Jingnan Liu, Priority date: March 6, 2012.
- [P4] Chinese patent: An automatic gyro calibration method. Application date: March 17, 2015, Applicant: Wuhan University, Completer: Xiaoji Niu, **You Li**, Qingli Li, and Peng Zhang.
- [P5] Chinese patent: Indoor navigation based on inertial sensors, WiFi, and magnetic matching. Application date: June 30, 2015, Applicant: Wuhan University, Completer: Xiaoji Niu, **You Li**, Peng Zhang, Yuan Zhuang, and Zheng Cheng.

REFERENCES

- ABDULRAHIM, K., HIDE, C., MOORE, T. & HILL, C. Aiding MEMS IMU with building heading for indoor pedestrian navigation. *Ubiquitous Positioning Indoor Navigation and Location Based Service (UPINLBS)*, 2010, 2010. IEEE, 1-6.
- AFZAL, M. H. 2011. Use of Earth's Magnetic Field for Pedestrian Navigation.
- AFZAL, M. H., RENAUDIN, V. & LACHAPELLE, G. 2011. Use of earth's magnetic field for mitigating gyroscope errors regardless of magnetic perturbation. *Sensors*, 11, 11390-11414.
- AGGARWAL, P., SYED, Z. & EL-SHEIMY, N. Hybrid extended particle filter (HEPF) for integrated civilian navigation system. *Position, Location and Navigation Symposium, 2008 IEEE/ION*, 2008. IEEE, 984-992.
- AKEILA, E., SALCIC, Z. & SWAIN, A. 2014. Reducing low-cost INS error accumulation in distance estimation using self-resetting. *Instrumentation and Measurement, IEEE Transactions on*, 63, 177-184.
- AKYILDIZ, I. F., SUN, Z. & VURAN, M. C. 2009. Signal propagation techniques for wireless underground communication networks. *Physical Communication*, 2, 167-183.
- ALVAREZ, D., GONZ LEZ, R. C., L PEZ, A. & ALVAREZ, J. C. Comparison of step length estimators from weareable accelerometer devices. *Engineering in Medicine and Biology Society, 2006. EMBS'06. 28th Annual International Conference of the IEEE*, 2006. IEEE, 5964-5967.
- ATIA, M. M., NOURELDIN, A. & KORENBERG, M. J. 2012. Dynamic Propagation Modeling for Mobile Users' Position and Heading Estimation in Wireless Local Area Networks. *Wireless Communications Letters, IEEE*, 1, 101-104.
- BAHL, P. & PADMANABHAN, V. N. RADAR: An in-building RF-based user location and tracking system. *INFOCOM 2000. Nineteenth Annual Joint Conference of the IEEE Computer and Communications Societies. Proceedings*. IEEE, 2000. IEEE, 775-784.
- BAN, R., KAJI, K., HIROI, K. & KAWAGUCHI, N. Indoor positioning method integrating pedestrian Dead Reckoning with magnetic field and WiFi fingerprints. *Mobile Computing and Ubiquitous Networking (ICMU), 2015 Eighth International Conference on*, 2015. IEEE, 167-172.
- BARNES, J., RIZOS, C., PAHWA, A., POLITI, N. & VAN CRANENBROECK, J. 2007. The potential of locata technology for structural monitoring applications. *Positioning*, 1.
- BEHZAD, K. P. & BEHROOZ, K. P. Vehicle localization on gravity maps. *Proceedings of SPIE-The International Society for Optical Engineering*, 1999. sl]:[sn], 182-191.
- BERGINSIGHT. 2014. Available: <http://www.berginsight.com/ReportPDF/ProductSheet/bi-lbs8-ps.pdf> [Accessed July 7 2014].
- BESL, P. J. & MCKAY, N. D. Method for registration of 3-D shapes. *Robotics-DL tentative*, 1992. International Society for Optics and Photonics, 586-606.
- BISIO, I., LAVAGETTO, F., MARCHESE, M. & SCIARRONE, A. Performance comparison of a probabilistic fingerprint-based indoor positioning system over different smartphones. *Performance Evaluation of Computer and Telecommunication Systems (SPECTS), 2013 International Symposium on*, 2013. IEEE, 161-166.
- BLOCH, A. M., MARSDEN, J. E. & ZENKOV, D. V. 2005. Nonholonomic Dynamics-Nonholonomic dynamical systems are mechanical systems, like a falling rolling disk, whose velocities have constraints that can't be derived from their position constraints. *Notices of the American Mathematical Society*, 52, 324-333.
- BOLLIGER, P. Redpin-adaptive, zero-configuration indoor localization through user collaboration. *Proceedings of the first ACM international workshop on Mobile entity localization and tracking in GPS-less environments*, 2008. ACM, 55-60.
- BOSE, A. & FOH, C. H. A practical path loss model for indoor WiFi positioning enhancement. *Information, Communications & Signal Processing, 2007 6th International Conference on*, 2007. IEEE, 1-5.

- BOUADI, H., BOUCHOUCHA, M. & TADJINE, M. 2007. Sliding mode control based on backstepping approach for an UAV type-quadrotor. *World Academy of Science, Engineering and Technology*, 26, 22-27.
- BOWDITCH, N. & BOWDITCH, J. I. 1802. *American Practical Navigator*, US Government Printing Office.
- BROWN, R. G. & HWANG, P. Y. C. 1992. *Introduction to random signals and applied Kalman filtering*, John Wiley & Sons New York.
- BRYSON, M. & SUKKARIEH, S. Vehicle model aided inertial navigation for a UAV using low-cost sensors. Proceedings of the Australasian Conference on Robotics and Automation, 2004.
- CAMPBELL, W. H. 2001. *Earth magnetism: a guided tour through magnetic fields*, Academic Press.
- CAMPS, F., HARASSE, S. & MONIN, A. Numerical calibration for 3-axis accelerometers and magnetometers. *Electro/Information Technology*, 2009. eit'09. IEEE International Conference on, 2009. IEEE, 217-221.
- CHAMBODUT, A. 2011. Geomagnetic Field, IGRF. *Encyclopedia of Solid Earth Geophysics*. Springer.
- CHEN, L.-H., WU, E. H.-K., JIN, M.-H. & CHEN, G.-H. 2014. Intelligent fusion of Wi-Fi and inertial sensor-based positioning systems for indoor pedestrian navigation. *Sensors Journal, IEEE*, 14, 4034-4042.
- CHEN, R., CHEN, W., CHEN, X., ZHANG, X. & CHEN, Y. 2011. Sensing strides using EMG signal for pedestrian navigation. *GPS solutions*, 15, 161-170.
- CHENG, J., YANG, L., LI, Y. & ZHANG, W. 2014. Seamless outdoor/indoor navigation with WIFI/GPS aided low cost Inertial Navigation System. *Physical Communication*.
- CHENG, Y.-C., CHAWATHE, Y., LAMARCA, A. & KRUMM, J. Accuracy characterization for metropolitan-scale Wi-Fi localization. Proceedings of the 3rd international conference on Mobile systems, applications, and services, 2005. ACM, 233-245.
- CHENG, Y., WANG, X., MORELANDE, M. & MORAN, B. 2013. Information geometry of target tracking sensor networks. *Information Fusion*, 14, 311-326.
- CHO, S. Y. & PARK, C. G. 2006. MEMS based pedestrian navigation system. *Journal of navigation*, 59, 135-153.
- COLOMBO, A., FONTANELLI, D., MACII, D. & PALOPOLI, L. 2014. Flexible Indoor Localization and Tracking Based on a Wearable Platform and Sensor Data Fusion.
- CRASSIDIS, J. L. 2006. Sigma-point Kalman filtering for integrated GPS and inertial navigation. *Aerospace and Electronic Systems, IEEE Transactions on*, 42, 750-756.
- DAVIDSON, P. & TAKALA, J. 2013. Algorithm for pedestrian navigation combining IMU measurements and gait models. *Gyroscopy and Navigation*, 4, 79-84.
- DAWADEE, A., CHAHL, J. & NANDAGOPAL, D. Method for landmark extraction for autonomous vision based navigation of UAVs. 2013. Australian International Aerospace Congress.
- DENG, Z., YU, Y., YUAN, X., WAN, N.; & YANG, L. 2013. Situation and development tendency of indoor positioning. *Communications, China*, 10, 42-55.
- DENNIS, T. E., RAYNER, M. J. & WALKER, M. M. 2007. Evidence that pigeons orient to geomagnetic intensity during homing. *Proceedings of the Royal Society of London B: Biological Sciences*, 274, 1153-1158.
- DISSANAYAKE, G., SUKKARIEH, S., NEBOT, E. & DURRANT-WHYTE, H. 2001. The aiding of a low-cost strapdown inertial measurement unit using vehicle model constraints for land vehicle applications. *Robotics and Automation, IEEE Transactions on*, 17, 731-747.
- DODGE, D. 2015. *Indoor Location startups innovating Indoor Positioning* [Online]. Available: http://dondodge.typepad.com/the_next_big_thing/2013/06/indoor-location-startups-innovating-indoor-positioning.html [Accessed July 29 2015].
- DOS SANTOS, I. L., PIRMEZ, L., LEMOS, É. T., DELICATO, F. C., PINTO, L. A. V., DE SOUZA, J. N. & ZOMAYA, A. Y. 2014. A localized algorithm for Structural Health Monitoring using wireless sensor networks. *Information Fusion*, 15, 114-129.

- DRAWIL, N. & BASIR, O. 2014. Modeling the impact of observation conditions on localization systems. *Information Fusion*, 15, 19-31.
- EL-SHEIMY, N. 2000. Least Squares Estimation. *ENGO 361-course notes*. Calgary, Canada: Department of Geomatics Engineering, University of Calgary.
- EL-SHEIMY, N. & NIU, X. 2007. The Promise of MEMS to the Navigation Community. *Inside GNSS*, 2, 26-56.
- EVENNOU, F. & MARX, F. 2006. Advanced integration of WiFi and inertial navigation systems for indoor mobile positioning. *Eurasip journal on applied signal processing*, 2006, 164-164.
- EZANI, M., FAHEEM, M., ABDULLAH, M. A. & HASEEB, S. A region-to-point indoor localization approach via RSS-magnetic fingerprinting. *Information and Communication Technology for The Muslim World (ICT4M)*, 2014 The 5th International Conference on, 2014. IEEE, 1-6.
- FALLAH, N., APOSTOLOPOULOS, I., BEKRIS, K. & FOLMER, E. 2013. Indoor human navigation systems: A survey. *Interacting with Computers*, 25, 21-33.
- FANG, J. & YANG, S. 2011. Study on innovation adaptive EKF for in-flight alignment of airborne POS. *Instrumentation and Measurement, IEEE Transactions on*, 60, 1378-1388.
- FANG, S.-H. & LIN, T.-N. Accurate indoor location estimation by incorporating the importance of access points in wireless local area networks. *Global Telecommunications Conference (GLOBECOM 2010)*, 2010 IEEE, 2010. IEEE, 1-5.
- FEDERAL COMMUNICATIONS, C. 2015. Wireless E911 location accuracy requirements. *PS Docket*.
- FONG, W., ONG, S. & NEE, A. 2008. Methods for in-field user calibration of an inertial measurement unit without external equipment. *Measurement Science and Technology*, 19, 085202.
- FOXLIN, E. 2005. Pedestrian tracking with shoe-mounted inertial sensors. *Computer Graphics and Applications, IEEE*, 25, 38-46.
- GANG, W., CHEN, H., YOUNG, L. & MING, J. 2012. On Received-Signal-Strength Based Localization with Unknown Transmit Power and Path Loss Exponent. *Wireless Communications Letters, IEEE*, 1, 536-539.
- GEORGY, J. 2010. Advanced nonlinear techniques for low cost land vehicle navigation.
- GEORGY, J., NOURELDIN, A., KORENBERG, M. J. & BAYOUMI, M. M. 2010. Modeling the stochastic drift of a MEMS-based gyroscope in gyro/odometer/GPS integrated navigation. *Intelligent Transportation Systems, IEEE Transactions on*, 11, 856-872.
- GOLDEN, J. P. Terrain contour matching (TERCOM): a cruise missile guidance aid. 24th Annual Technical Symposium, 1980. International Society for Optics and Photonics, 10-18.
- GONCALO, G. & HELENA, S. Indoor location system using ZigBee technology. *Sensor Technologies and Applications*, 2009. SENSORCOMM'09. Third International Conference on, 2009. IEEE, 152-157.
- GORDON, N., RISTIC, B. & ARULAMPALAM, S. 2004. Beyond the kalman filter: Particle filters for tracking applications. *Artech House, London*.
- GREJNER-BRZEZINSKA, D. A., MARKIEL, J., TOTH, C. K. & ZAYDAK, A. Cooperative navigation in transitional environments. *Position Location and Navigation Symposium (PLANS)*, 2012 IEEE/ION, 2012. IEEE, 334-340.
- GROVES, P. D. 2014. The Complexity Problem in Future Multisensor Navigation and Positioning Systems: A Modular Solution. *Journal of Navigation*, 67, 311-326.
- GUSTAFSSON, F., GUNNARSSON, F., BERGMAN, N., FORSELL, U., JANSSON, J., KARLSSON, R. & NORDLUND, P.-J. 2002. Particle filters for positioning, navigation, and tracking. *Signal Processing, IEEE Transactions on*, 50, 425-437.
- HACKETT, J. K. & SHAH, M. Multi-sensor fusion: a perspective. *Robotics and Automation, 1990. Proceedings.*, 1990 IEEE International Conference on, 1990. IEEE, 1324-1330.
- HAN, D., ANDERSEN, D. G., KAMINSKY, M., PAPAGIANNAKI, K. & SESAN, S. 2009. Access point localization using local signal strength gradient. *Passive and Active Network Measurement*. Springer.

- HARLE, R. 2013. A survey of indoor inertial positioning systems for pedestrians. *Communications Surveys & Tutorials, IEEE*, 15, 1281-1293.
- HAUG, A. J. 2005. A tutorial on Bayesian estimation and tracking techniques applicable to nonlinear and non-Gaussian processes. *MITRE Corporation, McLean*.
- HE, Z. 2013. High-Sensitivity GNSS Doppler and Velocity Estimation for Indoor Navigation.
- HEGREN S, Ø. & HALLINGSTAD, O. 2011. Model-aided INS with sea current estimation for robust underwater navigation. *Oceanic Engineering, IEEE Journal of*, 36, 316-337.
- HERRERA, E. P., KAUFMANN, H., SECUE, J., QUIR S, R. & FABREGAT, G. 2013. Improving data fusion in personal positioning systems for outdoor environments. *Information Fusion*, 14, 45-56.
- HOSEINI-TABATABAEI, S. A., GLUHAK, A. & TAFAZOLLI, R. 2013. A survey on smartphone-based systems for opportunistic user context recognition. *ACM Computing Surveys (CSUR)*, 45, 27.
- HUANG, C., LIAO, Z. & ZHAO, L. 2010. Synergism of INS and PDR in self-contained pedestrian tracking with a miniature sensor module. *Sensors Journal, IEEE*, 10, 1349-1359.
- INERTIALLABS. 2014. *Vertical Gyro System VG Interface Control Document* [Online]. Available: http://inertiallabs.com/downloads/new/VG_ICD_rev_1.4_Mar14.pdf [Accessed Jan 19 2015].
- INVENSENSE. 2014. *MPU-6500 Product Specification Revision 1.1* [Online]. Available: <http://www.invensense.com/mems/gyro/mpu6500.html> [Accessed November 20 2014].
- JEKABSONS, G., KAIRISH, V. & ZURAVLYOV, V. 2011. An Analysis of Wi-Fi Based Indoor Positioning Accuracy. *Scientific Journal of Riga Technical University. Computer Sciences*, 44, 131-137.
- JIM NEZ, A., ZAMPELLA, F. & SECO, F. Light-matching: A new signal of opportunity for pedestrian indoor navigation. *Indoor Positioning and Indoor Navigation (IPIN)*, 2013 International Conference on, 2013. IEEE, 1-10.
- JIM NEZ, A. R., SECO, F., ZAMPELLA, F., PRIETO, J. C. & GUEVARA, J. 2011. PDR with a foot-mounted IMU and ramp detection. *Sensors (Basel, Switzerland)*, 11, 9393.
- JIRAWIMUT, R., PRAKOONWIT, S., CECELJA, F. & BALACHANDRAN, W. 2003. Visual odometer for pedestrian navigation. *Instrumentation and Measurement, IEEE Transactions on*, 52, 1166-1173.
- JULIER, S. J., UHLMANN, J. K. & DURRANT-WHYTE, H. F. A new approach for filtering nonlinear systems. *American Control Conference, Proceedings of the 1995*, 1995. IEEE, 1628-1632.
- KAILATH, T., SAYED, A. H. & HASSIBI, B. 2000. *Linear estimation*, Prentice Hall Upper Saddle River, NJ.
- KAISER, S., KHIDER, M. & ROBERTSON, P. 2013. A pedestrian navigation system using a map-based angular motion model for indoor and outdoor environments. *Journal of Location Based Services*, 7, 44-63.
- KALMAN, R. E. 1960. A new approach to linear filtering and prediction problems. *Journal of Fluids Engineering*, 82, 35-45.
- KAMGAR-PARSI, B. & KAMGAR-PARSI, B. Vehicle localization on gravity maps. *AeroSense'99*, 1999. International Society for Optics and Photonics, 182-191.
- KANG, W. & HAN, Y. 2015. SmartPDR: smartphone-based pedestrian dead reckoning for indoor localization. *Sensors Journal, IEEE*, 15, 2906-2916.
- KANNAN, B., MENEGUZZI, F., DIAS, M. B. & SYCARA, K. Predictive indoor navigation using commercial smart-phones. *Proceedings of the 28th Annual ACM Symposium on Applied Computing*, 2013. ACM, 519-525.
- KARLSSON, R., SCH N, T. & GUSTAFSSON, F. 2004. Complexity analysis of the marginalized particle filter.
- KHALEGHI, B., KHAMIS, A., KARRAY, F. O. & RAZAVI, S. N. 2013. Multisensor data fusion: A review of the state-of-the-art. *Information Fusion*, 14, 28-44.

- KIM, Y., CHON, Y. & CHA, H. 2012. Smartphone-based collaborative and autonomous radio fingerprinting. *Systems, Man, and Cybernetics, Part C: Applications and Reviews, IEEE Transactions on*, 42, 112-122.
- KLEPAL, M. & BEAUREGARD, S. A backtracking particle filter for fusing building plans with PDR displacement estimates. *Positioning, Navigation and Communication, 2008. WPNC 2008. 5th Workshop on*, 2008. IEEE, 207-212.
- KODIPPLI, N. & DIAS, D. Integration of fingerprinting and trilateration techniques for improved indoor localization. *Wireless And Optical Communications Networks (WOCN), 2010 Seventh International Conference On*, 2010. IEEE, 1-6.
- KOUROGI, M., ISHIKAWA, T. & KURATA, T. A method of pedestrian dead reckoning using action recognition. *Position Location and Navigation Symposium (PLANS), 2010 IEEE/ION*, 2010. IEEE, 85-89.
- KRUSKAL, J. B. & LIBERMAN, M. 1983. The symmetric time-warping problem: from continuous to discrete. *Time Warps, String Edits and Macromolecules: The Theory and Practice of Sequence Comparison*, 125-161.
- KUSHKI, A., PLATANIOTIS, K. N. & VENETSANOPoulos, A. N. 2007. Kernel-based positioning in wireless local area networks. *Mobile Computing, IEEE Transactions on*, 6, 689-705.
- L TTTERS, J., SCHIPPER, J., VELTINK, P., OLTHUIS, W. & BERGVELD, P. 1998. Procedure for in-use calibration of triaxial accelerometers in medical applications. *Sensors and Actuators A: Physical*, 68, 221-228.
- LADETTO, Q., GABAGLIO, V. & MERMINOD, B. Combining gyroscopes, magnetic compass and GPS for pedestrian navigation. *Proceedings of the international symposium on kinematic systems in geodesy, geomatics, and navigation*, 2001. 205-213.
- LAOUDIAS, C., LARKOU, G., ZEINALIPOUR-YAZTI, D. & PANAYIOTOU, C. G. 2013a. Airplace: Indoor geolocation on smartphones through wifi fingerprinting. *Mobile Computing*, 37.
- LAOUDIAS, C., ZEINALIPOUR-YAZTI, D. & PANAYIOTOU, C. G. Crowdsourced indoor localization for diverse devices through radiomap fusion. *Indoor Positioning and Indoor Navigation (IPIN)*, 2013 International Conference on, 2013b. IEEE, 1-7.
- LAWRENCE, A. 2012. *Modern inertial technology: navigation, guidance, and control*, Springer Science & Business Media.
- LEE, J. K., PARK, E. J. & ROBINOVITCH, S. N. 2012. Estimation of attitude and external acceleration using inertial sensor measurement during various dynamic conditions. *Instrumentation and Measurement, IEEE Transactions on*, 61, 2262-2273.
- LEPP KOSKI, H., COLLIN, J. & TAKALA, J. 2013. Pedestrian navigation based on inertial sensors, indoor map, and WLAN signals. *Journal of Signal Processing Systems*, 71, 287-296.
- LI, B., GALLAGHER, T., DEMPSTER, A. G. & RIZOS, C. How feasible is the use of magnetic field alone for indoor positioning? *International Conference on Indoor Positioning and Indoor Navigation*, 2012a. 15th.
- LI, X., WANG, J. & LI, T. 2013. Seamless positioning and navigation by using Geo-referenced images and multi-sensor data. *Sensors*, 13, 9047-9069.
- LI, Y., GEORGY, J., NIU, X., LI, Q. & EL-SHEIMY, N. 2015a. Autonomous Calibration of MEMS Gyros in Consumer Portable Devices. *IEEE Sensors Journal*, 15, 4062-72.
- LI, Y., NIU, X., ZHANG, Q., ZHANG, H. & SHI, C. 2012b. An in situ hand calibration method using a pseudo-observation scheme for low-end inertial measurement units. *Measurement Science and Technology*, 23, 105104.
- LI, Y., ZHUANG, Y., LAN, H., ZHANG, P., NIU, X. & EL-SHEIMY, N. 2015b. WiFi-Aided Magnetic Matching for Indoor Navigation with Consumer Portable Devices. *Micromachines*, 6, 747-764.
- LIAO, I. E. & KAO, K.-F. 2008. Enhancing the accuracy of WLAN-based location determination systems using predicted orientation information. *Information Sciences*, 178, 1049-1068.

- LIN, P., LI, Q., FAN, Q., GAO, X. & HU, S. 2014. A Real-Time Location-Based Services System Using WiFi Fingerprinting Algorithm for Safety Risk Assessment of Workers in Tunnels. *Mathematical Problems in Engineering*, 2014.
- LIU, Y., WU, M., HU, X. & XIE, H. Research on geomagnetic matching method. *Industrial Electronics and Applications*, 2007. ICIEA 2007. 2nd IEEE Conference on, 2007. IEEE, 2707-2711.
- MAUTZ, R. 2012. *Indoor positioning technologies*. Habil. ETH Zürich, 2012.
- MAYBECK, P. S. 1982. *Stochastic models, estimation, and control*, Access Online via Elsevier.
- MILLER, P. A., FARRELL, J. A., ZHAO, Y. & DJAPIC, V. 2010. Autonomous underwater vehicle navigation. *Oceanic Engineering, IEEE Journal of*, 35, 663-678.
- MIROWSKI, P., HO, T. K., YI, S. & MACDONALD, M. Signalslam: simultaneous localization and mapping with mixed wifi, bluetooth, LTE and magnetic signals. *Indoor Positioning and Indoor Navigation (IPIN)*, 2013 International Conference on, 2013. IEEE, 1-10.
- MOK, E. & RETSCHER, G. 2007. Location determination using WiFi fingerprinting versus WiFi trilateration. *Journal of Location Based Services*, 1, 145-159.
- MOKBEL, M. F. & LEVANDOSKI, J. J. Toward context and preference-aware location-based services. *Proceedings of the Eighth ACM International Workshop on Data Engineering for Wireless and Mobile Access*, 2009. ACM, 25-32.
- MONTESERIN, J. J. M. 2014. *Multi Sensor System for Pedestrian Tracking and Activity Recognition in Indoor Environments*. University of South Florida.
- MORRISON, A., RENAUDIN, V., BANCROFT, J. B. & LACHAPELLE, G. 2012. Design and testing of a multi-sensor pedestrian location and navigation platform. *Sensors*, 12, 3720-3738.
- NASSAR, S. & EL-SHEIMY, N. 2005. Wavelet analysis for improving INS and INS/DGPS navigation accuracy. *Journal of Navigation*, 58, 119-134.
- NI, L. M., LIU, Y., LAU, Y. C. & PATIL, A. P. 2004. LANDMARC: indoor location sensing using active RFID. *Wireless networks*, 10, 701-710.
- NIEMINEN, T., KANGAS, J., SUURINIEMI, S. & KETTUNEN, L. 2010. An enhanced multi-position calibration method for consumer-grade inertial measurement units applied and tested. *Measurement Science and Technology*, 21, 105204.
- NIU, X. 2002. *Micromachined Attitude Measurement Unit with Application in Satellite TV Antenna Stabilization*. PhD, Tsinghua University.
- NIU, X., LI, Y., ZHANG, H., WANG, Q. & BAN, Y. 2013. Fast Thermal Calibration of Low-Grade Inertial Sensors and Inertial Measurement Units. *Sensors*, 13, 12192-12217.
- NIU, X., NASSAR, S. & EL-SHEIMY, N. 2007a. An accurate land-vehicle MEMS IMU/GPS navigation system using 3D auxiliary velocity updates. *Navigation*, 54, 177-188.
- NIU, X., NASSER, S., GOODALL, C. & EL-SHEIMY, N. 2007b. A universal approach for processing any MEMS inertial sensor configuration for land-vehicle navigation. *Journal of Navigation*, 60, 233-245.
- NIU, X., ZHANG, H., CHIANG, K.-W. & EL-SHEIMY, N. Using Land-Vehicle Steering Constraint to Improve the Heading Estimation of MEMS GPS/INS Georeferencing Systems. 2010. ISPRS.
- PENG, J., ZHU, M. & ZHANG, K. New algorithms based on sigma point Kalman filter technique for multi-sensor integrated RFID indoor/outdoor positioning. 2011 International Conference on Indoor Positioning and Indoor Navigation (IPIN) Guimaraes, Portugal, 2011. 21-23.
- PRITT, N. Indoor navigation with use of geomagnetic anomalies. *Geoscience and Remote Sensing Symposium (IGARSS)*, 2014 IEEE International, 2014. IEEE, 1859-1862.
- QIAN, J., PEI, L., ZOU, D. & P., L. 2014. Optical Flow Based Step Length Estimation for Indoor Pedestrian Navigation on a Smartphone. *ION/IEEE PLANS 2014*.
- RAHIM, K. A. 2012. *Heading Drift Mitigation for Low Cost Inertial Pedestrian Navigation*. PhD, The University of Nottingham.
- RANTAKOKKO, J., RYDELL, J., STROMBACK, P., HANDEL, P., CALLMER, J., TORNQVIST, D., GUSTAFSSON, F., JOBS, M. & GRUDEN, M. 2011. Accurate and reliable soldier and first responder

indoor positioning: multisensor systems and cooperative localization. *Wireless Communications, IEEE*, 18, 10-18.

RASHVAND, H. F., ABEDI, A., ALCARAZ-CALERO, J. M., MITCHELL, P. D. & MUKHOPADHYAY, S. C. 2014. Wireless sensor systems for space and extreme Environments: A Review. *Sensors Journal, IEEE*, 14, 3955-3970.

RISEMAN, E. M., HANSON, A. R. & BEVERIDGE, J. R. 2013. 11 LANDMARK-BASED NAVIGATION AND THE ACQUISITION OF ENVIRONMENTAL MODELS. *Visual Navigation: From Biological Systems to Unmanned Ground Vehicles*, 317.

RUIZ, A. R. J., GRANJA, F. S., PRIETO HONORATO, J. C. & ROSAS, J. I. G. 2012. Accurate pedestrian indoor navigation by tightly coupling foot-mounted IMU and RFID measurements. *Instrumentation and Measurement, IEEE Transactions on*, 61, 178-189.

RUOTSALAINEN, L., KUUSNIEMI, H., BHUIYAN, M. Z. H., CHEN, L. & CHEN, R. 2013. A two-dimensional pedestrian navigation solution aided with a visual gyroscope and a visual odometer. *Gps Solutions*, 17, 575-586.

S. JEON, J. L., H. HONG, S. SHIN, H. LEE 2014. Indoor WPS/PDR Performance Enhancement using Map Matching Algorithm with Mobile Phone. *ION/IEEE PLANS*.

SAEEDI, S. 2013. *Context-Aware Personal Navigation Services Using Multi-level Sensor Fusion Algorithms*. PhD, University of Calgary.

SAXENA, A., GUPTA, G., GERASIMOV, V. & OURSELIN, S. In use parameter estimation of inertial sensors by detecting multilevel quasi-static states. *Knowledge-Based Intelligent Information and Engineering Systems*, 2005. Springer, 595-601.

SCH N, T., GUSTAFSSON, F. & NORDLUND, P.-J. 2005. Marginalized particle filters for mixed linear/nonlinear state-space models. *Signal Processing, IEEE Transactions on*, 53, 2279-2289.

SCHMITT, S., ADLER, S. & KYAS, M. The Effects of Human Body Shadowing in RF-based Indoor Localization. International Conference on Indoor Positioning and Indoor Navigation, 2014. 30th.

SECO, F., PRIETO, C. & GUEVARA, J. A comparison of pedestrian dead-reckoning algorithms using a low-cost MEMS IMU. *Intelligent Signal Processing*, 2009. WISP 2009. IEEE International Symposium on, 2009. IEEE, 37-42.

SHIN, E.-H. 2005a. Estimation techniques for low-cost inertial navigation. *UCGE report*, 20219.

SHIN, E.-H. 2005b. *Estimation techniques for low-cost inertial navigation*. PhD Dissertation/Thesis, University of Calgary.

SHIN, E. & EL-SHEIMY, N. 2002. A new calibration method for strapdown inertial navigation systems. *Z. Vermess*, 127, 1-10.

SHIN, S. H., PARK, C. G., KIM, J. W., HONG, H. S. & LEE, J. M. Adaptive step length estimation algorithm using low-cost MEMS inertial sensors. *Sensors Applications Symposium*, 2007. SAS'07. IEEE, 2007. IEEE, 1-5.

SHU, Y., BO, C., SHEN, G., ZHAO, C. & ZHAO, F. Magicol: Indoor Localization Using Pervasive Magnetic Field and Opportunistic WiFi Sensing. *IEEE Journal on Selected Areas in Communications*, 1, 1-14.

SIMANEK, J., REINSTEIN, M. & KUBELKA, V. 2015. Evaluation of the EKF-based estimation architectures for data fusion in mobile robots. *Mechatronics, IEEE/ASME Transactions on*, 20, 985-990.

SKOG, I. & H NDEL, P. Calibration of a MEMS inertial measurement unit. XVII IMEKO World Congress, 2006.

SKOG, I. & HANDEL, P. 2009. In-car positioning and navigation technologies—A survey. *Intelligent Transportation Systems, IEEE Transactions on*, 10, 4-21.

SKYHOOK. 2014. *Skyhook products* [Online]. Available: <http://www.skyhookwireless.com/products/#optimized> [Accessed July 7 2014].

- ST-PIERRE, M. & GINGRAS, D. Comparison between the unscented Kalman filter and the extended Kalman filter for the position estimation module of an integrated navigation information system. *Intelligent Vehicles Symposium*, 2004 IEEE, 2004. IEEE, 831-835.
- STORMS, W. F. 2009. *Magnetic field aided indoor navigation*. Master thesis, DTIC.
- SUBBU, K. P., GOZICK, B. & DANTU, R. 2013. LocateMe: Magnetic-fields-based indoor localization using smartphones. *ACM Transactions on Intelligent Systems and Technology (TIST)*, 4, 73.
- SUSI, M. 2012. Gait Analysis for Pedestrian Navigation Using MEMS Handheld Devices.
- SYED, Z., AGGARWAL, P., GOODALL, C., NIU, X. & EL-SHEIMY, N. 2007. A new multi-position calibration method for MEMS inertial navigation systems. *Measurement Science and Technology*, 18, 1897.
- TABATABAEI, S. A. H., GLUHAK, A. & TAFAZOLLI, R. 2013. A Fast Calibration Method for Triaxial Magnetometers. *Instrumentation and Measurement, IEEE Transactions on*, 62, 2929-2937.
- TALVITIE, J., RENFORS, M. & LOHAN, E. S. 2015. Distance-Based Interpolation and Extrapolation Methods for RSS-Based Localization With Indoor Wireless Signals. *Vehicular Technology, IEEE Transactions on*, 64, 1340-1353.
- TIAN, Z., FANG, X., ZHOU, M. & LI, L. 2015. Smartphone-Based Indoor Integrated WiFi/MEMS Positioning Algorithm in a Multi-Floor Environment. *Micromachines*, 6, 347-363.
- TITTERTON, D. H. & WESTON, J. L. 2004. *Strapdown inertial navigation technology -2nd ed.*, the Institution of Electrical Engineers, London, United Kingdom.
- TORRES-SOLIS, J., FALK, T. H. & CHAU, T. 2010. A review of indoor localization technologies: towards navigational assistance for topographical disorientation. *Ambient Intelligence*, 51-84.
- TURCOT, P. & LOWE, D. G. Better matching with fewer features: The selection of useful features in large database recognition problems. Computer Vision Workshops (ICCV Workshops), 2009 IEEE 12th International Conference on, 2009. IEEE, 2109-2116.
- URI SCHATZBERG, L. B., YUVAL AMIZUR 2014. Intel - Enhanced WiFi ToF Indoor Positioning System with MEMS-based INS and Pedometric Information. *ION/IEEE PLANS*.
- VAN DER MERWE, R., DOUCET, A., DE FREITAS, N. & WAN, E. The unscented particle filter. *Nips*, 2000. 584-590.
- WAHDAN, A., GEORGY, J., ABDELFATAH, W. F. & NOURELDIN, A. Magnetometer Calibration for Portable Navigation Devices in Vehicles Using a Fast and Autonomous Technique.
- WAHDAN, A., GEORGY, J. & NOURELDIN, A. 2015. Three-Dimensional Magnetometer Calibration with Small Space Coverage for Pedestrians.
- WANG, L., GROVES, P. D. & ZIEBART, M. K. 2013. Urban Positioning on a Smartphone: Real-time Shadow Matching Using GNSS and 3D City Models.
- WANG, M., YANG, Y., HATCH, R. R. & ZHANG, Y. Adaptive filter for a miniature MEMS based attitude and heading reference system. Position Location and Navigation Symposium, 2004. PLANS 2004, 2004. IEEE, 193-200.
- WELCH, G. & BISHOP, G. 1995. An introduction to the Kalman filter.
- WINKLHOFER, M. 2009. The physics of geomagnetic-field transduction in animals. *Magnetics, IEEE Transactions on*, 45, 5259-5265.
- WU, F., NIE, J. & HE, Z. 2010. Low-cost GPS/INS integrated navigation algorithm in land vehicle system considering attitude update (in Chinese). *Jounral of Chinese Inertial Technology*, 18, 675-679.
- XIANG, Z., SONG, S., CHEN, J., WANG, H., HUANG, J. & GAO, X. 2004. A wireless LAN-based indoor positioning technology. *IBM Journal of research and development*, 48, 617-626.
- XIAO, L., WEI, S. & SUN, W. 2008. Research on the high accuracy rapid test method of IMU. *J. Astronaut.*, 29, 172-177.
- XIAO, Z., WEN, H., MARKHAM, A., TRIGONI, N., BLUNSMON, P. & FROLIK, J. 2015. Non-Line-of-Sight Identification and Mitigation Using Received Signal Strength. *Wireless Communications, IEEE Transactions on*, 14, 1689-1702.

- XIE, H., GU, T., TAO, X., YE, H. & LV, J. MaLoc: a practical magnetic fingerprinting approach to indoor localization using smartphones. Proceedings of the 2014 ACM International Joint Conference on Pervasive and Ubiquitous Computing, 2014. ACM, 243-253.
- YAN, L. & CUI, C. A new algorithm of gravity matching aided navigation. Second International Conference on Spatial Information Technology, 2007. International Society for Optics and Photonics, 679529-679529-6.
- YU, J., THANDAPANI VENKATARAMANI, X. Z. & JIA, Z. Bootstrapped learning of WiFi access point in hybrid positioning system. Proceedings of the 25th International Technical Meeting of The Satellite Division of the Institute of Navigation, ION GNSS, 2012a. 960-966.
- YU, Z., ZHONG, Z. & YI, F. 2012b. Study on Application of Zero Velocity Update Technology to Inertial Navigation System [J]. *Piezoelectrics & Acoustooptics*, 6, 009.
- ZAMPELLA, F., DE ANGELIS, A., SKOG, I., ZACHARIAH, D. & JIMENEZ, A. A constraint approach for UWB and PDR fusion. Indoor Positioning and Indoor Navigation (IPIN), 2012 International Conference on, 2012. IEEE, 1-9.
- ZHANG, C., SUBBU, K., LUO, J. & WU, J. 2014. GROPING: Geomagnetism and cROwdsensing Powered Indoor NaviGation.
- ZHANG, H., WU, Y., WU, W., WU, M. & HU, X. 2010. Improved multi-position calibration for inertial measurement units. *Measurement Science and Technology*, 21, 015107.
- ZHANG, H., YUAN, W., SHEN, Q., LI, T. & CHANG, H. 2015. A Handheld Inertial Pedestrian Navigation System With Accurate Step Modes and Device Poses Recognition. *Sensors Journal, IEEE*, 15, 1421-1429.
- ZHANG, R., HOFLINGER, F. & REINDL, L. 2013. Inertial sensor based indoor localization and monitoring system for emergency responders. *Sensors Journal, IEEE*, 13, 838-848.
- ZHANG, Z.-Q. & YANG, G.-Z. 2014. Calibration of miniature inertial and magnetic sensor units for robust attitude estimation. *Instrumentation and Measurement, IEEE Transactions on*, 63, 711-718.
- ZHAO, J., WANG, S. & WANG, A. Study on underwater navigation system based on geomagnetic match technique. *Electronic Measurement & Instruments*, 2009. ICEMI'09. 9th International Conference on, 2009. IEEE, 3-255-3-259.
- ZHAO, Z., HU, T., CUI, W., HUANGFU, J., LI, C. & RAN, L. 2014. Long-Distance Geomagnetic Navigation: Imitations of Animal Migration Based on a New Assumption.
- ZHEN, D., ZHAO, H., GU, F. & BALL, A. 2012. Phase-compensation-based dynamic time warping for fault diagnosis using the motor current signal. *Measurement Science and Technology*, 23, 055601.
- ZHUANG, Y. 2015. *Integration of WiFi and MEMS Sensors for Indoor Navigation*. PhD, University of Calgary.
- ZHUANG, Y., LAN, H., LI, Y. & EL-SHEIMY, N. 2015a. PDR/INS/WiFi Integration Based on Handheld Devices for Indoor Pedestrian Navigation. *Micromachines*, 6, 793-812.
- ZHUANG, Y., LI, Y., LAN, H., SYED, Z. & EL-SHEIMY, N. 2015b. Smartphone-based WiFi access point localisation and propagation parameter estimation using crowdsourcing. *Electronics Letters*, 51, 1380-1382.
- ZHUANG, Y., SYED, Z., GEORGY, J. & EL-SHEIMY, N. 2015c. Autonomous smartphone-based WiFi positioning system by using access points localization and crowdsourcing. *Pervasive and Mobile Computing*, 18, 118-136.